ERDC/CHL TR-11-10

Coastal and Hydraulic Laboratory

US Army Corps of Engineers®
Engineer Research and Development Center

Verification and Validation of the Coastal Modeling System

Report 3, CMS-Flow: Hydrodynamics

Alejandro Sánchez, Weiming Wu, Tanya M. Beck, Honghai Li,
James Rosati III, Robert Thomas, Julie Dean Rosati,
Zeki Demirbilek, Mitchell Brown, and Christopher Reed

December 2011

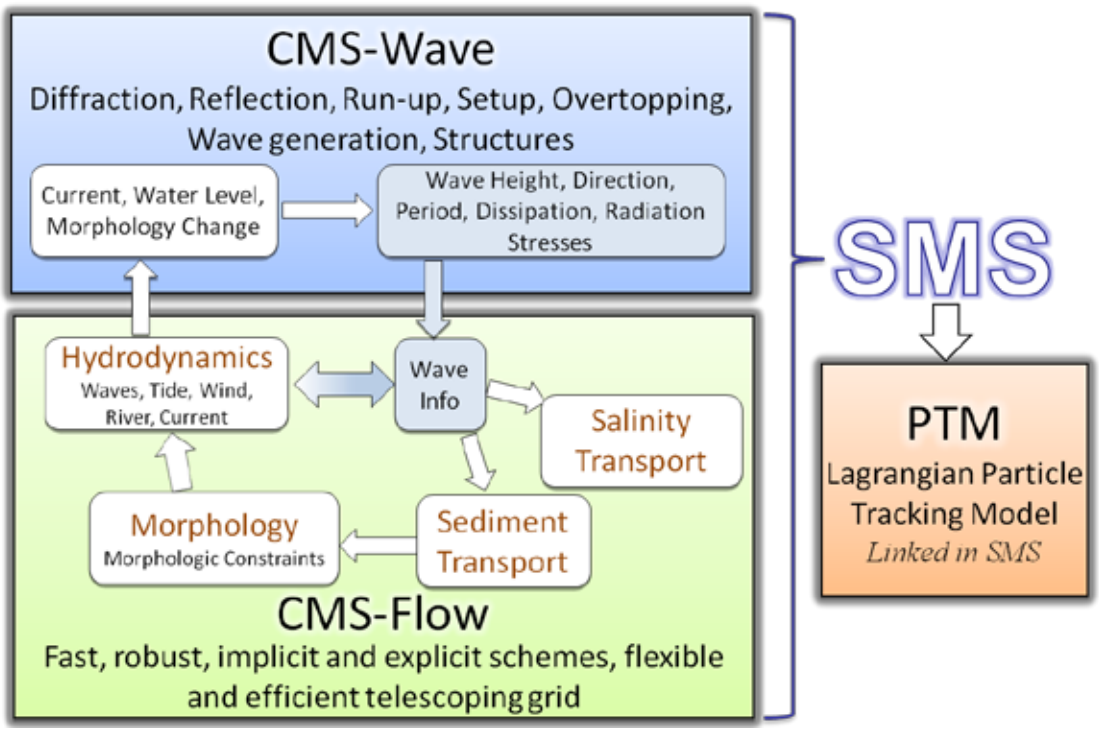

ERDC/CHL TR-11-10
December 2011

Verification and Validation of the Coastal Modeling System

Report 3, CMS-Flow: Hydrodynamics

Alejandro Sánchez, Weiming Wu, Tanya M. Beck, Honghai Li, James Rosati III, Robert Thomas, Julie Dean Rosati, Zeki Demirbilek, Mitchell Brown, and Christopher Reed

Coastal and Hydraulics Laboratory,
U.S. Army Engineer Research and Development Center
3909 Halls Ferry Road,
Vicksburg, MS 39180-6199

Report 3 of a series

Abstract: This is the third report, Report 3, in a series of four reports toward the Verification and Validation (V&V) of the Coastal Modeling System (CMS). The details of the V&V study specific to the hydrodynamic modeling are described in this report. The goal of this study was to perform a comprehensive assessment of the predictive skills of the CMS-Flow model for a wide range of problems encountered in coastal applications, with an emphasis on applications for coastal inlets and navigation projects. The evaluation study began by considering some simple and idealized test cases for checking the basic physics and computational algorithms implemented in the CMS-Flow model. After these fundamental comparisons, the model was evaluated with a large number of test cases representing idealized and real world problems. These application-oriented tests were selected carefully and only those which had data available from laboratory and field studies were considered. Included in this report are the descriptions of each test case, model setup, the boundary conditions used for each numerical simulation, and an assessment of the modeling results. Major findings and default parameters are provided as guidance to users for practical applications of CMS-Flow.

Contents

Figures and Tables

Figures

Tables

Preface

This study was performed by the Coastal Inlets Research Program (CIRP), funded by the Headquarters U.S. Army Corps of Engineers (HQUSACE). The CIRP is administered for Headquarters by the U.S. Army Engineer Research and Development Center (ERDC), Coastal and Hydraulics Laboratory (CHL), Vicksburg, MS, under the Navigation Program of the U.S. Army Corps of Engineers. James E. Walker is the HQUSACE Navigation Business Line Manager overseeing CIRP. Jeff Lillycrop, CHL, is the ERDC Technical Director for Navigation. Dr. Julie Rosati, CHL, is the CIRP Program Manager.

CIRP conducts applied research to improve USACE capabilities to manage federally maintained inlets and navigation channels, which are present on all coasts of the United States, including the Atlantic Ocean, Gulf of Mexico, Pacific Ocean, Great Lakes, and U.S. territories. The objectives of CIRP are to advance knowledge and provide quantitative predictive tools to (a) support management of federal coastal inlet navigation projects to facilitate more effective design, maintenance, and operation of channels and jetties, to reduce the cost of dredging, and (b) preserve the adjacent beaches and estuary in a systems approach that treats the inlet, beaches, and estuary as sediment-sharing components. To achieve these objectives, CIRP is organized in work units conducting research and development in hydrodynamics, sediment transport and morphology change modeling, navigation channels and adjacent beaches, navigation channels and estuaries, inlet structures and scour, laboratory and field investigations, and technology transfer.

For mission-specific requirements, CIRP has developed a finite-volume model based on nonlinear shallow-water wave equations, called the Coastal Modeling System CMS-Flow model, specifically for inlets, navigation, and nearshore project applications. The governing equations are solved using either explicit or implicit solvers in a finite-volume method on regular and refined (i.e., telescoping) Cartesian grids. The model is part of the CMS suite of models intended to simulate nearshore waves, flow, sediment transport, and morphology change affecting planning, design, maintenance, and reliability of federal navigation projects. In this assessment, verification and validation of CMS-Flow are performed to determine the capability and

versatility of the model for Corps projects. Validation of CMS-Flow is performed using real data collected from the field and laboratory to determine the accuracy of flow calculations.

Unless otherwise noted, the following are associated with ERDC-CHL, Vicksburg, MS. This report was prepared by Alejandro Sánchez and Zeki Demirbilek, Harbors Entrances and Structures Branch; Tanya Beck, James Rosati III, Dr. Honghai Li, Robert Thomas, and Mitchell Brown, Coastal Engineering Branch; Dr. Julie D. Rosati, Coastal Processes Branch; Dr. Weiming Wu, University of Mississippi; and Dr. Christopher Reed, Reed & Reed Consulting, Inc . The work described in the report was performed under the general administrative supervision of Dr. Jackie Pettway, Chief of Harbors Entrances and Structures Branch, Dr. Jeffrey Waters, Chief of Coastal Engineering Branch, Dr. Ty V. Wamsley, Chief of Coastal Processes Branch, Dr. Rose M. Kress, Chief of Navigation Division, and Bruce Ebersole, Chief of the Flood Control Division. Dr. Earl Hayter, Coastal Processes Branch, Dr. Joseph Letter, Estuarine Engineering Branch, and Dr. Jim Chen, Louisiana State University, reviewed the report, and Donnie F. Chandler, ERDC Editor, ITL, reviewed and format-edited the report. Jose Sanchez and Dr. William D. Martin were Deputy Director and Director of CHL, respectively, during the study and preparation of the report.

COL Kevin Wilson was ERDC Commander. Dr. Jeffery Holland was ERDC Director.

Unit Conversion Factors

Multiply	By	To Obtain
cubic yards	0.7645549	cubic meters
degrees (angle)	0.01745329	radians
feet	0.3048	meters
knots	0.5144444	meters per second
miles (nautical)	1,852	meters
miles (U.S. statute)	1,609.347	meters
miles per hour	0.44704	meters per second
pounds (force)	4.448222	newtons
pounds (force) per foot	14.59390	newtons per meter
pounds (force) per square foot	47.88026	pascals
square feet	0.09290304	square meters
square miles	2.589998 E+06	square meters
tons (force)	8,896.443	newtons
tons (force) per square foot	95.76052	kilopascals
yards	0.9144	meters

1 Introduction

1.1 Overview

The Coastal Modeling System (CMS) is an integrated numerical modeling system for simulating nearshore waves, currents, water levels, sediment transport, and morphology change (Militello et al. 2004; Buttolph et al. 2006a; Lin et al. 2008; Reed et al. 2011). The system is designed for coastal inlets and navigation applications including channel performance and sediment exchange between inlets and adjacent beaches. Modeling provides planners and engineers with essential information for improving the usage of USACE Operation and Maintenance Funds. The Coastal Inlets Research Program (CIRP) is developing, testing, improving, and transferring the CMS to Corps Districts and industry and assisting users in engineering studies. The overall framework of the CMS and its components are presented in Figure 1.

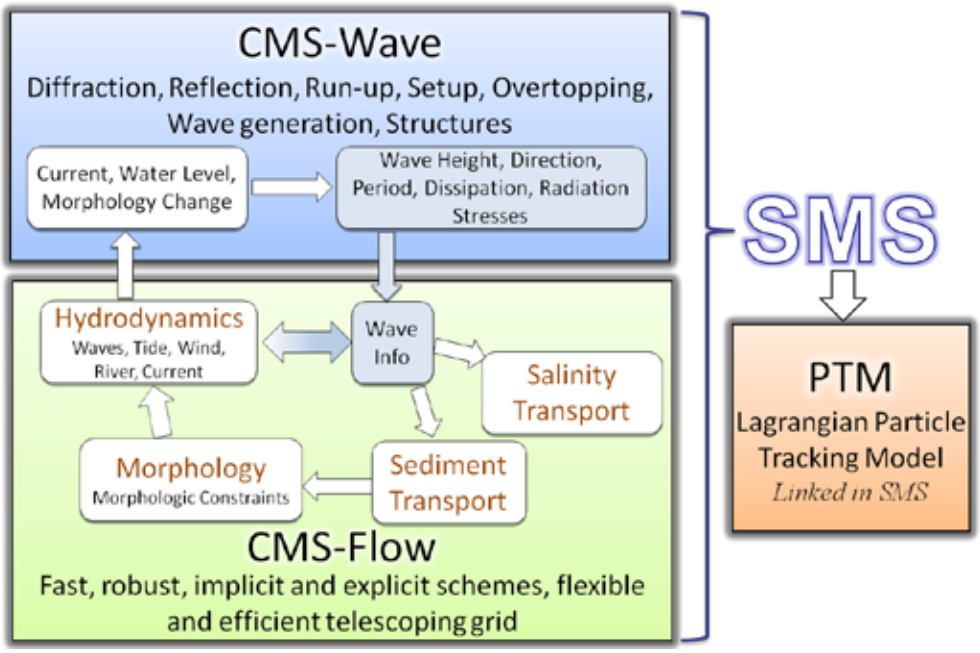

Figure 1. CMS framework and its components.

The CMS includes a flow model (CMS-Flow) which calculates hydrodynamics and sediment transport, and a wave model (CMS-Wave), all coupled together within the Surface-water Modeling System (SMS). The focus of this report, CMS-Flow, is a two-dimensional (2-D) depth-averaged nearshore circulation model. CMS-Flow calculates currents and water levels

including physical processes such as advection, turbulent mixing, combined wave-current bottom friction, wind, wave, river, tidal forcing, Coriolis force, and the influence of coastal structures (Buttolph et al. 2006a; Wu et al. 2011a, b). The implicit solver uses the SIMPLEC algorithm on a non-staggered grid to handle the coupling of water level and velocity. Primary variables u-, v-velocity, and water level are stored on the same set of grid points. Fluxes at cell faces are determined using a Rhie and Chow (1983) type momentum interpolation method (Wu et al. 2011a, b). The explicit solver uses a staggered grid with velocities at the cell faces and the water levels and water depths at the cell centers (Buttolph et al. 2006a). CMS-Flow also calculates salinity, sediment transport, and morphology change as discussed in a companion report (Sánchez et al. 2011). CMS-Wave is a spectral wave transformation model and solves the wave-action balance equation using a forward marching Finite Difference Method (Mase et al. 2005; Lin et al. 2008). CMS-Wave includes physical processes such as wave shoaling, refraction, diffraction, reflection, wave-current interaction, wave breaking, wind wave generation, white capping of waves, and the influence of coastal structures. The CMS takes advantage of the SMS interface (Zundel 2006) versions 8.2 through 11.1 for grid generation, model setup, plotting, and post-processing of modeling results. The SMS also provides a link between the CMS and the Lagrangian Particle Tracking Model (PTM) (MacDonald et al. 2006).

Typical applications of CMS-Flow include the analyses of navigation channel performance; wave, current, and wave-current interaction in channels and in the vicinity of navigation structures; and sediment management transport issues around coastal inlets and adjacent beaches. Some examples of CMS-Flow applications are: Batten and Kraus (2006), Buttolph et al. (2006b), Zarillo and Brehin (2007), Li et al. (2009), Li et al. (2011), Beck and Kraus (2010), Byrnes et al. (2010), Rosati et al. (2011), Reed and Lin (2011), Wang and Beck (2011), and Watts et al (2011).

1.2 Purpose of study

When a numerical model is developed, it should be verified and validated before it is applied in engineering practice. Verification is the process of determining the accuracy with which the governing equations of a specific model are being solved. It checks the numerical implementation of the governing equations. Validation is the process of determining the degree to which a model is an accurate representation of real world physics and processes from the perspective of the intended uses of the model. Another

important term in model application is calibration, which is the process of determining the unknown model parameters or variables that represent physical quantities. Almost all nearshore models for hydrodynamics, waves, and sediment transport have calibration parameters such as bottom friction and sediment transport scaling factors. Estimating appropriate values for these parameters based on the problem considered is still an active area of research. Many of the calibration parameters are due to simplification and parameterization of the physics. Even a well verified and validated model may still need to be calibrated for different practical problems.

This report documents details of the Verification and Validation (V&V) study conducted by CIRP to evaluate the hydrodynamic modeling capabilities of the CMS-Flow. The V&V study is divided into four separate reports:

1. Summary Report (Demirbilek and Rosati 2011),
2. CMS-Wave (Lin et al. 2011),
3. CMS-Flow: Hydrodynamics (present report), and
4. CMS-Flow: Sediment Transport and Morphology Change (Sánchez et al. 2011).

This is the third report, Report 3, in a series of four reports toward the Verification and Validation (V&V) of the Coastal Modeling System (CMS) that provides details of the V&V study specific to the hydrodynamic modeling. The details of the V&V protocol are described in Report 1 in this series. The CMS-Flow model hydrodynamic implementation is verified and validated using idealized, laboratory, and field test cases, and model performance is evaluated using several goodness-of-fit statistics described in Appendix A. The goal of this study was to perform a comprehensive assessment of the predictive skills of the CMS-Flow model for a wide range of problems encountered in coastal applications, with an emphasis on applications for coastal inlets and navigation projects. The evaluation study began by considering some simple and idealized test cases for checking the basic physics and computational algorithms implemented in the CMS-Flow model. After these fundamental comparisons, the model was evaluated with a large number of test cases representing idealized and real world problems. These application-oriented tests were selected carefully and only those which had data available from laboratory and field studies were considered. Included in this report are the descriptions of each test case, model setup, the boundary conditions used for each numerical simulation, and an

assessment of the modeling results. Major findings and default parameters are provided as guidance to users for practical applications of CMS-Flow. Future improvements are identified to enhance the model's features and computational capabilities. This Report 3 is the first documentation of hydrodynamic V&V of CMS-Flow, which will continue as the model advances and additional tests are conducted. A description of the present and future test cases will be posted to the CIRP website http://cirp.usace.army.mil/CMS.

1.3 CMS hydrodynamics

CMS-Flow calculates depth-averaged hydrodynamics by solving the conservative form of the shallow water equations using the Finite Volume Method on a regular or telescoping Cartesian mesh. The regular Cartesian mesh only allows a cell to have a maximum of four neighbors and has a fixed number of columns and rows, but may have a spatially variable grid resolution. When the grid resolution varies along either of the coordinates, the grid is referred to as a non-uniform Cartesian grid. The telescoping Cartesian grid allows a computational cell to have up to six neighbors and up to two on the same direction (e.g., North, South, East, and West). Telescoping grids are supported in SMS versions 11.0 and above. Presently, the SMS interface can only generate telescoping grids with a spatially constant cell aspect ratio and only supports isotropic grid refinement (one cell is split into four cells). These grids resemble quad-tree grids. However, the term quad-tree is avoided here because the data structure used is not a quad-tree and the numerical discretization is not limited to quad-tree grids. For both the regular and telescoping Cartesian grids, the inactive (permanently dry cells) portions of the grids are removed and variable information is stored in 1-D arrays with the cell connectivity specified by lookup tables in the same way as in an unstructured mesh. This approach reduces computational memory, allows for efficient vectorized computations, and provides a simple framework for anisotropic grid refinement (one cell is split into two cells).

An important aspect to any practical engineering hydrodynamic model is the boundary condition (BC) treatment and specification. CMS-Flow offers several types of BCs. For most coastal applications, the ocean boundary is assigned a water level time series from a measured station and applied along the whole boundary. This BC type is simply referred to as a Water Level BC. If water level measurements are not available, tidal constituents may be entered manually and applied on the whole ocean boundary (Tidal

Constituent BC). It is noted that in the implicit flow solver, the water level is applied as a source (forcing) term, and is not enforced strictly (clamped) which provides better stability and performance. In the explicit flow solver, the water level is clamped. For cases in which the ocean domain is relatively large and spatially variable water levels or velocities occur, water level and velocity (flux) BCs are available. The spatially variable water levels and velocities may be extracted from larger regional models such as ADCIRC (Luettich et al. 1992), CMS simulation, or from a tidal constituent database. When applying a Water Level BC to the nearshore, the wave-induced setup is not included and can lead to local flow reversals and boundary problems. In the explicit flow solver, this problem is avoided by implementing a Wave-adjusted Water Level BC (Reed and Militello 2005). In the implicit flow solver, a similar wave-adjusted BC is applied by solving the 1-D cross-shore momentum equation including wave and wind forcing (Wu et al. 2011a, b).

The hydrodynamics is coupled to sediment transport (also in CMS-Flow) and the wave model, CMS-Wave. Some important features and processes included are:

- Wetting and drying,
- Wave and surface roller stresses,
- Wave mass fluxes,
- Wave-enhanced bottom friction,
- Turbulent diffusion,
- Wall friction,
- Coriolis force,
- Spatially variable wind and atmospheric pressure, and
- Vegetation flow drag.

Both explicit and implicit time marching schemes are available. The explicit scheme is designed for highly transient flow and extreme wetting and drying problems which require small time steps. The implicit scheme is designed for tidal flow and long-term simulations where large time steps can be used on the order of 10 min. CMS versions 4.0 and higher have both CMS-Wave and CMS-Flow in a single executable (code) for faster and more efficient model coupling. The CMS is parallelized using OpenMP. Additional information about CMS-Flow is available from the CIRP website: http://cirp.usace.army.mil/CMS.

1.4 Study plan

Three Categories of data sources are used in this V&V study to evaluate the performance of CMS-Flow: analytical/empirical solutions (Category 1), laboratory studies (Category 2), and field experiments (Category 3). Test examples chosen include some known analytical solutions and idealized problems, laboratory studies with data, and field studies with data. Many test cases not included in this V&V report are being researched and these will be documented in future companion reports.

1.5 Report organization

This report is organized in five chapters. Chapter 1 presents the motivation, definitions, and an overview of the CMS-Flow V&V study. Chapter 2 discusses Verification of CMS-Flow with analytical solutions and idealized cases (Category 1). Chapters 3 and 4 present Validation of CMS-Flow with comparison of model calculations to laboratory (Category 2) and field (Category 3) data, respectively. In Chapters 2-4, test cases are identified by Category "C" and Example number "Ex" as C1-Ex1, etc. Chapter 5 summarizes the study and discusses future work. Appendix A provides a description of the goodness-of-fit statistics applied herein.

2 Analytical Solutions and Idealized Examples

2.1 Overview

The analytical and idealized test cases described in this chapter were selected for verification of CMS-Flow to confirm that the intended numerical algorithms have been correctly implemented. These cases have an ID, the first two characters identifies Category number, followed by a dash and the Example number under the Category. For example, test case C1-Ex1 refers to Category 1 - Example 1. This notation is used henceforth in this report. Four goodness-of-fit statistics are used to assess the model performance and are defined in Appendix A. The Category 1 V&V test cases completed are listed below. Additional cases are under investigation and will be included in future reports. Category 1 tests cases completed are:

1. Wind setup in a flat basin,
2. Wind-driven flow in a circular basin,
3. Tidal propagation in a quarter annulus,
4. Transcritical flow over a bump, and
5. Long-wave runup over a frictionless slope.

2.2 Test C1-Ex1: Wind setup in a flat basin

2.2.1 Purpose

This verification test is designed to test the most basic model capabilities by solving the most reduced or simplified form of the governing equations in which only the water level gradient balances the wind surface drag. The specific model features to be tested are

1. Spatially constant wind fields,
2. Water surface gradient implementation, and
3. Land-water boundary condition.

2.2.2 Problem and analytical solution

Assuming a closed basin with a spatially constant, steady state wind in one direction, and no advection, diffusion, bottom friction, waves, or Coriolis force, the momentum equations reduce to

$$\rho g h \frac{\partial \eta}{\partial y} = \rho_a C_d |W| W \tag{1}$$

where $h = \zeta + \eta$ is the total water depth, ζ is the still water depth, η is the water surface elevation (water level) with respect to the still water level, C_d is the wind drag coefficient, y is the coordinate in the direction of the wind, g is the gravitational acceleration, ρ is the water density, ρ_a is the air density, and W is the wind speed. Assuming a constant wind drag coefficient, the following analytical expression for the water level may be obtained by integrating the above equation (Dean and Dalrymple 1984)

$$\eta = \sqrt{\frac{2\rho_a C_d |W| W}{\rho g}(y + C) + \zeta^2} - \zeta \tag{2}$$

where C is a constant of integration.

2.2.3 Model setup

A computational grid with constant water depth of 5 m and irregular boundaries is used to verify the numerical methods. The computational grid has 60 columns and 70 rows and a constant resolution of 500 m. The irregular geometry is used intentionally to check for any discontinuities in processes near the land-water boundaries. The solution should be perfectly symmetric and independent of the geometry of the closed basin. The steady state solution is reached by increasing the wind speed over a 3-hr ramp period and by allowing the solution to reach steady state over a 48-hr time period. During the ramp period, all model forcing is increased slowly from the initial condition (not necessarily zero), to the specified boundary condition time series. The purpose of the ramp period is to allow the model to adjust slowly to the forcing conditions without "shocking" it with a step function. In CMS, a cosine ramp function of the form $f_R = 0.5 - 0.5 \cos[\min(t, T_R)/T_R]$ is used, where t is time and T_R is the ramp period duration. Table 1 summarizes the model setup for this case.

Table 1. CMS-Flow settings for the wind setup test case.

Parameter	Value
Solution scheme	Implicit
Time step	10 min
Simulation duration	48 hr
Ramp period duration	3 hr
Wind speed	10 m/sec
Drag coefficient	0.0016
Advection terms	Off
Mixing terms	Off
Bottom friction	Off
Wall friction	Off
Coriolis force	Off

The model is initialized from zero current velocities and water levels. The simulation is then allowed to reach steady state over 48 hr.

2.2.4 Results and discussion

The calculated wind setup (water surface elevation) is shown in Figure 2 for the case of wind from the north (left) and from west (right). For both cases, the calculated wind setup is symmetric and has straight contour lines, which is consistent with the analytical solution. Figure 3 shows the wind setup along the center line of the domain for the case with wind from the north compared to the analytical solution. The goodness-of-fit statistics along this transect include the Normalized Root Mean Square Error (NRMSE), Normalized Mean Absolute Error (NMAE), squared correlation coefficient (R^2), and Bias as given in Table 2.

2.2.5 Conclusions and recommendations

The steady wind set up in a closed basin with flat bed and irregular geometry was simulated and the model performance was measured using several goodness-of-fit statistics. The model calculated the water level accurately from wind setup with NRMSE of 0.01 percent, a NMAE of 0.02 percent, and R^2 of 0.999. The test case demonstrated the model capability in simulating wind induced setup and verifies the implementation of both the wind driving force and water surface elevation terms.

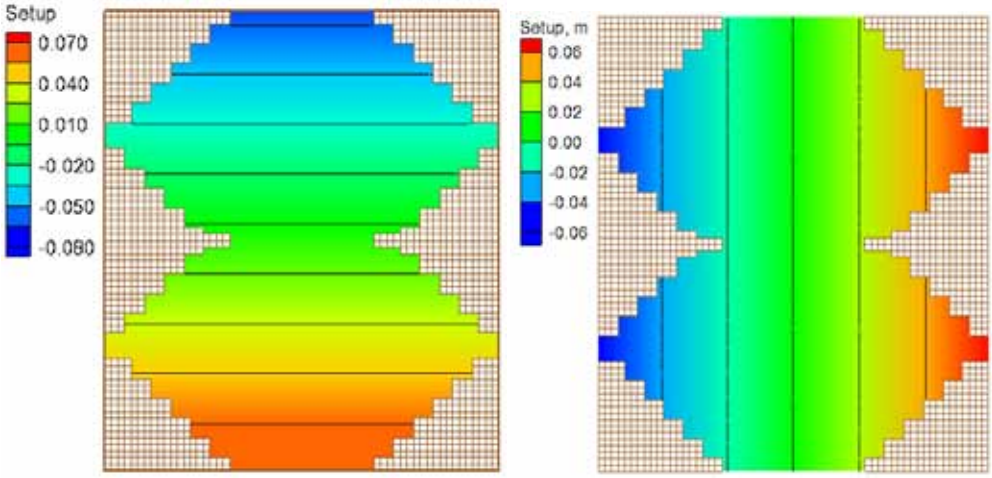

Figure 2. Calculated water levels in an irregular domain with a flat bed for the cases of wind from the north (left) and from the west (right).

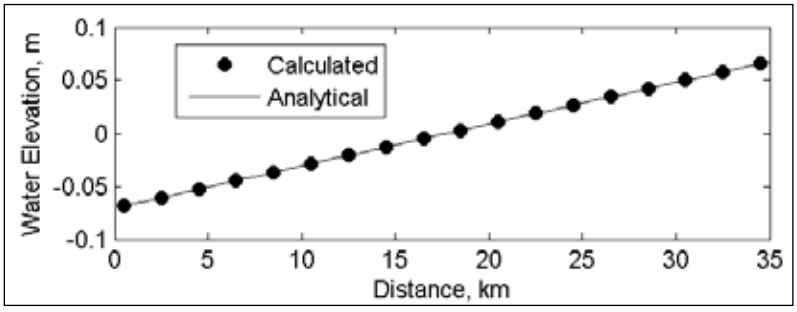

Figure 3. Analytical and calculated water level along the vertical centerline of an irregular basin with flat bed and winds from the south. The calculated results are shown on every 10th grid point for better visualization.

Table 2. Water level goodness-of-fit statistics* for in the idealized wind setup test case.

Statistic	Value
NRMSE, %	0.01
NMAE, %	0.02
R^2	0.999
Bias, m	0.000

*defined in Appendix A

2.3 Test C1-Ex2: Wind-driven flow in a circular basin

2.3.1 Purpose

The purpose of this test is to verify the steady state linear hydrodynamics when forced by spatially variable winds, a linear bottom friction, and with

and without Coriolis force. Specific model features evaluated in this problem are spatially variable winds and Coriolis force.

2.3.2 Problem

Assuming steady state conditions and no advection, diffusion, waves, or spatial gradients in atmospheric pressure, the governing equations reduce to

$$\frac{\partial(hU_j)}{\partial x_j} = 0 \tag{3}$$

$$-\varepsilon_{ij} f_c h U_j = -gh\frac{\partial \eta}{\partial x \rho} + \frac{1}{}\left(\tau_i^s - \tau_i^b\right) \tag{4}$$

where ε_{ij} is the permutation operator equal to 1 for *i, j*=1, 2; -1 for *i, j*=2, 1; and 0 for *i=j*, f_c is the Coriolis parameter, U_j is the depth-averaged current velocity in the j^{th} direction, τ_i^s is the wind driving force per unit water surface area, and τ_i^b is the bottom friction. The problem is further simplified by assuming a flat bed and deep water conditions, $h\eta >$, so that h may be considered constant. A linear bottom friction is specified as $\tau_i^b = \rho\kappa h U_i$ where κ is a linear bottom friction coefficient. The wind stress is given by $\tau_i^s = \varepsilon_{i2} x_j W / R$, where W is the gradient or slope of the wind speed and R is the radius of the circular basin.

2.3.3 Analytical solution

Dupont (2001) presented the analytical solution to the problem above. The water surface elevation is given by

$$\eta = \begin{cases} \dfrac{W x_1 x_2}{2ghR} & \text{for } f_c = 0 \\ \dfrac{W f_c}{Rgh\kappa}\left[\dfrac{R^2}{8} + \dfrac{1}{4}\left(\dfrac{2\kappa x_1 x_2}{f_c} - x_1^2 - x_2^2\right)\right] & \text{for } f_c \neq 0 \end{cases} \tag{4}$$

The current velocities are independent of the Coriolis coefficient and are given by

$$U_i = \frac{\varepsilon_{ij} x_j W}{2Rh\kappa} \tag{5}$$

2.3.4 Model setup

The computational grid, shown in Figure 4, has five levels of refinement from 2 km to 125 m and a total of 15,272 computational cells.

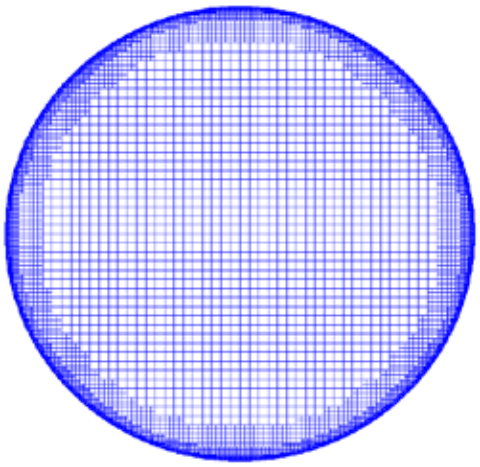

Figure 4. CMS-Flow computational grid used for the wind-driven flow in a circular basin.

The CMS model is run to steady state from zero current and water level as initial conditions. The relevant model parameters are summarized in Table 3. Two cases are run: one with Coriolis and one without.

Table 3. CMS-Flow setup for the circular basin test case.

Parameter	Value
Time step	1 hr
Simulation duration	72 hr
Ramp period duration	24 hr
Water depth	100 m
Mixing terms	Off
Wall friction	Off
Linear bottom friction coefficient	0.001
Coriolis	0.0, 0.0001 rad/sec
Wind gradient	0.0001 m^2/sec^2

2.3.5 Results and discussion

2.3.5.1 Without Coriolis force

A comparison of the calculated and analytical current velocities and water levels in the case without Coriolis force are shown in Figure 5. The

goodness-of-fit statistics for the velocity components and water level are shown in Table 4. The calculated water level shows excellent agreement with the analytical solution, even along the outer boundary, and is demonstrated by the NMAE of 0.02 percent. The current velocities agree well with the analytical solution. The largest errors for the current velocities occur near the outer boundary due to the staircase representation of the curved boundary. The error is reduced by increasing the refinement at the boundary.

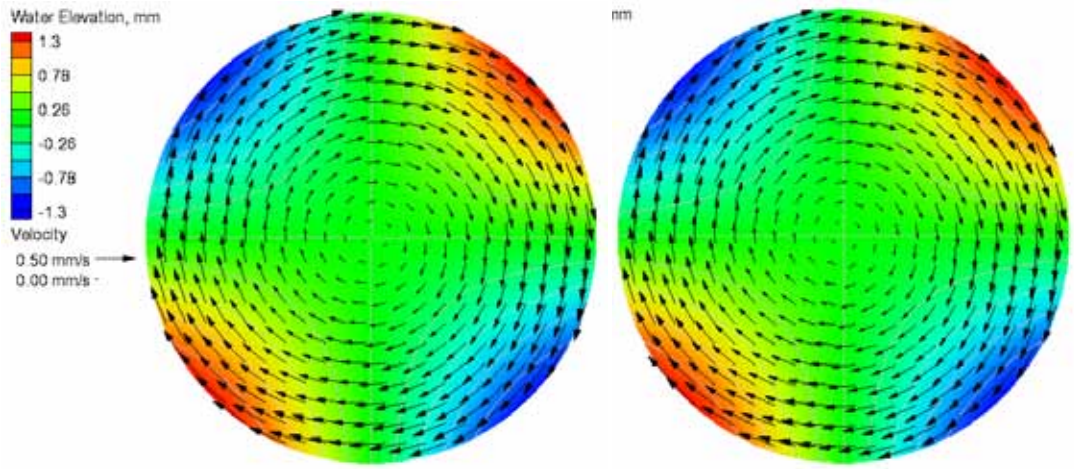

Figure 5. Analytical (left) and calculated (right) current velocities and water levels without Coriolis force.

Table 4. Water level and current velocity goodness-of-fit statistics* for the circular basin test case without Coriolis force.

Variable	NRMSE, %	NMAE, %	R^2	Bias
U-velocity	1.88	0.30	0.999	-4.5e-7 m/sec
V-velocity	2.51	0.37	0.998	9.7e-9 m/sec
Water level	0.03	0.02	0.999	3.14e-8 m

*defined in Appendix A

2.3.5.2 *With Coriolis force*

A comparison of the calculated and analytical solutions of current velocities and water levels for the case with Coriolis force is shown in Figure 6. The goodness-of-fit statistics for the velocity components and water level are shown in Table 5. Similar to the case without Coriolis force, agreement between the calculated water elevation and current velocity and the analytical solutions resulted in a NRMSE of 0.03 percent for water level and 2.53 percent for current velocities. The largest errors in current velocity occur adjacent to the outer boundary where the curved boundary exists. A

positive Coriolis parameter corresponds to the northern hemisphere where ocean currents are deflected to the right. For this case, the Coriolis force has the net effect of pushing water towards the center of the circular basin creating higher water levels and lower water levels around the perimeter. From Equation (4), it can be seen that the water level η at the basin center ($x_1 = x_2 =$ 0 m), is equal to $Wf_cR/(8gh)$ for $f_c \neq$ 0 sec^{-1}, and equal to 0 m for $f_c =$ 0 sec^{-1}.

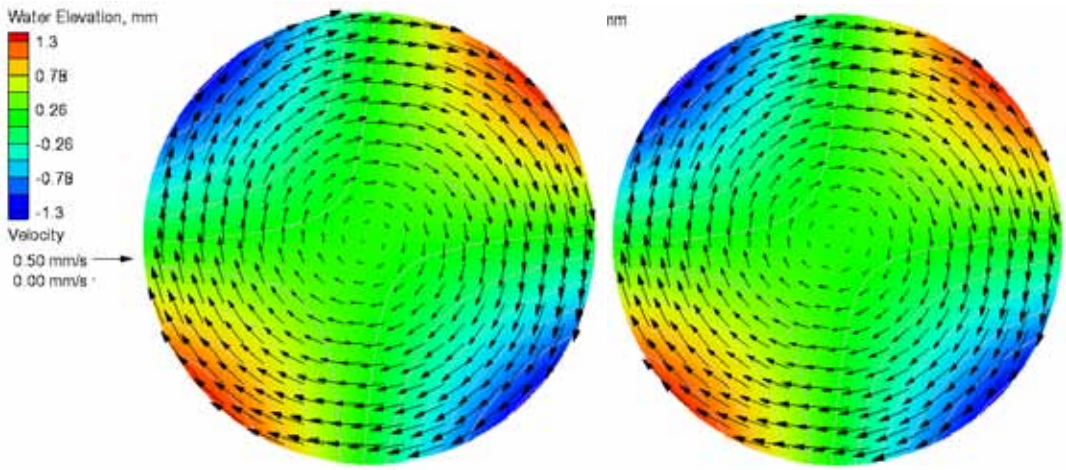

Figure 6. Analytical (left) and calculated (right) current velocities and water levels with Coriolis force.

Table 5. Water level and current velocity goodness-of-fit statistics* for the circular basin test case with Coriolis.

Variable	NRMSE, %	NMAE, %	R^2	Bias
U-Velocity	1.90	0.30	0.999	-4.5e-7 m/sec
V-Velocity	2.51	0.37	0.998	4.6e-9 m/sec
Water level	0.03	0.02	0.999	9.5e-8 m

*defined in Appendix A

2.3.6 Conclusions and recommendations

The analytical solution for the steady-state wind-induced linear hydrodynamics in a closed circular basin was simulated. Computed water levels were accurate within 0.03 percent NRMSE, and showed little influence from the staircase representation of the curved outer boundary. Current velocities were less accurate with a NRMSE of 2.53 percent due to errors near the outer boundary.

For most coastal applications open boundaries are represented by straight boundaries so the staircase boundary does not exist. Curved boundaries occur usually along the wet-dry interface in very shallow water where the current velocities are small, due usually to the increased bottom friction. However, if the curved boundary occurs in deep water or in areas where the current velocities are strong, errors will be incurred due to the staircase representation of the boundary. Nevertheless, the errors may be reduced by increasing the grid refinement along the specific boundary. In the future, this problem can be eliminated by implementing a boundary fitting method, such as a cut-cell or embedded boundary, or quadrilateral mesh.

2.4 Test C1-Ex3: Tidal propagation in a quarter annulus

2.4.1 Purpose

The purpose of this verification test is to assess the model performance in simulating long wave propagation. The case is useful for testing the model performance and symmetry for a non-rectangular domain with a tidal forcing specified on one of the curved boundaries. Because there is no bottom friction or mixing, the test case is also useful for looking at numerical dissipation.

2.4.2 Problem

Lynch and Gray (1978) presented the analytical solution for depth-averaged long-wave propagation in an annular domain. The case was for a linearly sloping bed, and without bottom friction, Coriolis force, or horizontal mixing. The offshore boundary consisted of a single tidal constituent (see Figure 7). Table 6 summarizes the important model settings used for this test.

2.4.3 Model setup

The computational grid (Figure 8) consists of a three-level telescoping Cartesian grid with resolution of 4, 2, and 1 km for the three levels. Higher resolution is specified near the inner and outer boundaries to reduce errors associated with the representation of the curved boundaries with squares. The grid has 1,160 active ocean cells. Model settings are shown in Table 7.

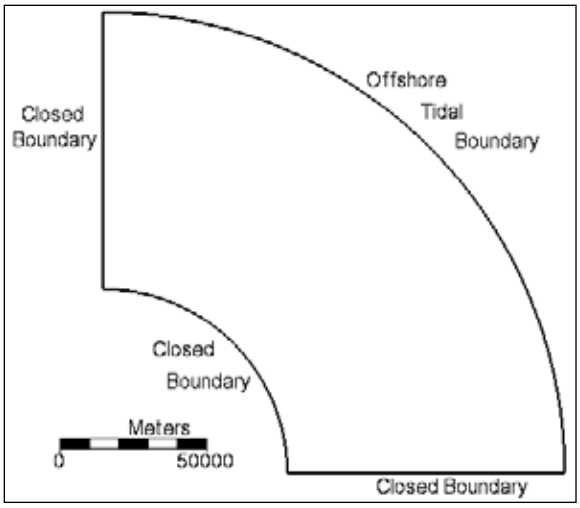

Figure 7. Computational domain for tidal propagation in a quarter annulus.

Table 6. Quarter annulus setup parameters.

Parameter	Value
Deepwater tidal amplitude	0.3048 m
Tidal period (M2 tide)	12.42 hr
Inner radius	60.96 km
Outer radius	152.4 km
Inner water depth	10.02 m
Outer water depth	25.05 m
Bathymetry profile	Linear
Bottom friction	None
Mixing terms	Off
Coriolis force	Off

2.4.4 Results and discussion

Figure 9 shows a time series of water levels at the inner edge of the simulation domain. The goodness-of-fit statistics are listed in Table 8. The model accurately predicts the wave phase but slightly overestimates the amplitude by approximately 0.01 m. No significant numerical dissipation is observed or numerical instability. The simulation takes about 1 min on a Windows PC on a single 2.67 GHz processor.

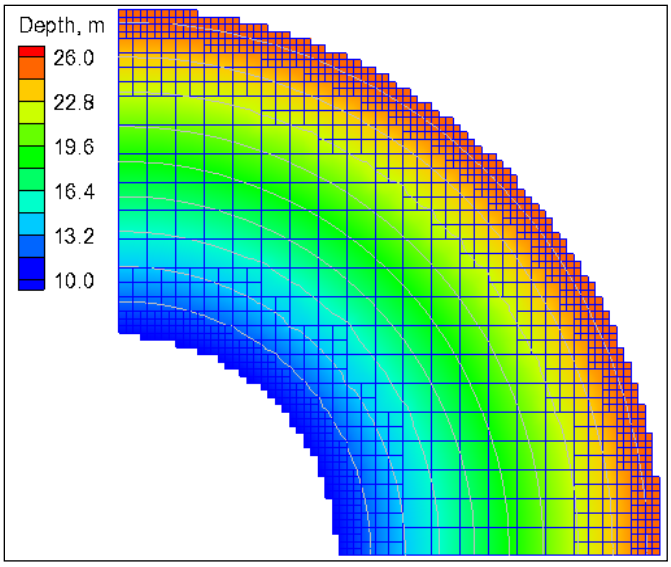

Figure 8. Computation grid used for tidal propagation in a quarter annulus.

Table 7. CMS-Flow setup parameters for the quarter annulus test case.

Parameter	Value
Solution scheme	Implicit
Time step	10 min
Simulation duration	120 hr
Ramp duration	24 hr
Mixing terms	Off
Advection terms	Off
Wall friction	Off
Coriolis force	Off

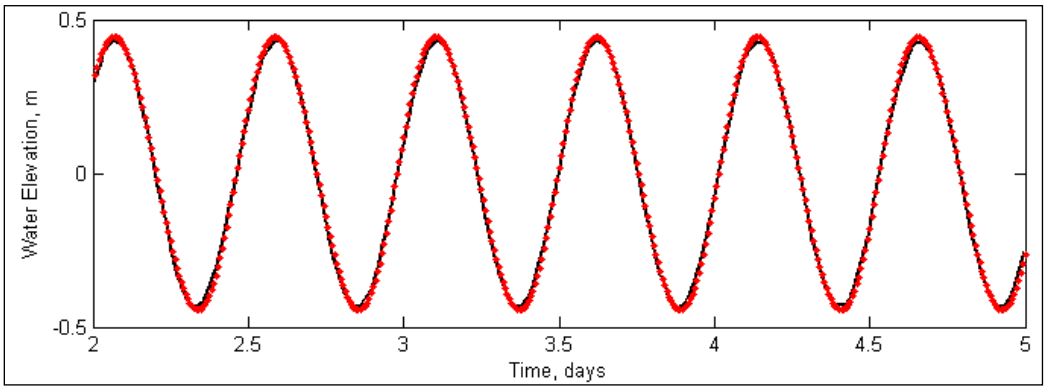

Figure 9. Comparison of analytical (solid black) and calculated (red dots) water surface elevations at the center of the inner radius.

Table 8. Water level goodness-of-fit statistics for the quarter annulus test case.

Statistic	Value
NRMSE, %	3.3
NMAE, %	2.7
R^2	0.999
Bias, m	0.002 m

An example of the simulated water level and current velocity magnitude fields is shown in Figure 10. The water level contours are very smooth and do not show any significant instability. However, the current magnitude shows some errors at the offshore boundary. This is due to staircase representation of the curved open boundary. This problem would be fixed by specifying the analytical current velocities at the offshore boundary, but it was not done in this example. Sensitivity tests with smaller time steps showed that the problem persists for smaller time steps. For practical applications all model forcing is specified on straight boundaries and this problem does not occur as demonstrated in subsequent test cases.

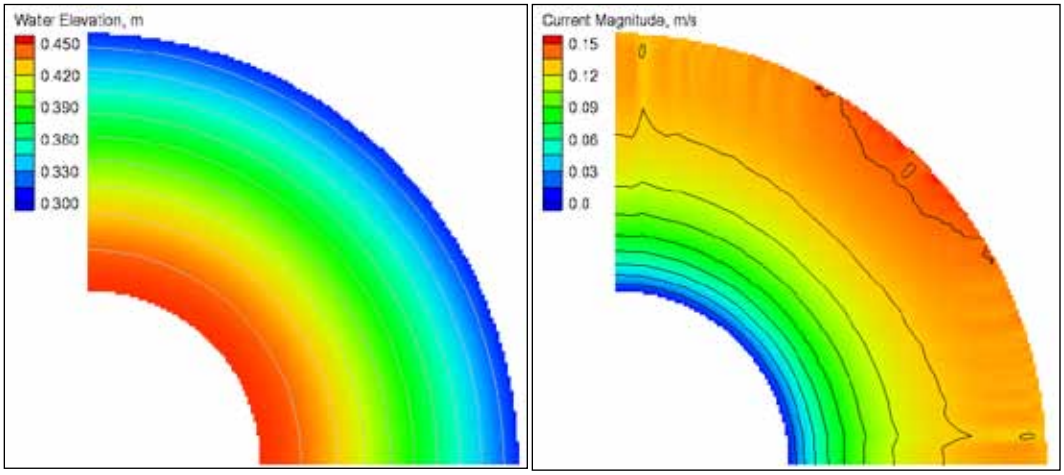

Figure 10. Snap shot of water levels at 62 hr (left) and current magnitude at 65.5 hr (right).

2.4.5 Conclusions and recommendations

The CMS-Flow can accurately simulate linear long-wave propagation in a quarter annulus with a linear bed, zero bottom friction, and Coriolis. The water level NRMSE, NMAE, and R^2 were 3.3 percent, 2.7 percent, and 0.999, respectively. For practical applications, water level conditions on straight boundaries should be specified. If a curved forcing boundary is

necessary, then it is recommended to specify both water levels and current velocities.

2.5 Test C1-Ex4: Transcritical flow over a bump

2.5.1 Purpose

This test case is used to assess the model performance in simulation of flow with mixed subcritical and supercritical regimes. Due to a steep change in bed elevation, the flow changes from subcritical to supercritical and back to subcritical. Because the bottom friction is not considered, an analytical solution is available for testing the water level calculations.

2.5.2 Problem

The one-dimensional problem (Caleffi et al. 2003) has a bed elevation given by

$$z_b = \begin{cases} 0, & \text{for } x < 8 \\ 0.2 - 0.05(x-10)^2, & \text{for } 8 \le x < 12 \\ 0, & \text{for } 12 \le x \end{cases} \quad (6)$$

where z_b is the bed elevation with respect to the still water level, and x is the horizontal distance. A constant flux boundary is specified at x = 0 m and a constant water level boundary is specified at x = 12 m. The bed is frictionless. Table 9 shows a summary of the important hydrodynamic parameters for this case.

Table 9. Hydrodynamic parameters for the test case of flow over a bump.

Parameter	Value
Flow discharge	0.18 m^3/sec
Downstream water depth	0.33 m
Bottom Friction	None

2.5.3 Model setup

The implicit CMS-Flow was applied with a computational domain of 25 m × 0.3 m, and a constant grid spacing of 0.1 m (see Figure 11). A flux boundary condition was specified at the upstream boundary and a constant water level boundary condition was applied to the downstream boundary. The

model was ramped from zero current velocity and a constant water level of 0.33 m over a period of 2.75 hr. For the implicit flow solver, an adaptive time step between 0.0781 to 20 sec was applied. Table 10 summarizes the CMS setup. For the explicit flow solver, a constant time step of 0.01 sec was applied. The computational times for the implicit and explicit solvers on a single 2.67 GHz processor were approximately 45 and 3.5 min, respectively.

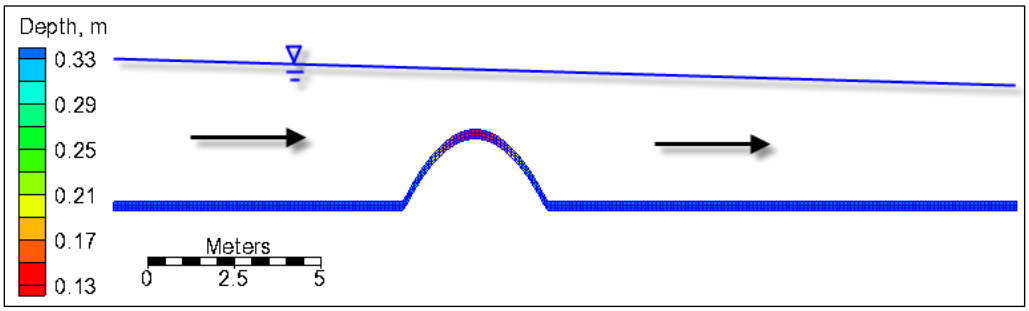

Figure 11. CMS-Flow computational grid for the flow over a bump test case.

Table 10. CMS-Flow setup parameters for the flow over a bump test case.

Parameter	Value
Solution scheme	Implicit, Explicit
Time step	Implicit: 0.0781-20 sec, Explicit: 0.015 sec
Simulation duration	3 hr
Ramp duration	2.75 hr
Wall friction	Off
Manning's coefficient	0.0 sec/m$^{1/3}$

2.5.4 Results and discussion

A comparison between the analytical and numerical solutions of water level is shown in Figure 12. The goodness-of-fit statistics summarized in Table 11 indicate that the mean calculated error is less than 3 percent and the squared correlation coefficient R^2 is 0.991. Both the implicit and explicit schemes produce accurate results with NMAE values equal to 1.28 percent and 1.30 percent, respectively. The location of the hydraulic jump is captured well with both the implicit and explicit schemes. In the case of the implicit scheme, the water level downstream of the bump is slightly underpredicted and demonstrates a slight negative bias shown in Table 11. The explicit scheme slightly overestimates the water level immediately downstream of the hydraulic jump and also slightly underestimates the water levels upstream of the bump. The overall bias of the explicit scheme

water levels is negative. It is noted that, although the implicit solution scheme is not designed or intended for flows with sharp discontinuities, the CMS has the capability to produce accurate results.

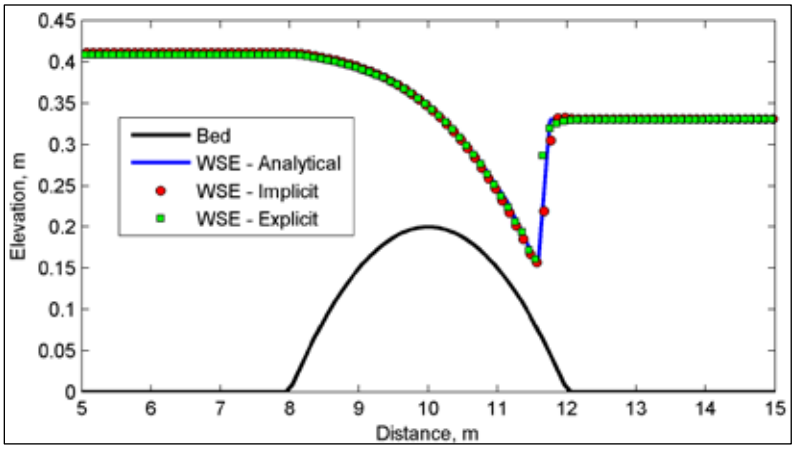

Figure 12. Comparison of analytical and calculated water surface elevations for the flow over a bump test case. The bed elevation is also shown for reference.

Table 11. Water level goodness-of-fit statistics* for the flow over a bump test case.

Statistic	Implicit	Explicit
NRMSE, %	2.86	3.31
NMAE, %	1.28	1.30
R2	0.991	0.991
Bias, m	0.0003	-0.0017

*defined in Appendix A

2.5.5 Conclusions and recommendations

Comparison of CMS-Flow to the analytical solution of flow over a bump verified that the calculated results are accurate for transcritical flows with sharp discontinuities. Both the implicit and explicit flow solvers produced similar results. The adaptive time step of the implicit solver increased the model efficiency and reduced the computational time. However, using the implicit solution scheme is not recommended for practical applications in which the physics require small time steps due to sharp discontinuities in the flow and/or extensive wetting and drying because the implicit solver will not be significantly more efficient than an explicit solver.

2.6 Test C1-Ex5: Long-wave runup over a frictionless slope

2.6.1 Purpose

The performance of the CMS-Flow in calculation of nonlinear long-wave runup over a frictionless planar slope is assessed by comparing the computed water levels and shoreline position with an analytical solution presented by Carrier et al. (2003).

2.6.2 Initial condition

The bed has a constant slope of 1:10 with the initial shoreline located at x = 0 m. Figure 13 shows that the initial water level is given by a leading depression N-wave (characteristic of the waves caused by submarine landslides). The initial current velocity is equal to zero everywhere.

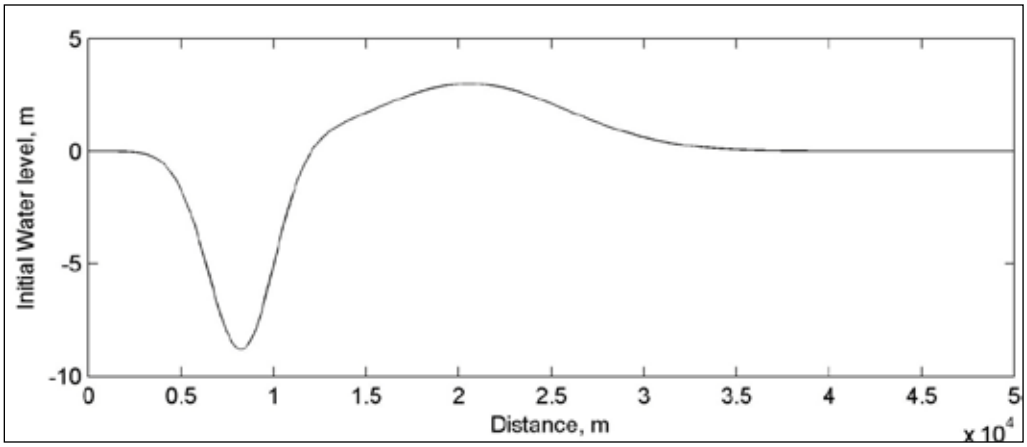

Figure 13 Initial water level profile for the long-wave runup test case.

2.6.3 Model setup

The computational grid has variable grid resolution of 3 m for x<300 m and increases to 10 m offshore with an aspect ratio of 1.05. The general model parameters used in the simulation are shown in Table 12. A relatively small time step of 0.1 sec is required due to the moving boundary. In CMS, the computational grid is fixed and the moving wetting and drying boundary is treated as an internal boundary. In CMS, cells are judged as wet or dry (no partial wet or dry cells) based on a threshold wetting/drying depth, and the interface between wet and dry cells is treated as a closed internal boundary with wall friction.

Table 12. Model parameters for the long-wave runup test case.

Parameter	Value
Solution scheme	Implicit
Time step	0.1 sec
Simulation duration	360 sec
Ramp duration	0.0 sec
Wetting/drying depth	0.01 m
Wall friction	Off
Mixing terms	Off
Bottom friction	Off

2.6.4 Results and discussion

Figure 14 shows a comparison of computed and analytical water surface elevations near the shoreline at four different elapsed times for the first 1,200 m from the initial shoreline position. The water level variation is characterized by a leading depression wave followed by a runup event. The model performance is generally good as demonstrated by the goodness-of-fit statistics shown in Table 13.

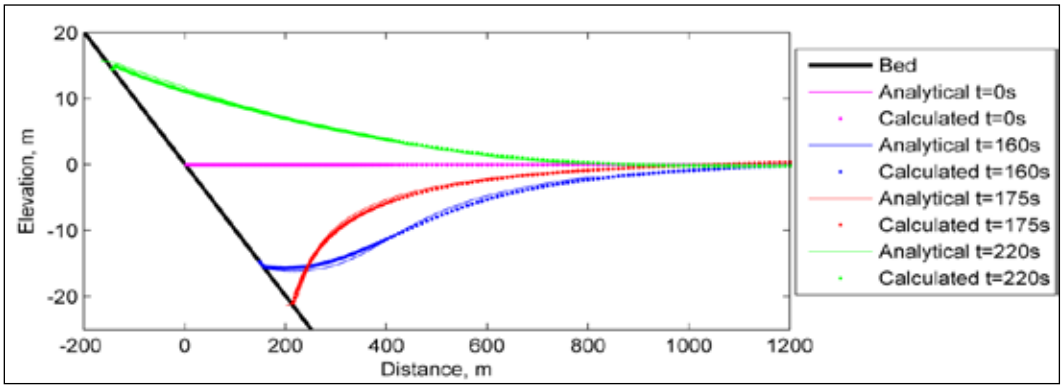

Figure 14. Comparison of analytical and calculated water levels at different elapsed times for the long-wave runup test case.

Table 13. Water level goodness-of-fit statistics* for the long-wave runup test case.

Time, s	NRMSE, %	NMAE, %	R^2	Bias, m
160	3.7	3.8	0.999	-0.012
175	6.5	5.9	0.997	-0.113
220	4.6	5.4	0.999	-0.066

*defined in Appendix A

A comparison of the numerical and analytical solutions for the shoreline position is shown in Figure 15. The water shoreline position of the leading depression wave is well captured including the peak shoreline position. However the shoreline position during the inundation or advancement of the first wave is slightly underpredicted. This is due to the small instability which is shown at 220 sec near the shoreline position in Figure 15. The small instability is formed during the up rush of water but does not grow significantly and does not cause significant error in the computed water levels. Further tests can be done in the future to investigate if the instability can be reduced by reducing the grid spacing or time step. Once the first wave begins to recede, the calculated shoreline position again agrees well with the analytical solution.

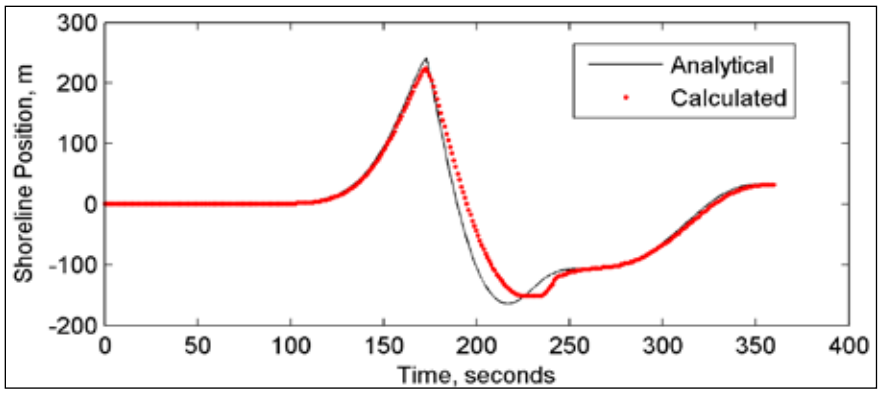

Figure 15. Time series comparison of calculated and analytical shoreline positions for the long-wave runup test case.

It is noted that for practical field applications, the bottom is not frictionless or inviscid, which will improve the model stability. In general, the CMS model's wetting and drying performance is considered satisfactory for the purposes of the model. The implicit solution scheme is designed for practical applications of tidal flow and wind- and wave-induced currents. This verification test provides a good case for testing the nonlinear hydrodynamics and wetting and drying algorithm.

2.6.5 Conclusions and recommendations

The CMS-Flow performance in simulating nonlinear hydrodynamics is tested using the analytical solution for long-wave runup over a planar frictionless slope presented by Carrier et al. (2003). Comparison of computed and analytical water levels and shoreline positions indicate good model performance as demonstrated by the goodness-of-fit statistics. The wetting and drying algorithm was found to be robust and led to an accurate prediction of the shoreline position.

3 Laboratory Studies

3.1 Overview

The test cases presented in this Chapter are the Category 2 type of problems. These laboratory cases provide experimental data from physical models and are useful for determining appropriate ranges for calibration parameters as well as validation. The Category 2 V&V test cases completed are listed below. Remaining cases are under investigation and will be included in future reports. Category 2 tests cases completed are:

1. Rectangular flume with a spur dike
2. Rectangular flume with a sudden expansion
3. Planar sloping beach with oblique incident regular waves
4. Idealized jettied inlet with equilibrium beach profile and oblique incident regular waves

3.2 Test C2-Ex1: Steady flow in a rectangular flume with a spur dike

3.2.1 Purpose

The CMS is applied to an experimental case of steady flow in a flume with a spur dike. The CMS performance is assessed by comparing the measured and calculated current velocities behind the spur dike. The specific model features tested are the non-uniform Cartesian grid, inflow flux boundary condition, outflow water level boundary condition, wall boundary condition and subgrid eddy viscosity (turbulence) model (Smagorinsky 1963).

3.2.2 Experiment setup

The laboratory flume experiment of Rajaratnam and Nwachukwu (1983) investigated a steady flow in a 37-m long, 0.92-m-widerectangular flume with a thin plate 0.1524-m long used to simulate a groin-like structure. Here, the numerical model is compared to the experimental run A1. In this case, the flow discharge and water depth were 0.0453 m^3/sec and 0.189 m, respectively. A summary of the hydrodynamic parameters is provided in Table 14.

Table 14. Hydrodynamic parameters for the spur-dike case.

Parameter	Value
Flow discharge	0.0453 m^3/sec
Water depth	0.189 m

3.2.3 Model setup

The computational grid consists of 152 x 36 nodes in the longitudinal and lateral directions and has a variable grid resolution of 0.01 to 0.05 m (see Figure 16). The mesh was refined near the structure and near the walls within the recirculation zone behind the structure. A constant flux (flow discharge) at the inflow boundary and a constant water depth at the outflow boundary was specified. A summary of the important model parameters for CMS-Flow is shown in Table 15.

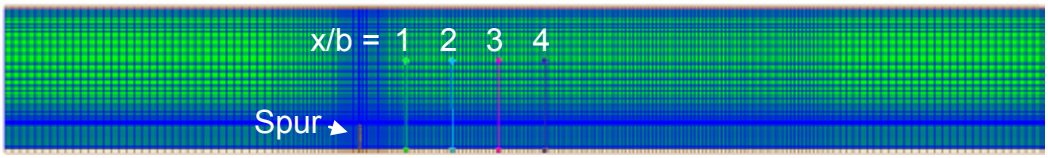

Figure 16. CMS-Flow computational grid for the spur-dike case. Colored lines represent the location of where calculated current velocities in the x-direction were extracted and compared to measurements (see Figure 17).

Table 15. CMS-Flow set up parameters for the spur-dike test case.

Parameter	Value
Solution scheme	Implicit
Time step	1 min
Simulation duration	3 hr
Ramp duration	2.5 hr
Manning's coefficient	0.02 sec/$m^{1/3}$
Wall friction	On
Turbulence model	Subgrid

3.2.4 Results and discussion

Steady-state depth-averaged velocities were interpolated using the SMS 10.1 interface along the four cross-sections located downstream of the spur dike and are indicated by vertical colored lines (observation arcs) in Figure 16. Velocity measurements were collected at several locations along these cross-sections and at two elevations above the bed. Here, the

measured velocities at 0.85 times the water depth are compared with the calculated depth-averaged velocities in Figure 17 and the corresponding goodness-of-fit statistics are presented in Table 16. The computed steady state water levels and current velocities are shown in Figure 18.

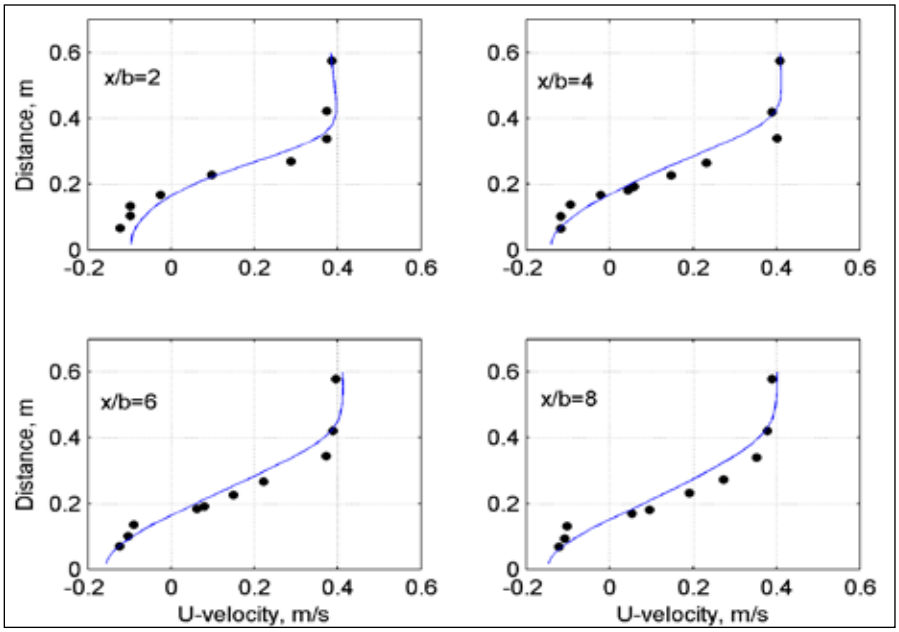

Figure 17. Comparison of measured and calculated flow velocities for the spur dike case. The location of transects x/b=2, x/b=4, x/b=6, and x/b=8, are shown in Figure 16 as green, blue, pink, and purple, respectively.

Table 16. U-velocity goodness-of-fit statistics* for spur dike test case.

Statistic	Cross-section location			
	x/b=2	x/b=4	x/b=6	x/b=8
RMSE, m/s	0.0504	0.0690	0.0557	0.0627
NMAE, %	2.39	7.25	8.84	10.38
R2	0.978	0.951	0.975	0.993

*defined in Appendix A

3.2.5 Conclusions and recommendations

The CMS-Flow performance was analyzed for a laboratory experiment of steady flow in a rectangular flume with a spur dike. In general, the computed current velocities agree well with measurements using the default subgrid turbulence model with a NRMSE of 0.05 to 0.69 percent, a NMAE of 2.39 to 10.38 percent, and a R^2 of 0.962 to 0.993. Further tests using different turbulence models and grid resolutions are needed to assess the model sensitivity. The non-uniform Cartesian grid allows local refinement and is simpler to set up compared to the telescoping grid.

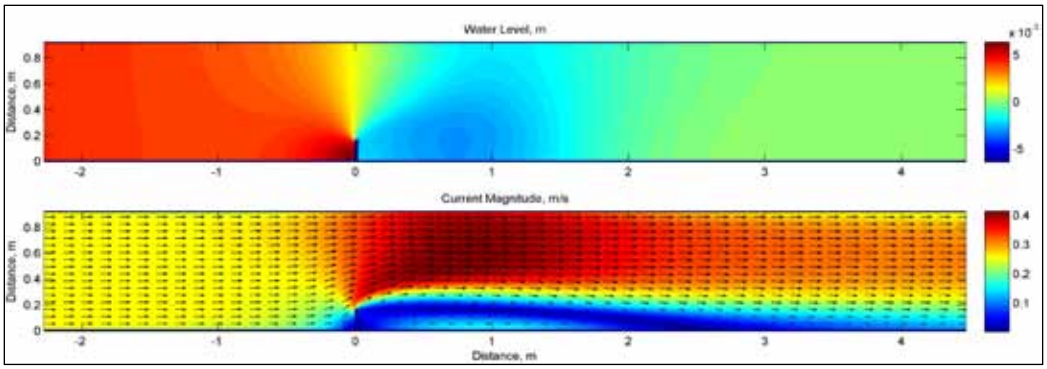

Figure 18. Calculated water level (top) and current velocities (bottom) for the spur dike test case.

3.3 Test C2-Ex2: Steady flow in a rectangular flume with a sudden expansion

3.3.1 Purpose

The CMS is applied to an experimental case of steady flow in a flume with a sudden expansion in width. The CMS performance is assessed by comparing the measured and calculated current velocities behind the sudden expansion. The intended specific model features to be tested are the stretched telescoping grid capability, inflow flux boundary condition, outflow water level boundary condition, wall boundary condition, and mixing-length eddy viscosity (turbulence) model (Wu et al. 2011a, b).

3.3.2 Experimental setup

The flume experiment of Xie (1996) consisted of a rectangular flume 18-m long, with an inflow section 0.6-m wide that abruptly expands into a section 1.2-m wide. The experiment conditions are shown in Table 17.

Table 17. Hydrodynamic conditions for the Xie (1996) experiment

Parameter	Value
Inflow	0.03854 m^3/sec
Bed slope	1/1000
Downstream water depth	0.115 m

3.3.3 Model setup

The stretched 3-level telescoping grid is shown in Figure 19. The grid has a resolution between 0.03 and 0.45 m with 2,625 active cells. A flux boundary condition is applied at the inflow boundary and a constant water level is

specified at the downstream boundary. The initial condition was still water for the entire grid. The model parameters are given in Table 18. The mixing-length turbulence model was applied for this case (Wu et al. 2011a, b). Future studies will compare other eddy viscosity models available in CMS. The bottom friction was estimated to have a Manning's coefficient of 0.015 sec/m$^{1/3}$, which is consistent with the concrete bottom used in the flume. The horizontal shear eddy viscosity coefficient was estimated to be 0.3 which is very close to the default value of 0.4 used in CMS. The computational time was approximately 1 min on a 2.67 GHz single processor.

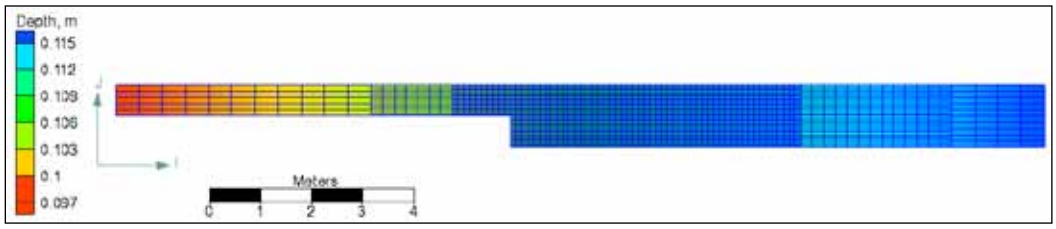

Figure 19. Computational grid for the Xie (1996) experiment test case.

Table 18. CMS-Flow settings for the Xie (1996) experiment test case.

Parameter	Value
Solution scheme	Implicit
Time step	30 sec
Simulation duration	1 hr
Ramp duration	0.5 hr
Manning's coefficient	0.015 sec/m$^{1/3}$
Turbulence model	Mixing-length
Bottom shear viscosity coefficient	0.067 (=default)
Horizontal shear viscosity coefficient	0.3 (default =0.4)

3.3.4 Results and discussion

Current velocities were measured along transects located every meter from the flume expansion. Figure 20 shows a comparison of the measured and computed current velocities in the x-direction. The recirculation zone behind the sudden expansion extends approximately 7 m downstream (see Figures 20-21). In general, the computed current velocities agree well with measurements as demonstrated by the goodness-of-fit statistics shown in Table 19. The NRMSE ranges from 1.60 to 13.98 percent for transects 1-5, increasing in error away from the expansion area.

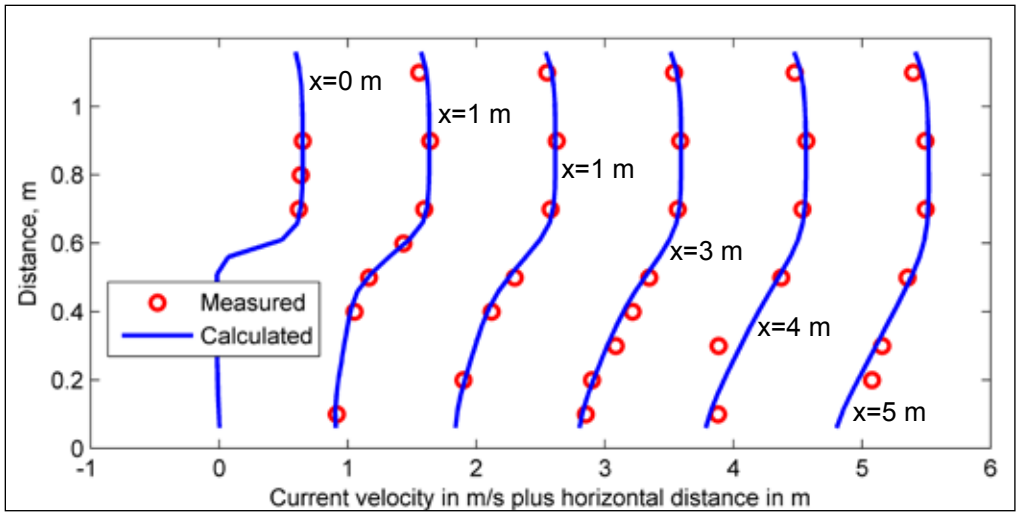

Figure 20. Measured and calculated current velocities along 6 cross-sections for the Xie (1996) experiment. For each transect the horizontal distance is added to the current velocity. Transects are spaced 1 m apart starting at 0 m.

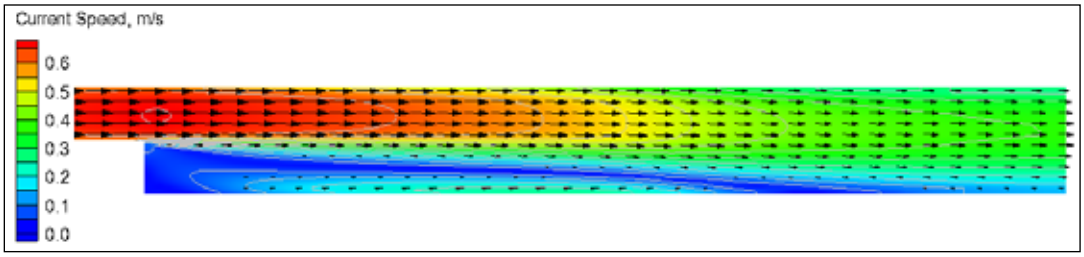

Figure 21. Computed current velocity field for the Xie (1996) experiment test case.

Table 19. Current velocity goodness-of-fit statistics* for the Xie (1996) experiment test case

Statistic	Cross-section location					
	x=0	x=1	x=2	x=3	x=4	x=5
RMSE, m/sec	0.0106	0.0259	0.0293	0.0386	0.0775	0.0584
NRMSE, %	1.60	3.58	4.04	5.26	11.29	13.98
NMAE, %	1.33	2.78	3.61	4.24	7.82	11.80
R^2	0.789	0.995	0.990	0.989	0.936	0.980
Bias, m/sec	0.0083	0.0046	-0.0035	-0.0187	0.0246	-0.0022

*defined in Appendix A

3.3.5 Conclusions and recommendations

The CMS-Flow performance was analyzed for a laboratory experiment of steady flow in a rectangular flume with a sudden expansion. The computed current velocities agreed well with measurements using the mixing-length

turbulence model as demonstrated by the NRMSE of 1.6 to 13.98 percent and R^2 ranging of 0.789 to 0.995. Further tests using different turbulence models and grid resolutions are needed to assess the model sensitivity. The stretched telescoping grid capability reduces the number of computational cells needed significantly. It is recommended that the stretched telescoping grid be used for practical applications whenever possible.

3.4 Test C2-Ex3: Planar sloping beach with oblique incident regular waves

3.4.1 Purpose

The CMS is applied to a laboratory experiment of wave-induced currents and water levels due to regular waves. The large cross-shore gradient of wave height in the surf zone produces a large forcing useful for testing hydrodynamic model stability and performance under strong wave forcing. The specific CMS-Flow features tested are the surface roller, cross-shore boundary conditions, and combined wave-current bottom shear stress parameterization.

3.4.2 Experiment

In 1991, Visser conducted eight laboratory experiments of monochromatic waves on a planar beach and collected measurements on waves, currents and water levels. In this report, experiments (Cases) 4 and 7 are selected as representative test cases. The bathymetry consisted of a 1:10 slope for the first 1 m from shore, a 1:20 slope for the next 5 m, followed by 5.9-m flat bottom to the wave generator. Cases 4 and 7 had an incident wave height of 0.078 m, peak period of 1.02 sec, and incident wave angle of 15.4 deg. Case 4 was run over a concrete bed and Case 7 was run over a thin (0.005 to 0.01-m) layer of gravel grouted onto the concrete floor. A summary of the wave conditions is provided in Table 20.

Table 20. Wave conditions for the Visser (1991) test cases.

Parameter	Value
Wave height (regular)	0.078 m
Wave period	1.02 sec
Incident wave angle	15.4°

3.4.3 Model setup

The computational grid (Figure 22) consists of 84 rows and 147 columns with a constant grid resolution in the longshore direction of 0.15 m, and a variable grid resolution between 0.04 and 0.15 m in the cross-shore direction. A constant zero water level was forced at the offshore boundary and cross-shore boundaries were applied on each side of the shoreline. The boundary type solves the 1-D cross-shore momentum equations for the longshore current and water level, and applies a flux boundary condition for inflow conditions and a water level condition for outflow conditions. The combined wave-current bottom shear stress model of Fredsoe (1984) is used. The cases were simulated as steady-state solutions with pseudo-time stepping to reach steady-state while coupling waves, currents, and water levels. The initial condition was specified as zero current velocity and water level for the whole domain. Waves and hydrodynamics were coupled every 20 min (steering interval) and run until steady-state. The surface roller model (Stive and De Vriend 1994) was run after each CMS-Wave run and the roller surface stresses were then added to the wave radiation stresses before running CMS-Flow. A summary of the important simulation settings for CMS-Flow and CMS-Wave is given in Tables 21 and 22 respectively. The experiments were simulated in laboratory scale, which is why some of the parameters like the wetting/drying depth were decreased.

The wave breaking formulations in CMS-Wave are designed for random waves. However the Visser (1991) laboratory experiments were run with regular (monochromatic) waves which are not useful for validating the CMS-Wave. Since the objective of this test case was to assess the performance of the hydrodynamics, it was necessary to calibrate the waves to obtain the most accurate wave results to analyze the performance of the hydrodynamic model by itself and not have the analysis impacted by the results from an inadequately calibrated wave model. The procedure consisted of first calibrating the location of the breaker using the breaker index γ. The flow was then calibrated using the Manning's coefficient and roller efficiency coefficient (Stive and de Vriend 1994) (Table 23). Additional tests were run for comparison with the same settings except the roller model was turned off.

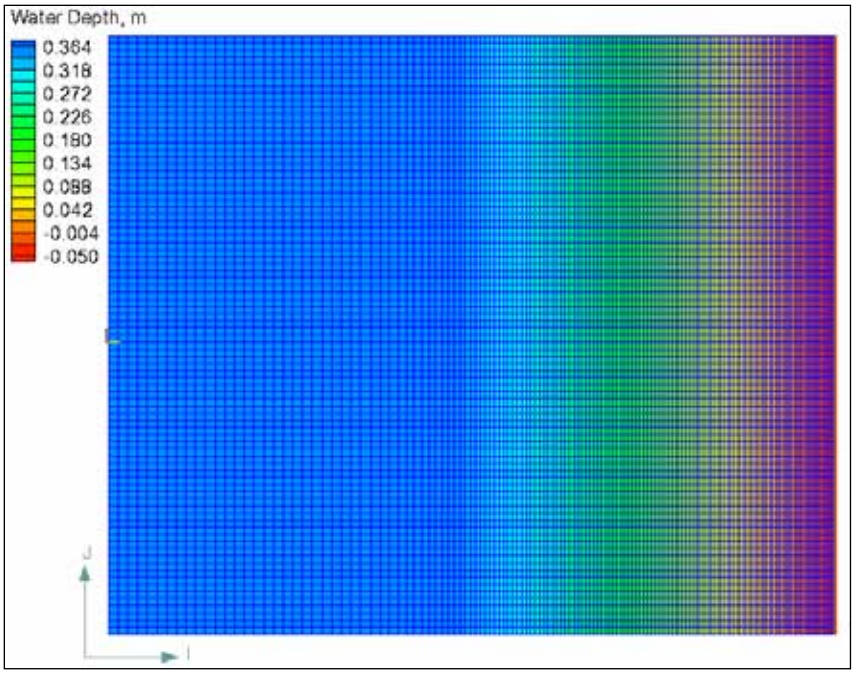

Figure 22. CMS computational grid for the Visser (1991) test cases.

Table 21. CMS-Flow settings for the Visser (1991) test cases.

Parameter	Value
Solution scheme	Implicit
Time step	1 min
Wetting/drying depth	0.006 m
Simulation duration	3 hr
Ramp duration	2 hr
Wave-current bottom friction	Fredsoe (1984)

Table 22. CMS-Wave settings for the Visser (1991) test cases.

Parameter	Value
Wave breaking formulation	Battjes and Janssen (1978)
Bottom friction	Off (default)
Steering interval	20 min

Table 23. Calibration parameters for the Visser (1991) test cases.

Parameter	Case 4	Case 7	Default
Manning's coefficient, sec/m$^{1/3}$ (flow only)	0.0115	0.018	None
Breaker coefficient	0.64	0.9	Automatic (random waves)
Roller dissipation coefficient	0.1	0.1	0.1
Roller efficiency factor	0.8	0.8	1.0

3.4.4 Results and discussion

3.4.4.1 Case 4

The measured and computed wave heights, longshore currents, and water levels for Case 4 are compared in Figure 23. Results are shown with and without the surface roller. The results are improved significantly when the surface roller is included, as demonstrated by the goodness-of-fit statistics shown in Table 24. The NMAE for longshore current was reduced from approximately 20 to 5 percent. The roller has the effect of spreading the peak longshore current and moving it closer to the shore. The surface roller also reduces the setup at the breaker and increases it in the surf zone and near the shoreline. Although the water levels and currents are affected significantly by the surface roller, the wave height profile shows only a minor difference when the roller is included. This is due to the fact that, in this case, the dominant wave process in the surf zone is the wave breaking and the current-wave interaction is relatively weak in the wave model.

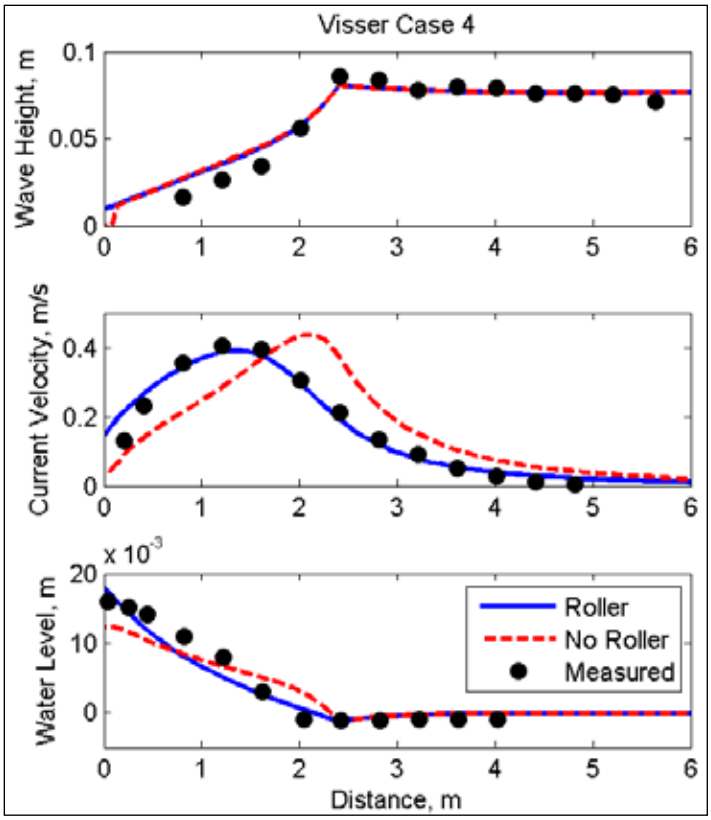

Figure 23. Measured and calculated wave height (top), longshore current (middle), and water level (bottom) for Visser (1991) Case 4.

Table 24. Goodness-of-fit statistics for the Visser (1991) Case 4.

		NRMSE, %	NMAE, %	R^2	Bias
No Roller	Wave height	7.10	5.35	0.985	0.002 m
	Longshore current	22.59	19.91	0.609	0.018 m/sec
	Water level	13.95	11.66	0.954	0.000 m
Roller	Wave height	6.70	5.11	0.985	0.002 m
	Longshore current	7.14	5.11	0.962	0.007 m/sec
	Water level	9.04	7.38	0.957	0.000 m

3.4.4.2 Case 7

The measured and computed wave heights, longshore currents, and water levels with and without the roller for Case 7 are shown in Figure 24. It is interesting to note that, although the offshore wave height, period, and direction are the same as Case 4, the location of the breaker for Case 7 is significantly further offshore. It is suspected that Case 7 actually had a larger wave height than Case 4 which produced a larger breaker further offshore. However, because no measurements were available further offshore of the breaker, no changes were made to the incident wave height. The results are similar to those of Case 4 in that the longshore current velocities are improved significantly when the roller is included (see Table 25). No measurements of water levels were available for Case 7. Similarly to Case 4 the longshore current is well predicted when the roller is included except for the first 1 m from the shoreline where the current velocity is overpredicted.

3.4.5 Conclusions and recommendations

Wave-induced currents and water levels were simulated with the CMS for the case of monochromatic waves over a planar bathymetry. Results were calculated with and without the surface roller and the best results were obtained with the roller turned on, using a roller dissipation coefficient of 0.1 and a roller efficiency factor of 0.8. Both currents and water levels were predicted with errors less than 10 percent. Additional tests will be conducted in the future to show model sensitivity to the calibration parameters and to better determine these parameters based on field conditions. The wave calibration and results shown here are related to regular waves and are not directly applicable to field conditions. However, the purpose of these tests was to test the performance of the hydrodynamic model as quantified by the comparison between measured and simulated longshore current velocities and water levels under strong wave forcing.

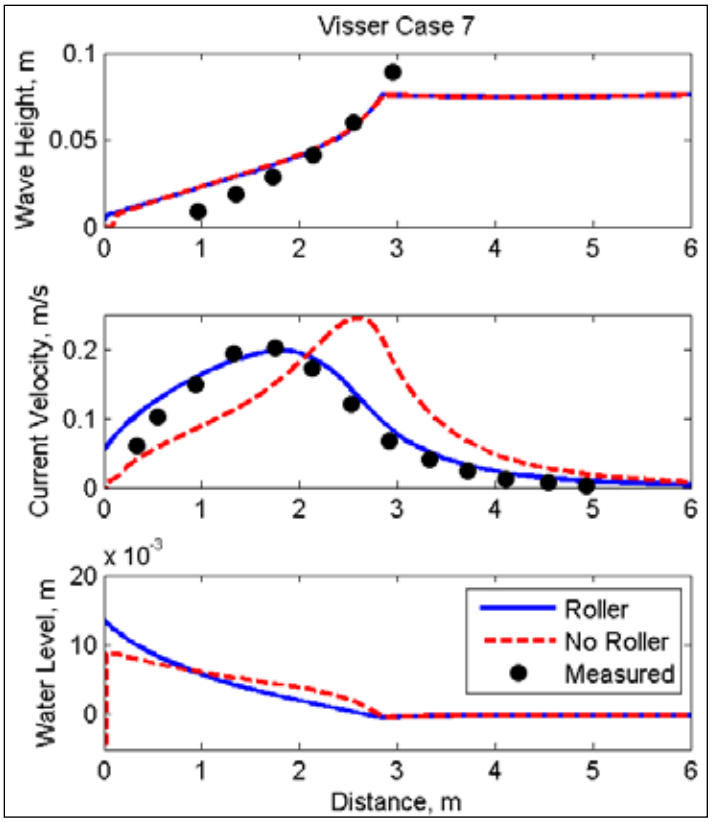

Figure 24. Measured and computed longshore currents (top), water levels (middle) and wave heights (bottom) for Visser (1991) Case 7.

Table 25. Goodness-of-fit statistics for the Visser (1991) Case 7.

Roller	Variable	NRMSE, %	NMAE, %	R^2	Bias
Off	Wave height	7.10	5.35	0.985	0.002 m
	Longshore current	22.59	19.91	0.609	0.018 m/sec
	Water level	13.95	11.66	0.954	0.000 m
On	Wave height	6.70	5.11	0.985	0.002 m
	Longshore current	7.14	5.11	0.962	0.007 m/sec
	Water level	9.04	7.38	0.957	0.000 m

3.5 Test C2-Ex4: Idealized jettied inlet with equilibrium beach profile and oblique incident regular waves

3.5.1 Purpose

The purpose of this validation case was to evaluate the CMS for wave-induced hydrodynamics in the vicinity of an inlet with two absorbing jetties. The specific model features to be tested are the inline flow and wave coupling, wave-adjusted lateral boundary conditions, and Stokes velocities in the continuity and momentum equations.

3.5.2 Physical experiment

In 2005, the USACE conducted a physical model study to collect both current and wave measurements in the vicinity of an idealized dual jetty inlet (Seabergh et al. 2005). The idealized inlet experiment was in a 46-m wide by 99-m long concrete basin with 0.6-m high walls. Figure 25 shows a map of the facility and basin area. A 1:50 undistorted Froude model scale was used to represent the dimensions of a medium-sized U.S. Atlantic coast inlet. The ocean side parallel contours correspond to an equilibrium profile $h = Ax^{2/3}$, where h is the still water depth, x is the cross-shore coordinate from the shoreline and A is a grain size dependant empirical coefficient (equal to 0.1615 $m^{1/3}$ here). For further details on the physical model and previous modeling results with CMS the reader is referred to Seabergh et al. (2005) and Lin and Demirbilek (2005). Fully reflective and absorbing jetties were constructed for inlet geometries studied in the physical model. However, all of the tests shown here are for the absorbing jetties since they represent those found typically in coastal applications. The incident wave conditions for the test cases used here are shown in Table 26. The three cases were chosen to cover a wide range of wave heights.

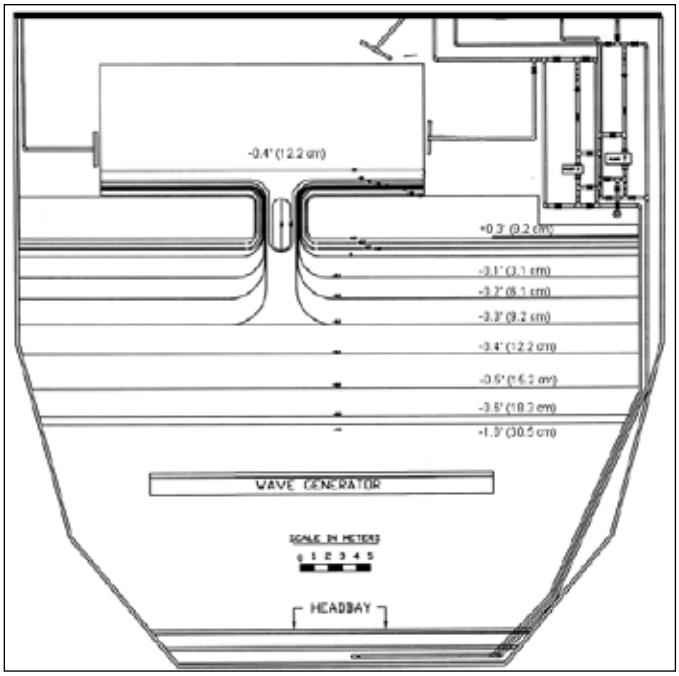

Figure 25. Physical model setup for the idealized inlet case (from Seabergh et al. (2005).

Table 26. Wave conditions (prototype scale) of three test cases from Seabergh et al. (2005).

Case	Wave height*, m	Wave period, sec	Wave Direction**
1	1.65	11.0	-20°
2	2.0	11.0	-20°
3	3.25	8.0	-20°

*Measured at the first offshore station approximately 50 m (prototype) from the jetty tips (see Figure 26).

**Clockwise from shore normal.

3.5.3 Model setup

The computational grid and bathymetry for both CMS-Flow and CMS-Wave is shown in Figure 26. The grid has 31,422 active cells and a constant resolution of 10 m (prototype scale). A list of the basic model setup parameters is given in Table 27. A constant zero water level boundary condition was assigned to the offshore boundary of CMS-Flow. A wall boundary condition was used at all boundaries inside the bay.

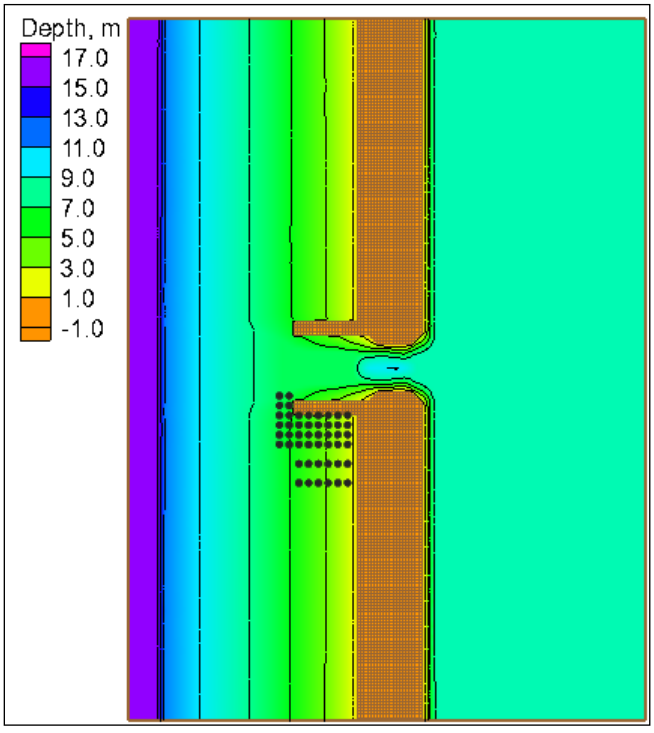

Figure 26. CMS computational grid showing the model bathymetry. Black circles indicate current velocity and wave height measurement stations used in this study.

Table 27. CMS settings for the Seabergh et al. (2005) experiment.

Parameter	Value
Flow time step	6 min
Simulation duration	4 hr
Ramp period duration	3 hr
Manning's *n* (both flow and wave grids)	0.025 sec/m$^{1/3}$
Steering interval	1 hr
Roller	On
Roller dissipation coefficient	0.05 (default for regular waves)
Stokes velocities	On
Wave reflection coefficient	0.0

Default CMS settings were used where possible with the Manning's coefficient being the only calibrated parameter (n = 0.025 sec/m$^{1/3}$) for this case study. The roller dissipation coefficient β_D was set to the recommended value for regular waves (β_D = 0.05). Both parameters were held constant for all test cases. Including the roller is very important for regular waves because it improves the prediction of the longshore current. The wave- and depth-averaged hydrodynamics equations are solved for depth-uniform currents according to Phillips (1977) and Svendsen (2006). The formulation includes Stokes velocities in both the continuity and momentum equations and provides a better prediction of cross-shore currents.

3.5.4 Results and discussion

The measured and calculated wave heights and wave-induced nearshore currents are presented in plan-view vector plots and also cross-shore transects as discussed below. Note that the wave height and cross-shore profiles are offset by a number indicated to left of each transect which are plotted using different colors. Demirbilek et al. (2009) reported similar results for the wave height using a previous version of CMS. The current velocities reported here are improved significantly with respect to Demirbilek et al. (2009) due to the implementation of the surface roller and Stokes velocities.

3.5.4.1 Case 1 (H=1.65 m, T=11 sec)

The calculated wave height magnitudes and directions agree well with the measurements with a NMAE of 10.62 percent (see Figures 27 and 28 and Table 28). The wave model tends to over predict wave refraction near the

structure and shoreline. The breaker is located at approximately the third cross-shore measurement station from the shoreline and was well predicted by the model (Figure 28). Measured and computed current velocities for Case 1 are compared in Figures 27 and 29. The velocity field is characterized by a narrow longshore current approximately 75-m wide which is deflected seaward by the south jetty. The NRMSE and NMAE values for the longshore current are approximately 24 and 19 percent, respectively, while for the cross-shore current, they are significantly smaller at 14 and 10 percent, respectively (see Table 28). Most of the longshore current is located within the first two measurement stations from the shoreline. The calculated cross-shore currents agree well with the measurements except near the jetty where it was overestimated.

3.5.4.2 Case 2 (H=2.0 m, T=11 sec)

The calculated wave height magnitudes and directions of Case 2 agree well with the measurements especially far away from the jetty (see Figures 30 and 31). The wave height NRMSE, NMAE, and R^2 are 12.33 percent, 8.05 percent, and 0.889, respectively (see Table 29). Closer to the jetty, the differences are larger possibly due to reflected wave energy from the jetty. Even though the jetties were made of small stones and absorbed most of the wave energy, a small portion of the wave energy was reflected. CMS-Wave has the capability to simulate reflecting waves. However, for this study it was assumed that the jetty reflectance was negligible. Additional tests will be conducted in the future to test this hypothesis. The breaker is located at approximately the fourth cross-shore measurement station from the shoreline and was well predicted by the model.

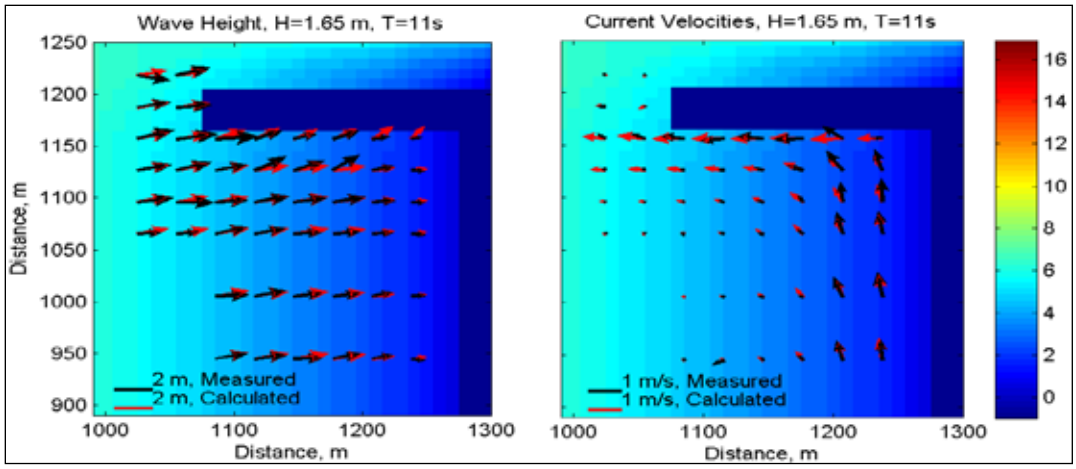

Figure 27. Measured and calculated wave height (left) and mean current (right) vectors for Case 1. Background colors indicate the local water depth corresponding to the right color bar.

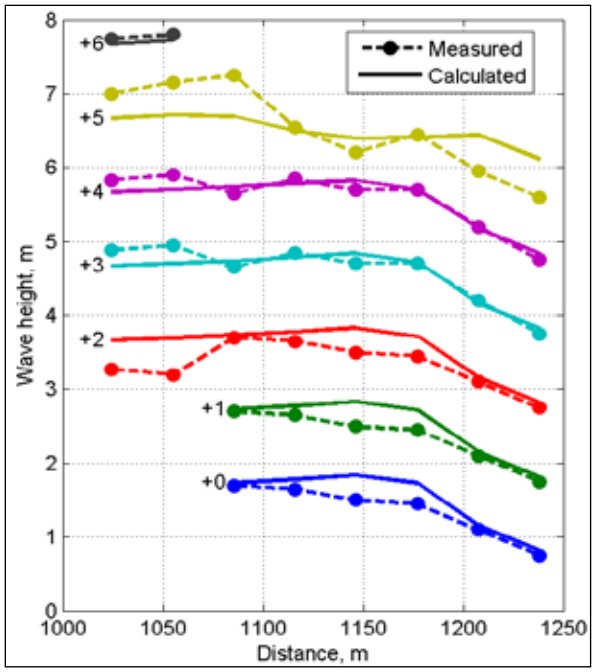

Figure 28. Cross-shore transects of measured and calculated wave heights for Case 1 (H = 1.65 m, T = 11 sec). For display purposes, wave heights are shifted by the number indicated on the left hand side of each transect.

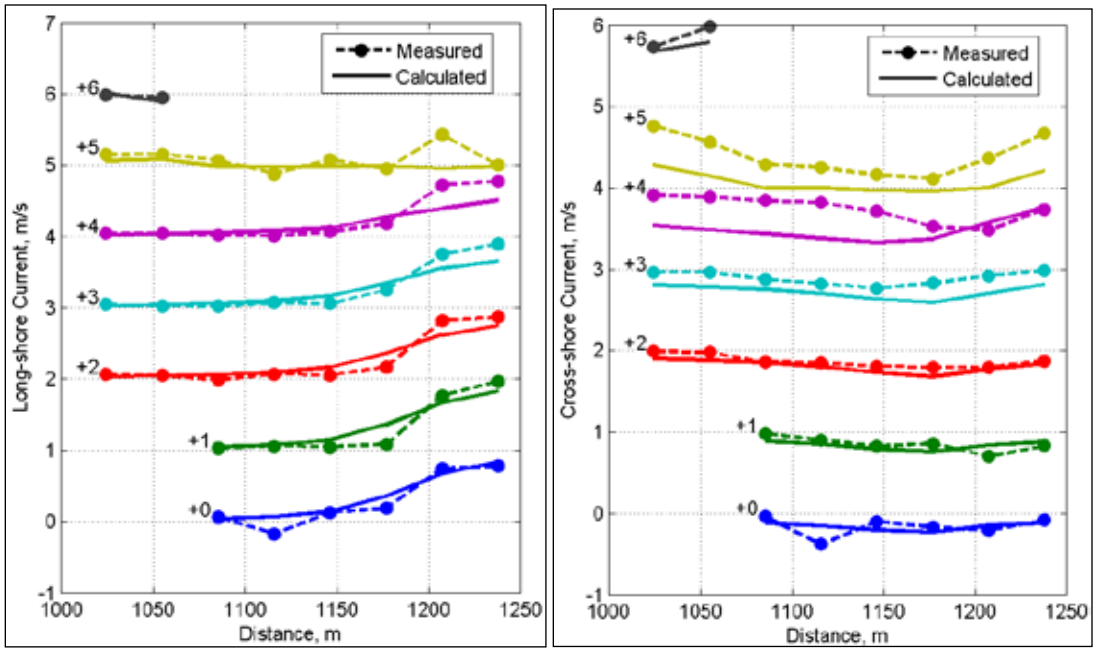

Figure 29. Cross-shore transects of measured and calculated longshore (left) and cross-shore (right) currents for Case 1 (H = 1.65 m, T = 11 sec). For display purposes, current velocities are shifted by the number indicated on the left hand side of each transect.

Table 28. Goodness-of-fit statistics* for Case 1 (H = 1.65 m, T = 11 sec)

Variable	NRMSE,%	NMAE,%	R^2	Bias
Longshore current	24.11	18.74	0.836	-0.141 m/sec
Cross-shore current	14.27	10.30	0.907	0.017 m/sec
Wave Height	13.96	10.62	0.826	0.051 m

*defined in Appendix A

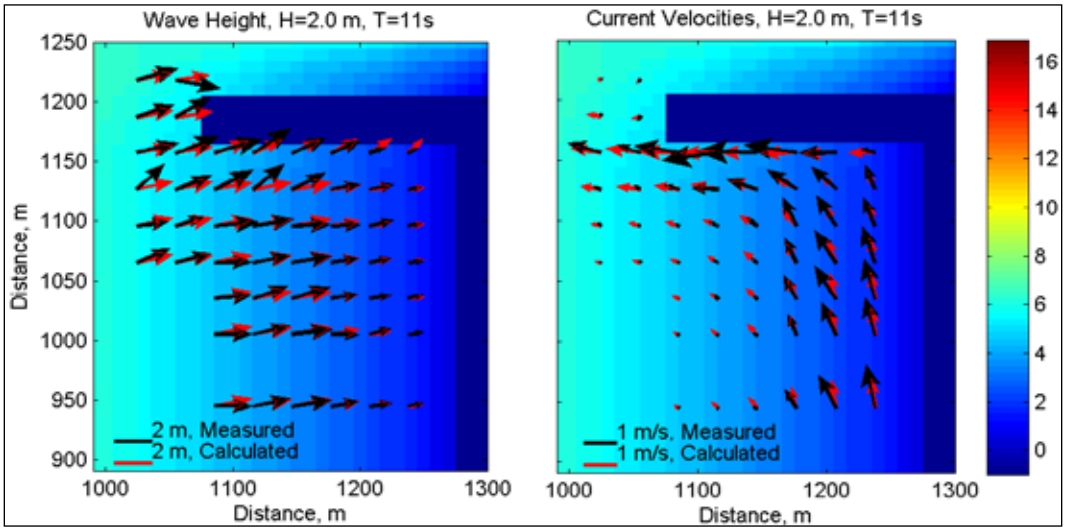

Figure 30. Measured and calculate wave height (left) and mean current (right) vectors for Case 2. Background colors indicate the local water depth corresponding to the right color bar.

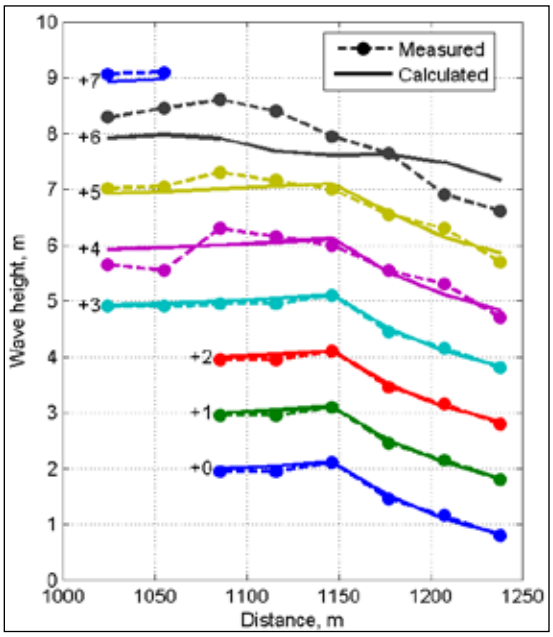

Figure 31. Cross-shore transects of measured and calculated wave heights for Case 2 (H = 2.0 m, T = 11 sec). For display purposes, wave heights are shifted by the number indicated on the left hand side of each transect.

Table 29. Goodness-of-fit statistics* for Case 2 (H = 2.0 m, T = 11 sec)

Variable	NRMSE,%	NMAE,%	R^2	Bias
Longshore current	14.43	12.24	0.797	-0.007 m/sec
Cross-shore current	14.69	11.49	0.930	-0.065 m/sec
Wave Height	12.33	8.05	0.889	-0.040 m

*defined in Appendix A

Measured and calculated current velocities for Case 2 along cross-sectional transects, shown in Figure 32, have NRMSE and NMAE values less than 15 and 13 percent, respectively. Although the breaker zone for Case 2 is wider than in Case 1, most of the long-shore current is still located within the first 3 measurement stations from the shoreline. The calculated cross-shore currents tend to be underestimated near the shoreline and slightly overestimated outside of the breaker for all cross-shore transects except the one adjacent to the jetty.

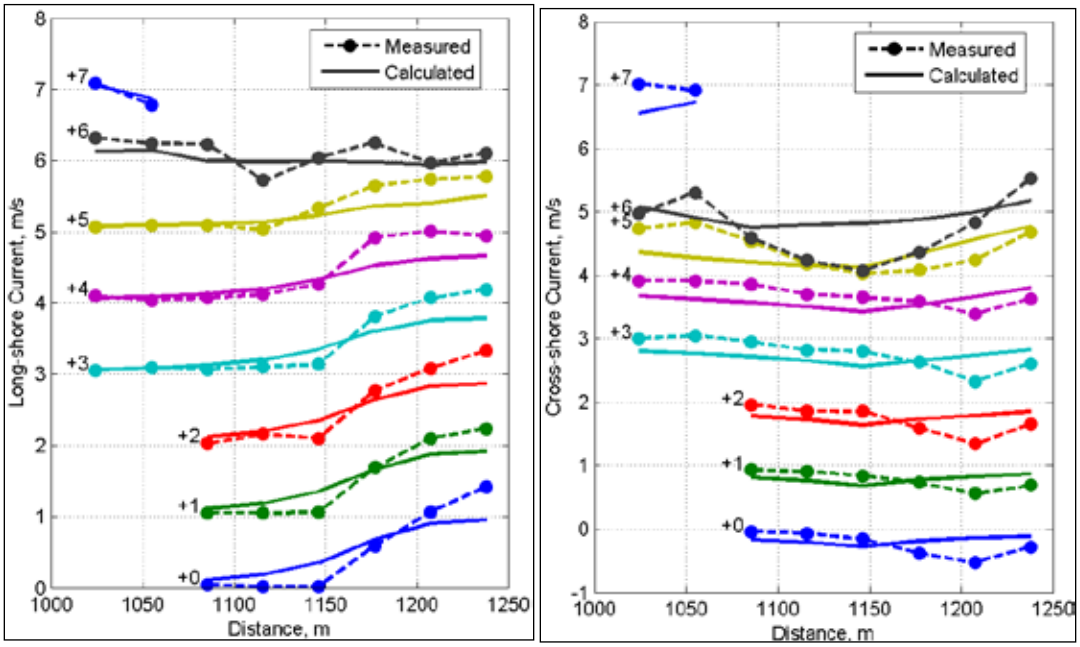

Figure 32. Cross-shore transects of measured and calculated long-shore (left) and cross-shore (right) currents for Case 2 (H = 2.0 m, T = 11 sec). For display purposes, current velocities are shifted by the number indicated on the left hand side of each transect.

3.5.4.3 Case 3 (H=3.25 m, T=8 sec)

Figure 33 shows plan-view vector plots of the measured and computed wave heights and current velocities for Case 3. Cross-shore profiles of measured and computed wave heights and current velocities are plotted in Figures 34 and 35.

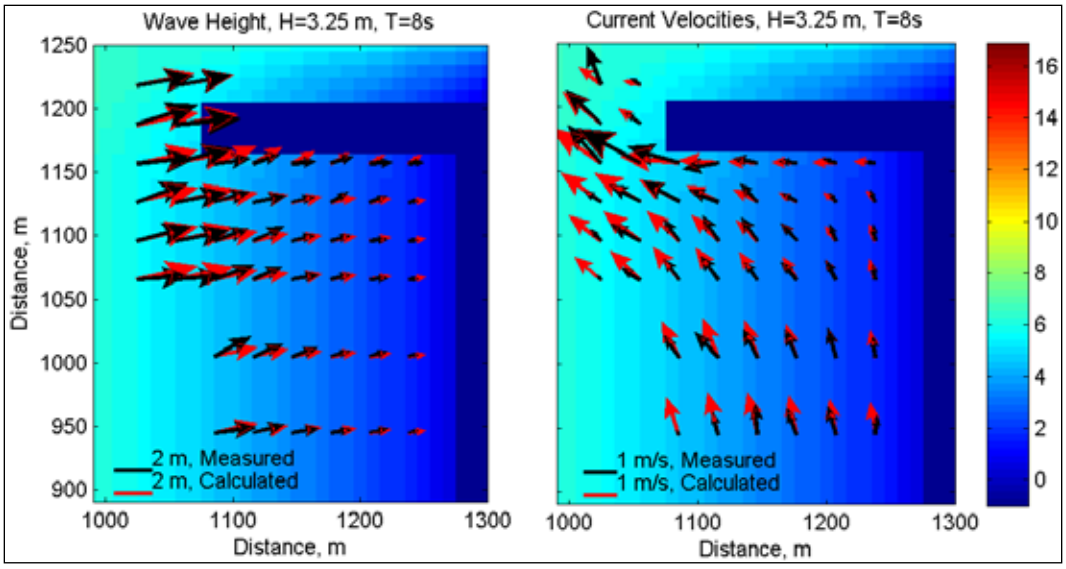

Figure 33. Measured and calculated wave height (left) and mean current (right) vectors for Case 3. Background colors indicate the local water depth corresponding to the right color bar.

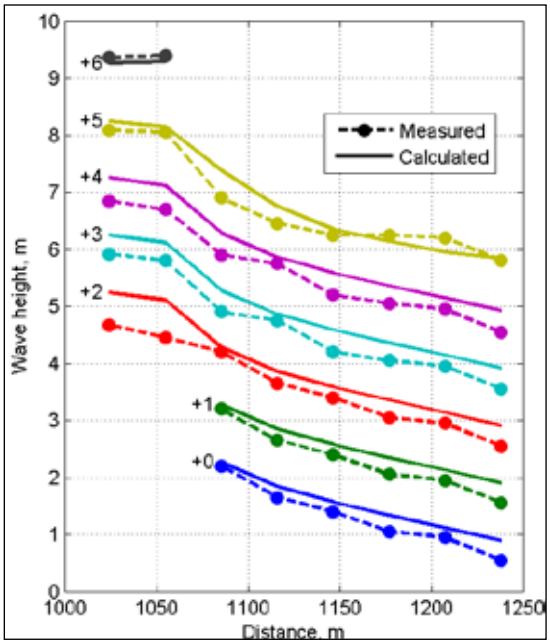

Figure 34. Cross-shore transects of measured and calculated wave heights for Case 3 (H = 3.25 m, T = 8 sec). For display purposes, wave heights are shifted by the number indicated on the left hand side of each transect.

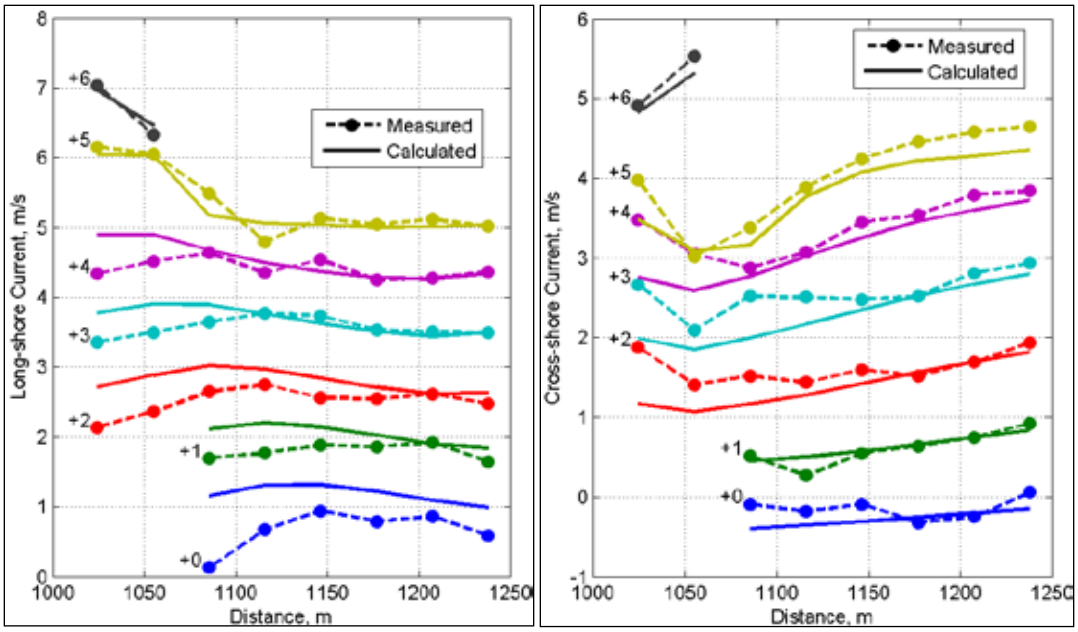

Figure 35. Cross-shore transects of measured and calculated long-shore (left) and cross-shore (right) currents for Case 3 (H = 3.25 m, *T* = 8 sec). For display purposes, current velocities are shifted by the number indicated on the left hand side of each transect.

For this case, the calculated wave heights are slightly overestimated for most of the measurement locations indicating the wave breaker coefficient was slightly overestimated for this steep wave condition. It is noted that wave breaker coefficient calculation is intended for irregular waves and has not been calibrated for regular waves. Wave directions agree well with the measurements with the exception of a few measurement stations where significant differences are observed in the incident wave angles. From the measurements it appears that the location of the breaker is outside of the measurement stations. The calculated longshore current velocities show the smallest NRMSE and NMAE of all three cases with values of 14 and 11 percent, respectively. The cross-shore velocities conversely, show the largest NRMSE and NMAE values of all three cases with values of 28 and 20 percent, respectively (Table 30). Measured and computed current velocities for Case 3 agree reasonably well. However, the long-shore current speed tends to be overestimated near the breaker.

Table 30. Goodness-of-fit statistics* for Case 3 (*H* = 3.25 m, *T* = 8 sec)

Variable	NRMSE, %	NMAE, %	R^2	Bias
Longshore current	13.86	10.61	0.886	-0.189 m/sec
Cross-shore current	27.75	20.48	0.676	0.158 m/sec
Wave Height	9.98	8.68	0.978	0.223 m

*defined in Appendix A

3.5.5 Conclusions and recommendations

Laboratory experiments were used to validate the CMS for cross-shore and longshore currents and waves near an idealized inlet with two fully-absorbing jetties. Measurements of regular waves and wave-induced currents were compared with CMS simulations at the prototype scale. The CMS was run using mostly default settings, except for the Manning's coefficient (n = 0.025 sec/m$^{1/3}$) and roller dissipation coefficient (β_D = 0.05). Both parameters were held constant for all three cases. The value of the roller dissipation coefficient applied is the recommended value for regular waves. Model performance and behavior varied case by case but in general the calculated wave heights and wave-induced current velocities agreed reasonably well with measurements as indicated by the goodness-of-fit statistics. Calculated nearshore wave heights and currents upstream of a jetty were found to be within approximately 10 to15 percent and 10 to30 percent, respectively, of measurements. CMS-Wave was able to predict the location of the wave breaker accurately. However, tests were conducted in a physical model without tidal currents, winds, and with well known bathymetry and wave conditions which all represent additional potential sources of error in field applications.

These results indicate that once the model is calibrated for a specific site, using mainly the bottom roughness, the model may be applied at the same site for different wave conditions without having to recalibrate the model. Using the wave- and depth-averaged hydrodynamic equations for depth-uniform currents as derived by Svendsen (2006) significantly improved the nearshore currents most noticeably by producing an offshore directed flow or undertow. Including the surface roller improved the longshore currents by moving the peak longshore current closer to the shoreline.

4 Field Studies

4.1 Overview

The field cases described in this chapter were selected for validation of CMS-Flow to confirm the degree to which the model is an accurate representation of the real world for its intended uses. The Category 3 V&V test cases completed are listed below. Additional cases are under investigation and will be included in future reports. Category 3 tests cases completed are:

1. Gironde Estuary, France
2. Grays Harbor, WA
3. Ocean Beach, CA
4. St. Augustine Inlet, FL
5. Shark River Inlet, NJ
6. Galveston Bay, TX
7. Ship Island, MS
8. Hazaki Oceanographic Research Facility, Japan
9. Duck, NC
10. Matagorda Ship Channel, TX

4.2 Test C3-Ex1: Gironde Estuary, France

4.2.1 Purpose

Application of CMS to the Gironde Estuary demonstrates specification of the flow boundary condition within an estuary, with validation measurements of water level and current speed spaced along the axis of the estuary.

4.2.2 Field study

The Gironde Estuary is located in southwestern France. It receives runoff from the Garonne and the Dordogne Rivers and opens up to the Atlantic Ocean, as shown in Figure 36. The water-surface width varies from 2 to 14 km, and the flow depth in the navigation channel ranges from 6 to 30 m. The estuary is partially mixed and macrotidal, with a 12 hr and 25 min tidal lunar period and a tidal amplitude of 1.5 to 5 m at the mouth (Li et al. 1994).

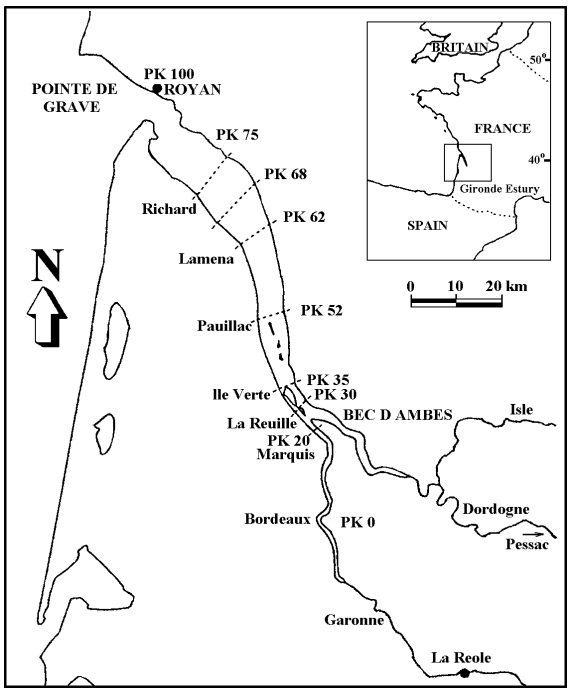

Figure 36. Sketch of the Gironde Estuary, France (from Wu and Wang 2004).

4.2.3 Model setup

The implicit CMS was applied to this test case, with the simulation domain extending 80 km starting from the mouth at the Atlantic Ocean to the Garonne and Dordogne Rivers. The bed topography was provided on a uniform mesh, with a size of 250 by 125 m for each cell. The grid has approximately 16,000 active cells. Because the domain is relatively simple, a uniform mesh was used. The data measured from 19-25May 1975 were used to validate the model for water level and current speed. The computational time step was set to 30 min. At the estuary mouth, the tidal elevation was given by the recorded time series at the station "Pointe de Grave" (see Figure 36). At the two upstream ends, the flow discharges of the Garonne River and the Dordogne River were specified according to the measured data at La Réole and Pessac. The Manning's roughness coefficient was set to 0.018 sec/$m^{1/3}$. Figure 37 shows the computational grid and observation stations. The Coriolis force is included using the f-plane approximation. Winds were not included in the simulation. The 100-hr simulation took approximately 12 min to run on a 2.67 GHz processor.

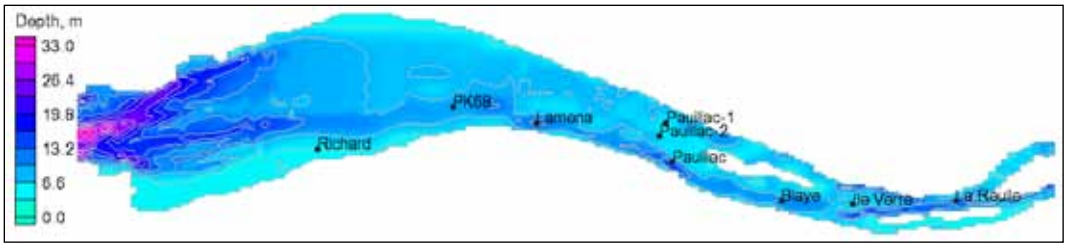

Figure 37. Computational grid and observation stations for the Gironde Estuary Test Case.

The inland boundaries along the Dordogne and Garonne rivers were assigned as flux boundary conditions according to the data from La Réole and Pessac, and the inflow discharges were set to 387 and 846 m^3/sec, respectively. The initial condition was specified as still water in the whole domain. A 1-hr ramp period was used at the start of the simulation. Table 31 summarizes the setup parameters for CMS.

Table 31. CMS-Flow setup parameters for the Gironde Estuary test case.

Parameter	Value
Solution scheme	Implicit
Simulation duration	100 hr
Ramp period duration	1 hr
Time step	6 min
Manning's n coefficient	0.018 sec/$m^{1/3}$
Latitude	45.5°

4.2.4 Results and discussion

The flow fields in flood and ebb tides are shown in Figure 38. The ebb flow is characterized by a funnel effect at the entrance (mouth or inlet) caused by the narrowing of the estuary in this region. The increase in velocity is likely to be the cause of the channel deepening in this region, as shown by the depth contours (see Figure 37). The flood tide is also characterized by a funnel effect near Ile Verte which also seems to cause some deepening of the estuary to the south of the island.

Figure 39 compares the measured and simulated water levels at five stations within the Gironde Estuary (stations shown in Figure 37). In general, the results show good agreement with the measured data both in amplitude and phase. Table 32 summarizes the goodness–of-fit statistics for water level. NRMSE and NMAE values for the water levels range from 5 to7 percent.

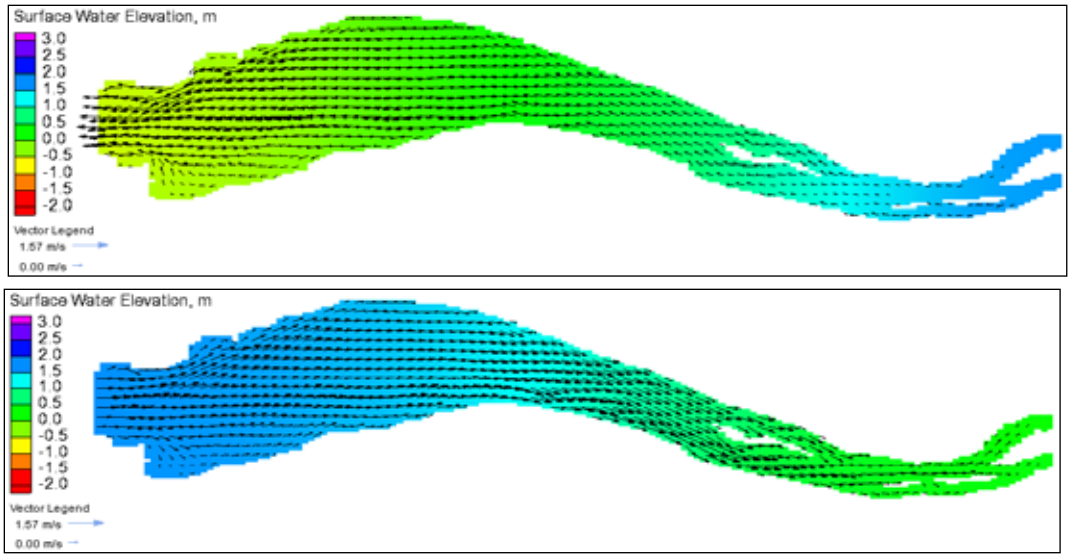

Figure 38. Examples of ebb (top) and flood (bottom) tidal currents and water surface elevations in the Gironde Estuary.

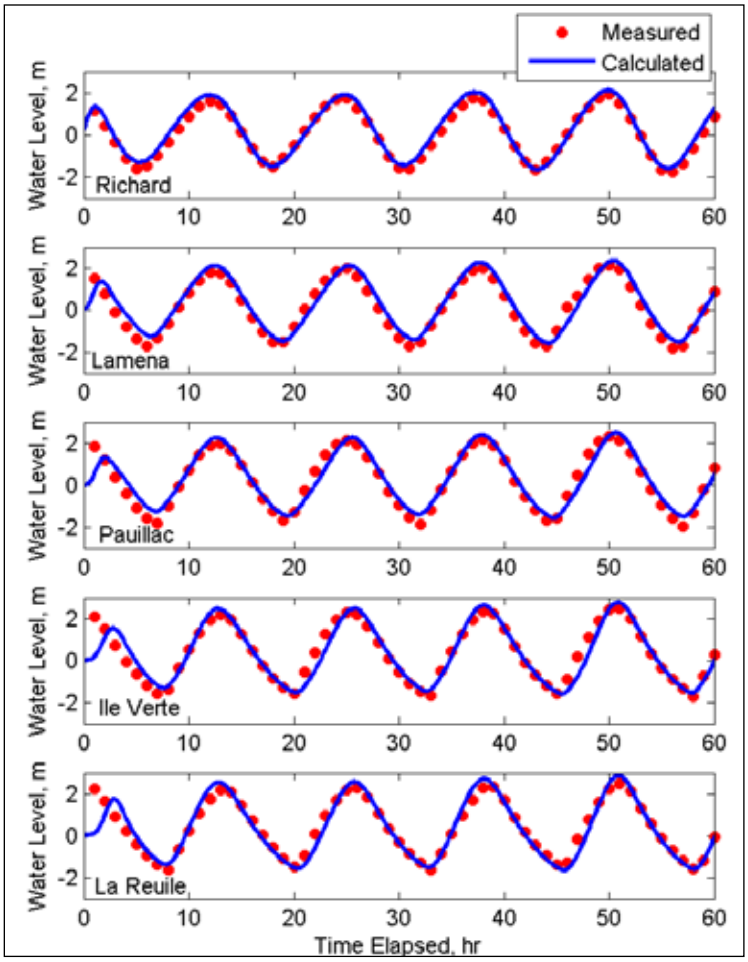

Figure 39. Comparison of measured and calculated water levels at five stations in the Gironde Estuary (stations shown in Figure 37).

Table 32. Water level goodness-of-fit statistics* for the Gironde Estuary test case.

	Station (see Figure 37 for location)				
Statistic	Richard	Lamena	Pauillac	Ile Verte	La Reuille
NRMSE, %	5.10	7.02	6.74	6.40	6.63
NMAE, %	4.33	6.21	5.63	4.34	5.08
R2	0.982	0.956	0.951	0.962	0.972
Bias, m	0.094	0.128	0.043	-0.060	-0.0252

*defined in Appendix A

Figure 40 shows the comparison of the measured and simulated flow velocities at several stations (stations shown in Figure 37). The velocities were measured 1 m below the water surface and 1 m above the river bed, respectively. In this figure, positive current velocities correspond to flood tides and negative velocities to ebb tides. The current measurements at both elevations are relatively similar for all stations except Richard and Lamena. This might be due to baroclinic circulation produced by wind, fresh water intrusion, or other factors near these two stations.

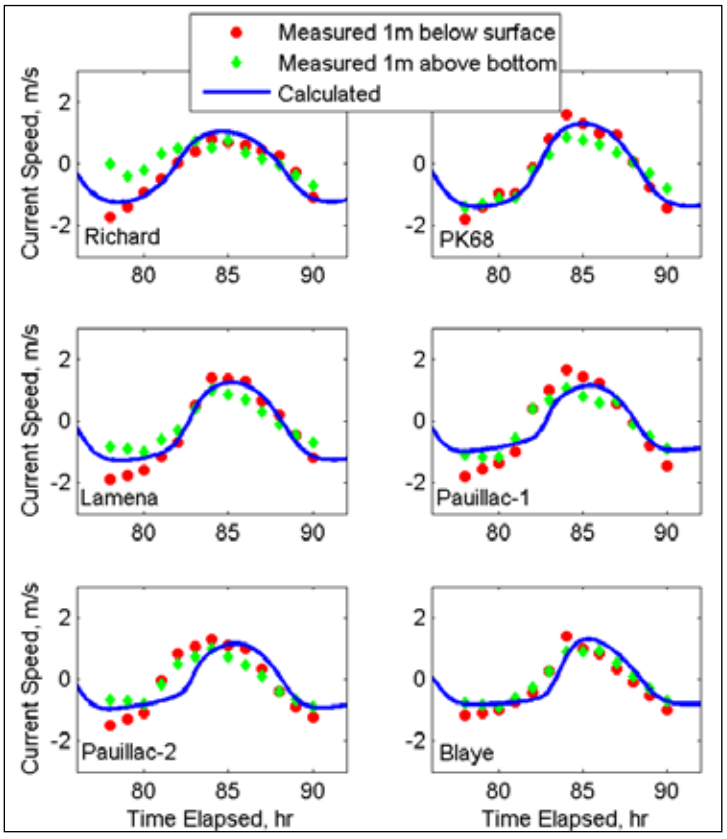

Figure 40. Measured and calculated current speed in the Gironde Estuary (stations shown in Figure 37).

Some of the differences in water surface elevations and current velocities may be due to inaccuracies in the boundary conditions. The boundary conditions at the estuary entrance were obtained from a nearby station and therefore a slight phase lag of about 45 min was subtracted from calculated water surface elevations to match the measured time series. However, since the boundary condition used was not measured exactly at the location of the boundary, some error in phase lag may be expected from this approximation.

Another probable source of error is the bottom roughness coefficient, which was assumed to be constant. Other field experiments show that the bottom roughness in an estuary can vary significantly due to changes in bed forms and grain sizes within the estuary. Although the CMS has the capability to use a spatially variable bottom roughness coefficient, there were no data available in this case. The agreement between measured and calculated current speeds is summarized in Table 33. NRMSE and NMAE in current speed range from 7 to 21 percent. Comparable results were obtained by Wu and Wang (2004) using a similar depth-averaged flow model.

Table 33. Current speed goodness of fit statistics for the Gironde Estuary test case.

	Station (see Figure 37 for location)					
Statistic	Richard	PK68	Lamena	Pauillac-1	Pauillac-2	Blaye
NRMSE, %	10.70	7.27	8.81	15.89	20.73	14.98
NMAE, %	9.15	5.71	6.93	13.67	17.05	13.17
R2	0.911	0.957	0.968	0.856	0.680	0.804
Bias, m/sec	0.070	-0.057	0.062	0.022	-0.031	0.095

*defined in Appendix A

4.2.5 Conclusions and recommendations

CMS calculations of tidal flow in a large estuary were compared to measured water level and current speed. Calculations agreed with measurements with errors ranging from 5 to 7 percent for water level and 7 to 21 percent for currents. The boundary condition used in the model was not measured exactly at the location of the boundary; therefore, the calculations incurred some error in phase lag of water surface elevation and in current velocities. This application demonstrates the accuracy of CMS within a macrotidal estuarine environment, for measurements distributed along the channel. It

is recommended that the bottom roughness should be estimated based on the bottom type (sandy, rocky outcrops, vegetation, etc.), and then adjusted (calibrated) based on field measurements of water levels and currents. When developing a new model setup and grid for engineering applications, it is useful to start simple as far as grid size and model forcing, and increase the model complexity slowly, only as needed until satisfactory results are obtained for the purpose of the project. This iterative process has the added benefit of providing insights on the importance of physical processes and model sensitivity to setup parameters and grid geometry.

4.3 Test C3-Ex2: Grays Harbor, WA

4.3.1 Purpose

The CMS performance in simulating the hydrodynamics and wave transformation at a relatively large and complex inlet and estuary at Grays Harbor, WA, is analyzed using field measurements of water levels and current velocities. The specific model features to be tested are the wave-flow coupling, user-defined water level boundary condition, and wetting and drying.

4.3.2 Field study

Grays Harbor is located on the southwest Washington coast about 45 miles north of the Columbia River. The estuary has a wetted surface area of approximately 91 square miles at mean higher high water and 28 squares miles at mean lower low water. The main input of fresh water is from the Chehalis River. The 3-mile-wide entrance has two convergent rock jetties which extend from spit points, as shown in Figure 41. In 1999 and 2001, the USACE conducted several field experiments at Grays Harbor as part of a navigation study to better understand the sediment transport and functionality of the northern jetty (Osborne et al. 2002). During 1999, measurements of water levels, current velocities, and suspended sediment were collected at seven locations (black dots in Figure 41). Here in the current velocity data collected September - October 1999 are used for validation. For further details on the field experiment, the reader is referred to Osborne et al. (2002). For water levels, NOAA tide gauge stations were used due to their distal location from the inlet entrance (red dots in Figure 41).

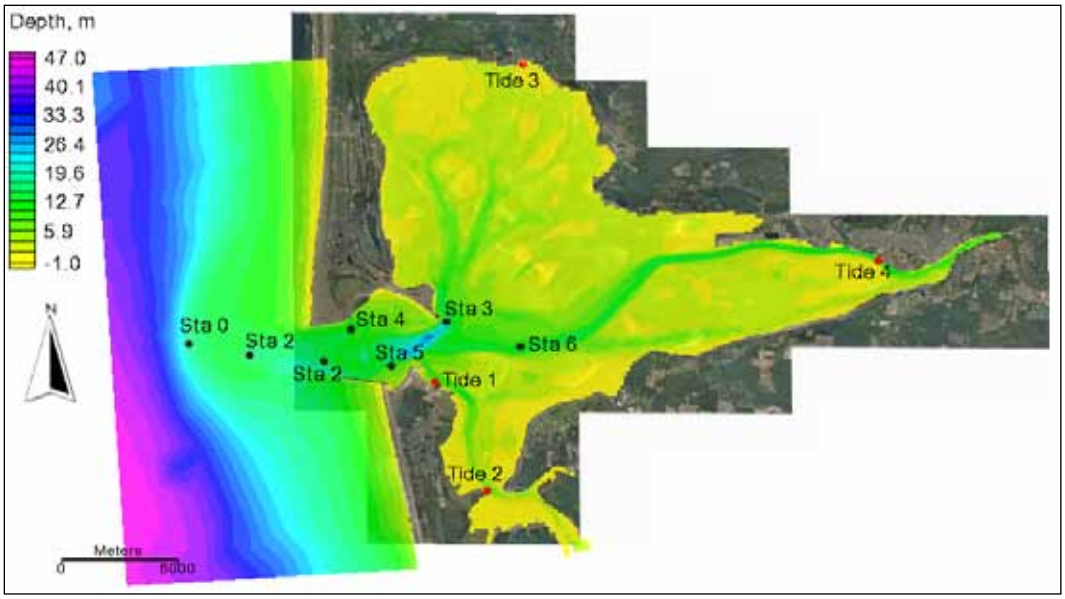

Figure 41. CMS computational domain for the Grays Harbor, WA test case.

4.3.3 Model setup

The computational grid consisted of 67,000 cells and had a non-uniform spacing from 28 to 200 m. The model domain is shown in Figure 41. Both the wave and flow models used the same grid. The spectral waves from the NOAA buoy 46029 were input at the model boundaries every 3 hr. Wind from the same buoy was included in the wave model. The hydrodynamic, sediment transport and morphologic time steps were set to 15 min. A spatially constant Manning's roughness coefficient was calibrated as 0.018 $s/m^{1/3}$ using water level measurements and was the only parameter calibrated. The hydrodynamic model was forced with water level measurements taken at Station 0. The 27-day period from 14 September to 15 October 1999 was calculated with CMS. The model setup is summarized in Table 34. For further details on the model setup and results see Wu et al. (2010). The 27-day simulation took approximately 7 hr on a single 2.67GHz processor.

Table 34. CMS model settings for the Grays Harbor test case.

Parameter	Value
Time step	15 min
Simulation duration	27 days
Ramp period	24 hr
Manning's coefficient	0.018 $1/m^{1/3}$
Steering interval	3 hr

4.3.4 Results and discussion

Figures 42-43 compare the computed and measured water levels and current velocities at selected stations. The agreement between calculated and measured water levels is generally good, as demonstrated by the goodness-of-fit statistics presented in Table 35. There is a slight over prediction of the water level at Stations 3 and 4 during low tide that may be associated with bathymetric error or an over estimation of bottom roughness which prevents the water from ebbing during low tide. It is possible that the results may be improved by using a spatially variable bottom roughness based on the bottom and this is planned for future work. Different time steps between 5 to 30 min were tested and the differences were negligible. The only areas which show significant differences are those with extensive wetting and drying. However, these areas contain a relatively small tidal prism and do not impact the dynamics near the inlet entrance significantly. It is interesting to note from the water levels (see Figure 42) that the hydrodynamics took approximately 250 hr to eliminate the effect of the initial condition. This suggests that the model needs a spin-up period of approximately 11 days, possibly due to the presence of resonance inside the bay which takes time for the model to build up.

Measured (estimated from vertical velocity profile) and calculated depth-averaged current velocities are compared along the current principle axis because it represents the major component of the current velocity variance. Peak ebb and flood current velocities range from approximately 1 to 1.5 m/sec. In general, the model predicts well the amplitude and phase of the principle current velocities well. Normalized errors for the principle current velocities are less than 10 percent, indicating a good model performance (see Table 36).

Table 35. Goodness-of-fit statistics for the water levels at Grays Harbor, WA.

Statistic	Sta1	Sta2	Sta3	Sta4
NRMSE, %	2.61	2.87	7.17	5.14
NMAE, %	2.03	2.41	5.38	3.78
R^2	0.990	0.991	0.968	0.979
Bias, m	-0.017	-0.049	-0.132	-0.106

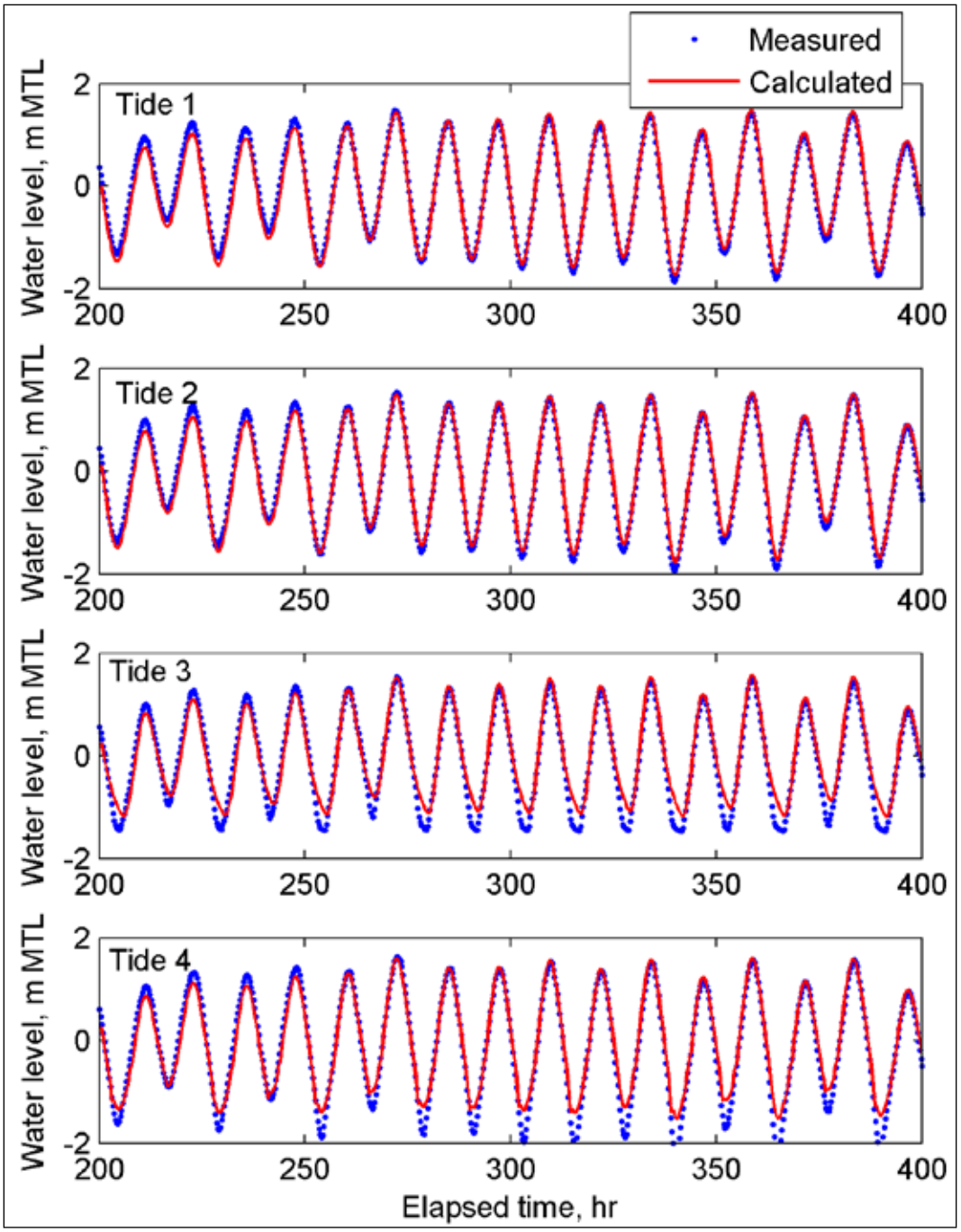

Figure 42. Measured and calculated tide levels at Grays Harbor, WA. MTL = Mean Tide Level. Elapsed times are with respect to September 14, 1999.

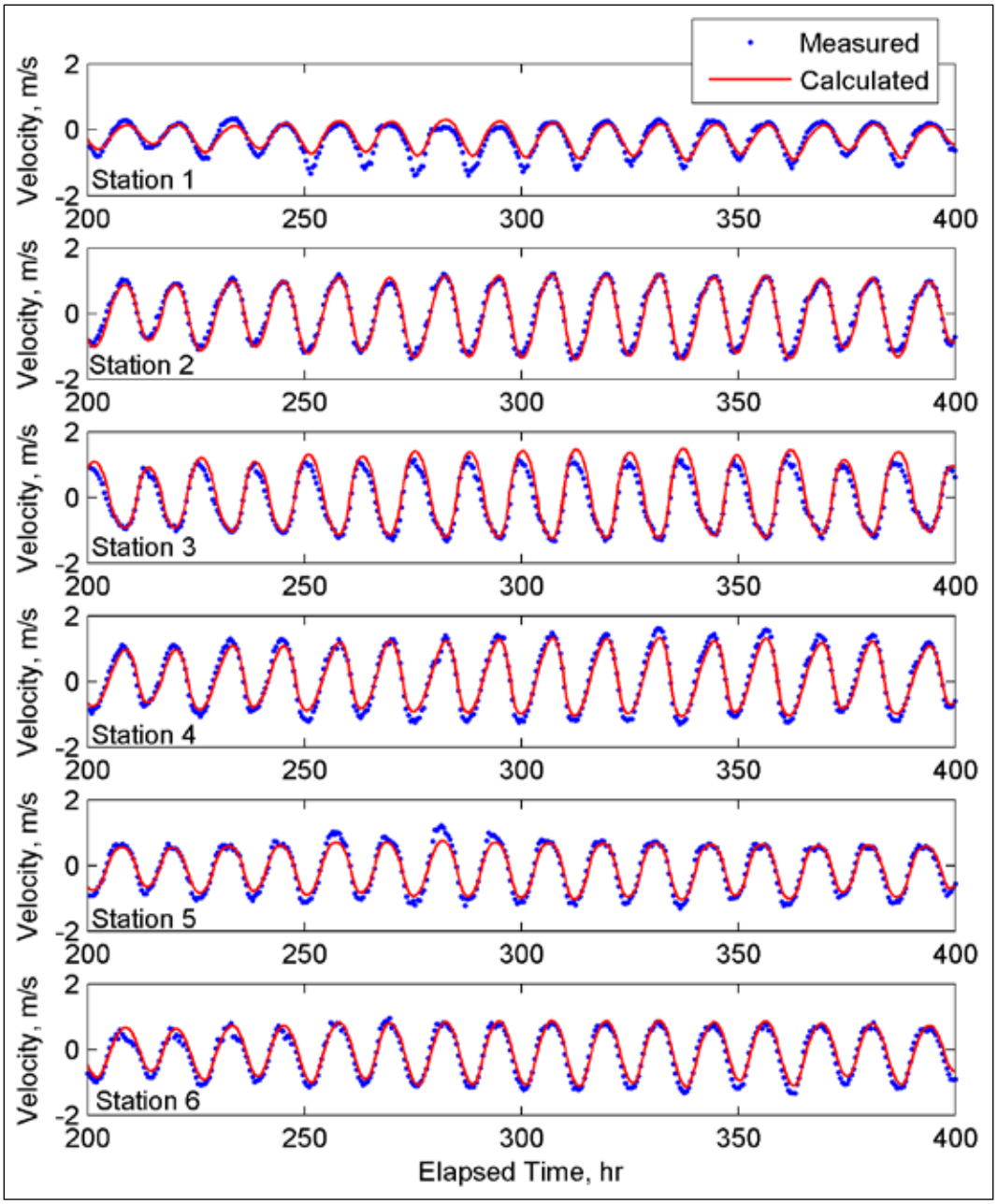

Figure 43. Measured and calculated principle current velocities at Grays Harbor, WA. Elapsed times are with respect to 14 September 1999.

Table 36. Principle current velocity goodness-of-fit statistics for Grays Harbor, WA.

Statistic	Sta 1	Sta 2	Sta 3	Sta 4	Sta 5	Sta 6
NRMSE, %	10.09	6.74	8.15	6.13	6.14	7.33
NMAE, %	8.53	5.11	5.93	5.04	4.74	6.08
R^2	0.916	0.970	0.979	0.981	0.974	0.9702
Bias, m/sec	0.053	-0.041	0.123	-0.027	0.0244	0.0816

As stated in Chapter 1, validation is the process of determining whether the governing equations represent the physics of the specific problem studied. When a single time-series measurement is used for calibration, the comparison between measured and computed values cannot be considered validation. However, if a model is reasonably calibrated using several measurement locations and variables such as water levels, velocities, fluxes, etc, it is then arguable that the calibration results also serve to demonstrate the model validity since it would be highly improbable, if not impossible, to obtain a good agreement at several locations for all variables without the model representing the physics of the problem being studied accurately. A reasonable calibration is one which uses few calibration parameters and uses parameters within physically meaningful or previously reported limits. Rigorous validation requires that the calibration dataset be separate and independent of the calibration dataset. However, in coastal hydrodynamics, this can be difficult due to limited data and the fact that different study periods may have significantly different geometries due to changing bathymetry and physics (tidal vs wind- and wave-induced currents, stratified vs non-stratified, time varying bed composition and friction, exposed vs unexposed hard bottom, etc.).

4.3.5 Conclusions and recommendations

The CMS performance in simulating tidal hydrodynamics at a coastal inlet in the presence of wave and wind was tested for Grays Harbor, WA, using field measurements of water levels and current velocities. Water levels and depth-averaged principle current velocities were compared at several stations and four goodness-of-fit statistics were used to assess the model performance. In general, the model results agree well with measurements. Although the model ramp period was only 24 hr, the time period for the model hydrodynamics to reach dynamic equilibrium in the bay (i.e., to fully spin-up) was approximately 250 hr. The model results demonstrate that it is reasonable to use large time steps, on the order of 15 min, for similar tidal inlet hydrodynamic studies. Using such a large time step will however, reduce the accuracy of the wetting and drying. If this is considered to be an important aspect of the study, than a smaller time step may be more adequate.

4.4 Test C3-Ex3: Ocean Beach, CA

4.4.1 Purpose

A hydrodynamics, wave, and sediment transport modeling study was conducted to evaluate a designated dredged-material placement site in the nearshore along a beach erosional hot spot, and to evaluate onshore nourishment alternatives at Ocean Beach, CA. A wide range of field data, including shoreline change, water levels, waves, current, and topographic mapping, have been collected by the San Francisco District (SPN) and the United States Geological Survey (USGS) at Ocean Beach and in San Francisco Bight from 2004 through 2010. For this application, the offshore bathymetry data were obtained from GEOphysical DAta System (GEODAS) database, which has been developed and managed by the National Geophysical Data Center (NGDC) of NOAA.

4.4.2 Model setup

Figure 44 illustrates the entire CMS domain and bathymetric features of San Francisco Bay, San Francisco Bight, and adjoining nearshore areas. The model domain extends approximately 80 km alongshore and 60 km offshore, and the offshore boundary of the domain reaches to the 80-m isobath. The grid system has a non-uniform Cartesian grid of 287 by 341 cells and permits much finer resolution in areas of high interest with a cell size of 20 by 20 m such as in front of Ocean Beach and the Golden Gate Channel, with larger cells offshore equal to 400 by 400 m. The depth contours from the combination of the SPN/USGS and GEODAS datasets show that the depth range in the San Francisco Bay is from 0 to 40 m relative to Mean Sea Level (MSL) and the maximum depth in the Golden Gate channel is more than 110 m. The ebb-tidal delta is located offshore of the Golden Gate Bridge.

The forcing datasets required by the CMS come from a variety of sources. The time-dependent water surface elevation data at open boundary locations were specified through water level observations at Point Reyes (NOAA 9415020) and Port Chicago (NOAA 9415144), CA. Time varying wave spectra and wind forcing data were retrieved from the offshore NDBC Buoy 46026 (Figure 45).

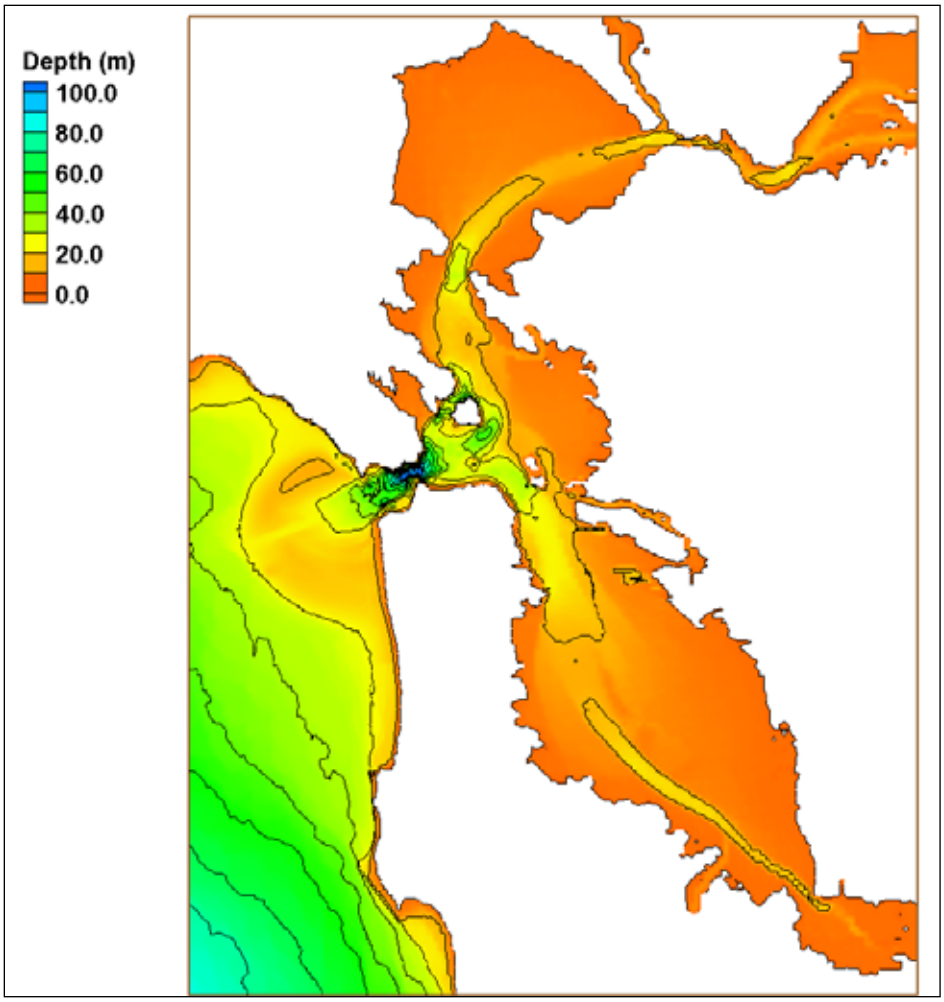

Figure 44. CMS domain in San Francisco Bay and San Francisco Bight.

Figure 45. Tidal gages and buoy locations used as model forcing for the Ocean Beach, CA test case.

Three ADCPs were deployed to collect current and water level data nearshore along Ocean Beach (Figure 46). Even though the Bay is partially stratified, the measurements used in this study were located outside of the bay near Ocean Beach in shallow water where the stratification is weak. The water depths of the measurement stations 1, 2, and 3 were 7.5, 10.9, and 14.1 m, respectively.

Figure 46. ADCP stations at Ocean Beach.

The explicit time marching scheme of the CMS is used for this application and the basic model parameters are listed in Table 37. A 20-hr spin-up period was sufficient for this study since the measurement stations were located outside of the bay.

Table 37. CMS-Flow model parameters for the Ocean Beach, CA test case.

Parameter	Value
Solution scheme	Explicit
Hydrodynamic time step	0.3 s
Simulation duration	10 day
Ramp period duration	12 hr
Manning's n	0.025 sec/$m^{1/3}$
Horizontal mixing scheme	Falconer
Wetting/drying depth	0.05 m
Steering interval	3 hr

4.4.3 Results

The calculated results are compared with the measured data at those locations during a 10-day simulation period from 20-29 June 2005. Figure 47 shows water surface elevation comparisons at Site 3. Both the observations and the calculations show mixed and predominantly semi-diurnal tidal signals. The calculated tide at this location has a good agreement with the measurements both in amplitude and phase. The correlation coefficient between the CMS and the data is 0.988, the RMSE is 0.107 m, and the NRMSE is 3.8 percent.

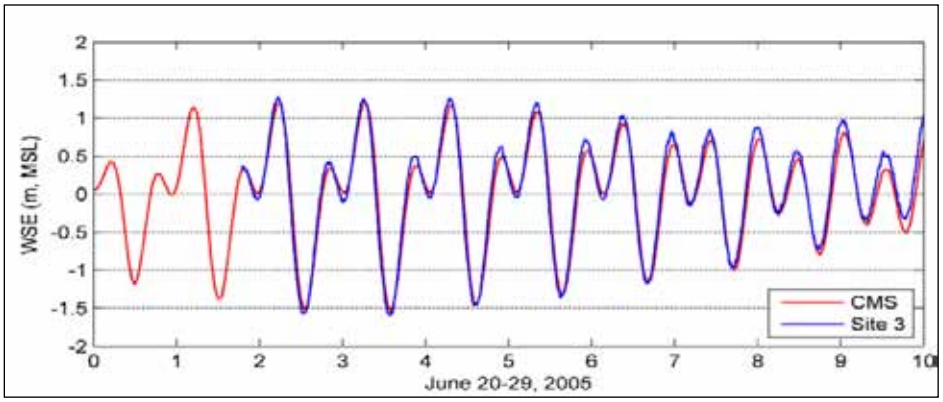

Figure 47. Measured and calculated water surface elevation at Site 3 for the Ocean Beach, CA test case.

Current comparisons at Sites 1, 2, and 3 are shown in Figure 48. The tidal current is predominantly alongshore, and the cross-shore component is relatively small. Nearshore current measurements show that the depth-averaged flood and ebb velocity magnitudes can be as large as 1.0 to 1.5 m/sec in the northern part of Ocean Beach (Site 1), adjacent to the Golden Gate entrance. The current magnitude decreases towards the south along Ocean Beach. CMS simulation results are in good agreement with the current measurements at all of the three sites, as demonstrated by the correlation coefficient, RMSE and NRMSE provided in Table 38.

4.4.4 Conclusions

The CMS calculations are validated by the measured water surface elevation and current in the San Francisco Bight. The results show that there is excellent correlation and a relatively small NRMSE of 8.4 to 11.7 percent between the model output and the ADCP measurements. The coupled waves and current calculations demonstrate a successful application of CMS in this high wave energy and strong tidal current region.

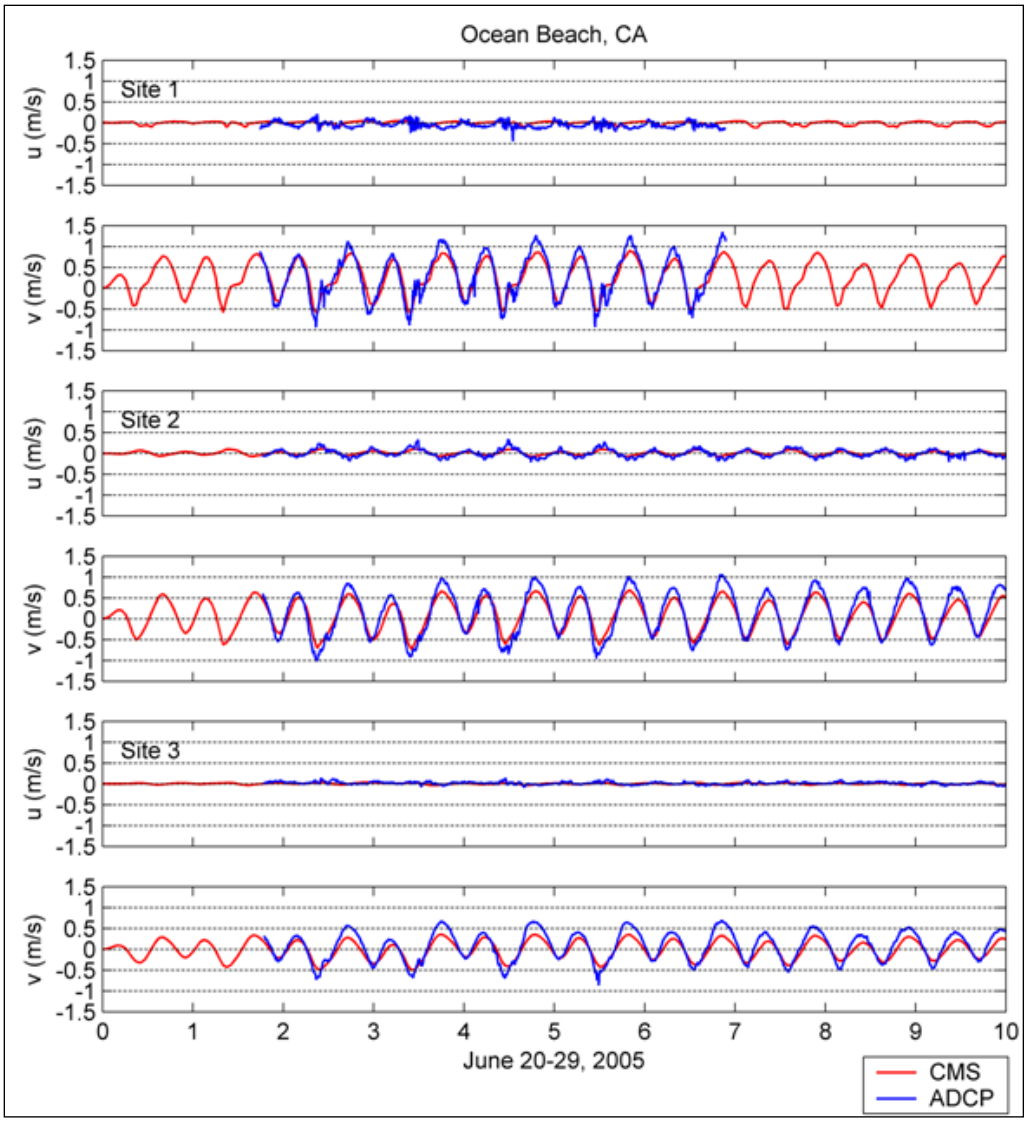

Figure 48. Measured and calculated current velocities at Sites 1, 2, and 3 for the Ocean Beach, CA test case.

Table 38. Longshore current goodness-of-fit statistics* for the Ocean Beach field test case.

Statistic	Station		
	1	2	3
R	0.960	0.966	0.963
RMSE, m/sec	0.176	0.199	0.164
NRMSE, %	8.4	11.1	11.7

*defined in Appendix A

4.4.5 Recommendations

With the default horizontal eddy viscosity scheme and bottom friction parameters, the calibrated and validated hydrodynamic results can be applied to conduct dredge and navigation related sediment transport and morphology change in coastal regions.

4.5 Test C3-Ex4: St. Augustine Inlet, FL

4.5.1 Purpose

The CMS performance in simulating tidal inlet hydrodynamics was tested using measured water levels and currents at St. Augustine Inlet, FL, in a study of mid-term evolution of the ebb tidal shoal in response to mining (U.S. Army Engineer District, Jacksonville 2010). This section presents the setup and validation of CMS to hydrodynamic measurements; validation of morphology change at St. Augustine Inlet is documented in Sánchez et al. (2011). Full documentation of the study is provided by U.S. Army Corps of Engineer Jacksonville District (2010).

4.5.2 Model setup

Two CMS model grids were developed for representing St. Augustine Inlet, one for CMS-Wave and the other for CMS-Flow and sand transport. The lateral extent of the CMS-Flow grid was determined through initial calibration of the hydrodynamics to resolve the appropriate bay boundaries for comparison to the measured tidal prism. Additionally, the lateral extent of the model domain was defined to include several focus areas of shoreline to the north and south of the inlet. The cross-shore distance of the CMS-Flow grid was set to the same location as the CMS-Wave grid, which was set to the offshore location of the contour depth of the forcing (wave data). Therefore, the resultant two grids cover the same alongshore distance of 23.5 km, and a cross-shore distance of 9 km, extending from the land seaward to the ocean boundary. The finest resolution of the model grid cells were set to 15 m in the inlet throat, and 30 m in the main bay channels, ebb-tidal delta, and nearshore. Maximum cells sizes in the bay reached 120 m over large open bay expanses, and increased to 240 m along the offshore boundary (Figure 49).

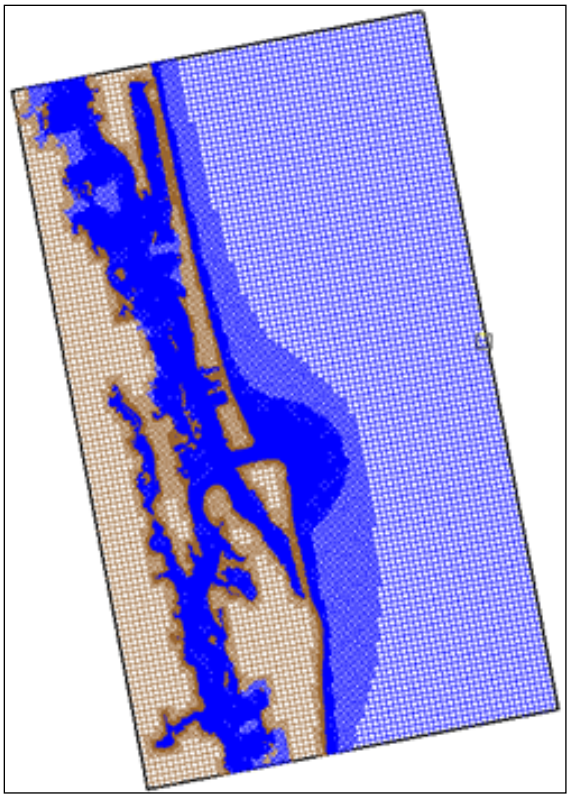

Figure 49. CMS-Flow grid for St. Augustine Inlet, Florida.

The inline version of CMS-Flow was applied in this study which contains CMS-Flow and CMS-Wave within a single code for model efficiency. Each CMS grid was forced along the ocean boundary. CMS-Wave was not included in the hydrodynamics calibration due to a lack of wave data for the calibration modeled time period. The forcing in the CMS-Flow grid for this project was a water-surface elevation as defined by tidal constituent forcing for the full perimeter of the ocean boundary. The vertical datums of the model grids were set to mean sea level. The tidal constituents used were developed by NOAA for the present epoch (1983-2001) for the St. Augustine Beach gauge (Station ID# 8720587, Figure 50).

The extent of the grid in the bay was determined by an iterative process to recreate the bay tidal prism. Because the bay system includes a secondary inlet to the south, Matanzas Inlet, there is some uncertainty involved in delineating the boundary for tidal prism between the two inlets. Calibration to both water levels and spatial current velocities was necessary to approximate this delineation of alongshore grid length, which was ultimately selected as 23.5 km. Following this, further calibration of the bottom friction, or Manning's n, was applied to account for bridge piling locations

Figure 50. Location of water level ocean forcing gauge (St. Augustine Beach Pier), and validation measurements (Vilano Beach Pier and St. Augustine Municipal Marina).

and lag effects from the marsh and extensive lateral shape of the bay (Figure 51). This modification of Manning's *n* also addressed an over prediction of flood currents in the inlet throat which improved significantly the predicted velocity magnitudes and phase spatially through the inlet throat. Winds were not included because they do not generate significant currents or waves in the bay due to limited fetch.

The model run was set for a ramp period of 6 hr, which is more than is needed typically for implicit model runs. The hydrodynamic time step was 5 min, which was found to be sufficiently short enough to capture the tidal circulation within the bay. Table 39 summarizes the CMS-Flow setup parameters.

4.5.3 Results and discussion

Calculations from 7-9 April 2010 serve as the calibration period. Because there are no other available recent (within the last decade) measurement periods, hydrodynamics are calibrated and then validated with two different

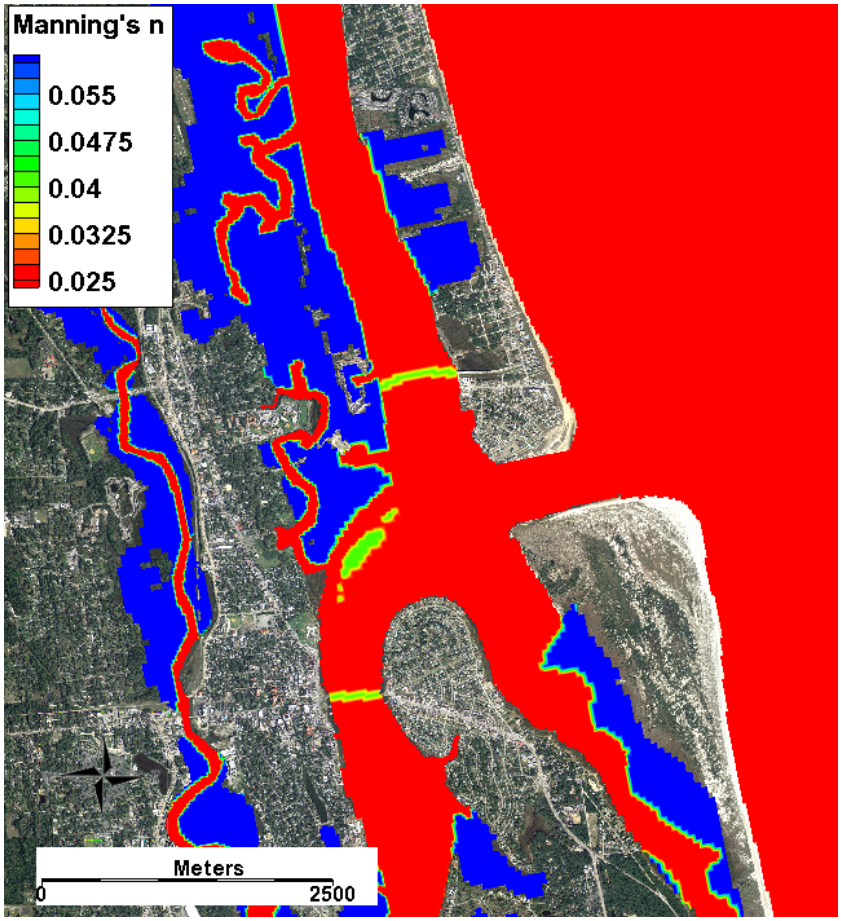

Figure 51. Variation of Manning's n in the back bay and river reaches of the CMS-Flow St. Augustine Inlet grid.

Table 39 CMS-Flow setup parameters for the St. Augustine Inlet field test case.

Parameter	Value
Solution scheme	Implicit
Simulation duration	2 days
Ramp period duration	6 hours
Time step	5 min
Manning's coefficient	0.025 – 0.06 sec/$m^{1/3}$

measurement datasets from the same period. Calibration of the CMS for St. Augustine Inlet was completed in two parts: first, through comparison of measured and calculated hydrodynamics discussed here, and second, through comparison of morphologic end-states discussed in Sánchez et al. (2011). The hydrodynamics were calibrated through comparing measurements of water level and currents collected from 7-9 April 2010 to a simulation that was forced with the measured open ocean tide, at the St. Augustine Beach Pier (see Figure 49).

Water levels measured at the St. Augustine Municipal Marina and Vilano Beach Pier by the two H-ADCP gauges are illustrated as red and green points, respectively in Figure 50. Peak measurements at the St. Augustine Municipal Marina show inconsistency, likely due to the proximal location to bridge-related construction and boat traffic. Other than these small fluctuations, water level measurements for the two day measurement period had similar peaks and range in comparison to the offshore measurements which were used for the CMS forcing for initial calibration. Measurements from two current meters were also part of the calibration to water level and currents. They were equipped with pressure gauges to measure water level and were deployed at fixed locations within 1 to 2 km of the inlet entrance channel and covered 50 to 70 m across the deepest part of the Tolomato River and the Matanzas River (Figure 50). Measured water levels were not correlated to a benchmark, and therefore, can only be compared to model calculations with demeaned (averaged to represent a zero mean) water levels. The measured horizontal current profiles provided temporal resolution for comparison to the calculated current velocity, and are discussed by U.S. Army Engineer District, Jacksonville (2010).

Figures 52 and 53 show a comparison between the measured and calculated water levels at the two bay gauges. The correlation coefficient, or R^2 values, between measurements and calculated results are 0.82 for the St. Augustine Municipal Marina gauge, and 0.93 for the Vilano Beach Pier gauge.

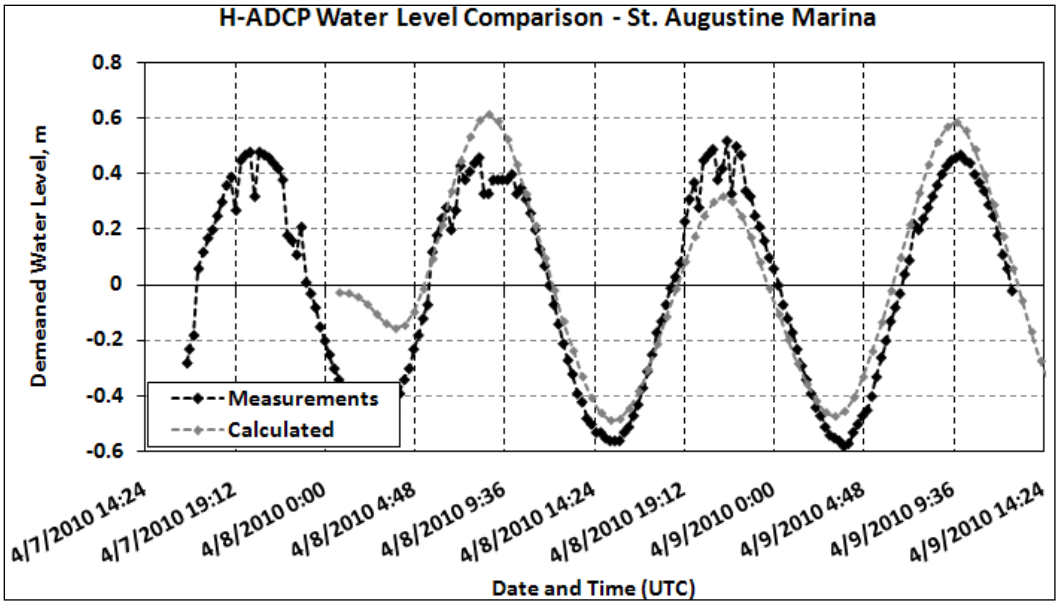

Figure 52. Measured and calculated water levels at St. Augustine Marina from 7-9 April 2010; R^2=0.82 (see Figure 50 for location).

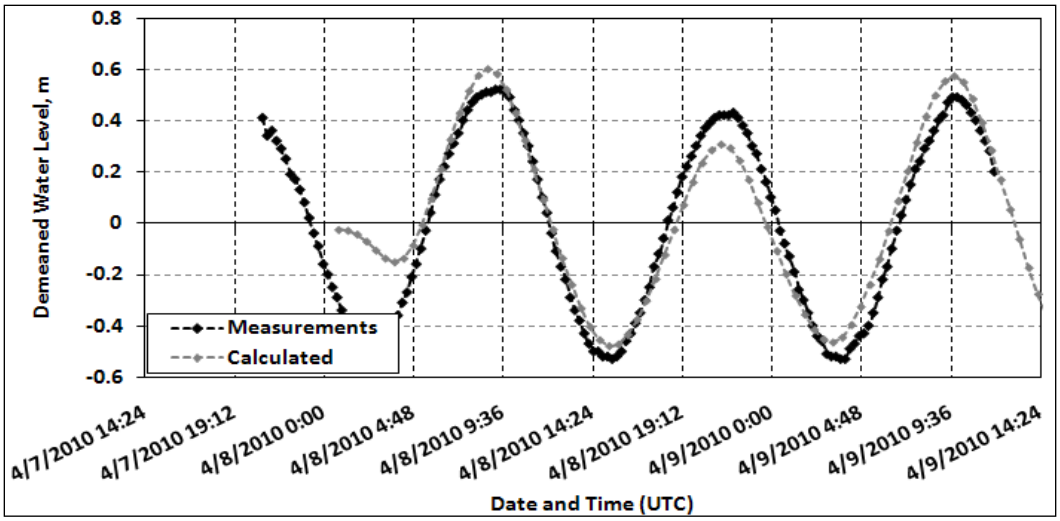

Figure 53. Measured and calculated water levels at Vilano Beach Pier from 7-9 April 2010, R^2=0.93 (see Figure 50 for location).

Hydrodynamics were further calibrated to current measurements collected by a boat-mounted, downward-looking acoustic Doppler current profiler (D-ADCP). The measurements compared here include depth-averaged currents across inlet throat cross-sections and several channel transects, as illustrated in Figure 54. Measurements, including two ebb-shoal transects and three inlet throat cross-sections, were made at the end of an ebbing cycle. At the beginning of the flood cycle, transects were made over the northern Tolomato River and southern Matanzas River main channels. Four inlet throat cross-sections were made at or close to capturing peak flooding currents.

Roaming vertical profiles of ebb and flood currents were also measured across reaches of the two rivers, through the inlet entrance, and over the ebb-tidal delta, and were used to calibrate the spatial distribution of current velocity. These profiles are compared to the modeled currents below in Figures 55-60 and serve as the primary calibration measurements because of the strong correlation between current velocities over the ebb shoal and the resulting sediment transport as discussed in Sanchez et al. (2011).

Inlet throat cross-section measurements show good agreement with the calculated measurements, resulting in a NMAE of 1 to 12 percent for ebbing currents (Figures 55 and 56). The velocity profile in Figure 55 shows the strong currents near the inlet throat decreasing.

Comparison between measurements and calculated agreed with a NMAE of 4 to 8 percent for flooding currents (Figures 57 and 58).

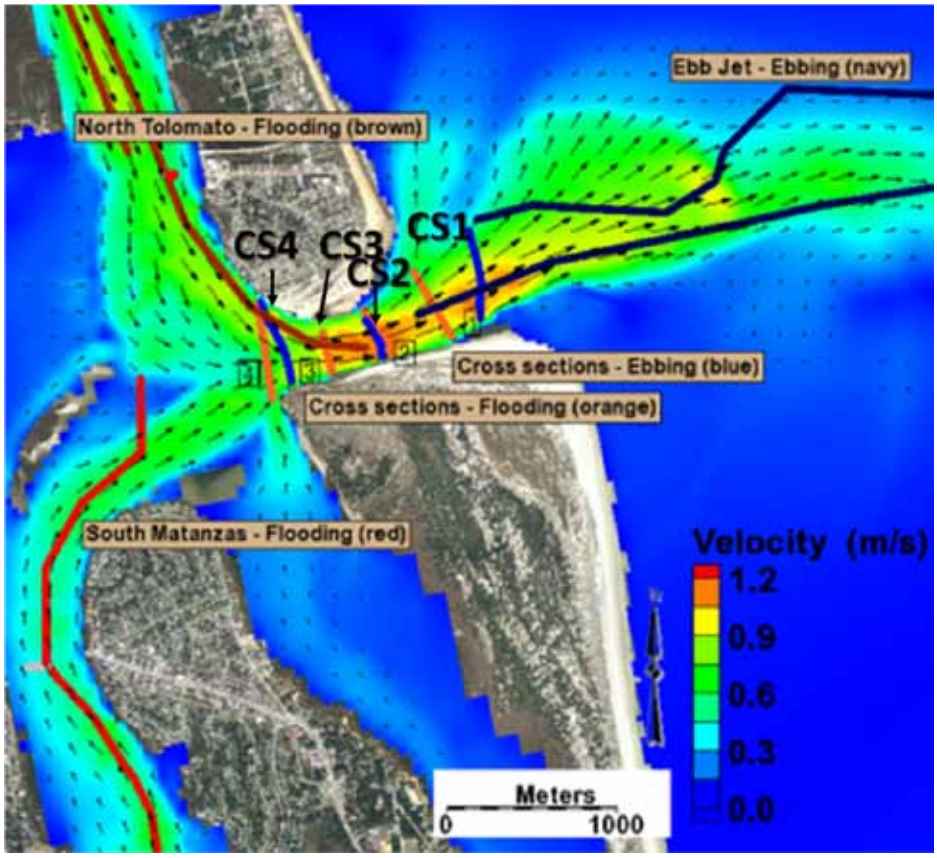

Figure 54. Location of roving D-ADCP transects at St. Augustine Inlet, FL, on 9 April 2010.

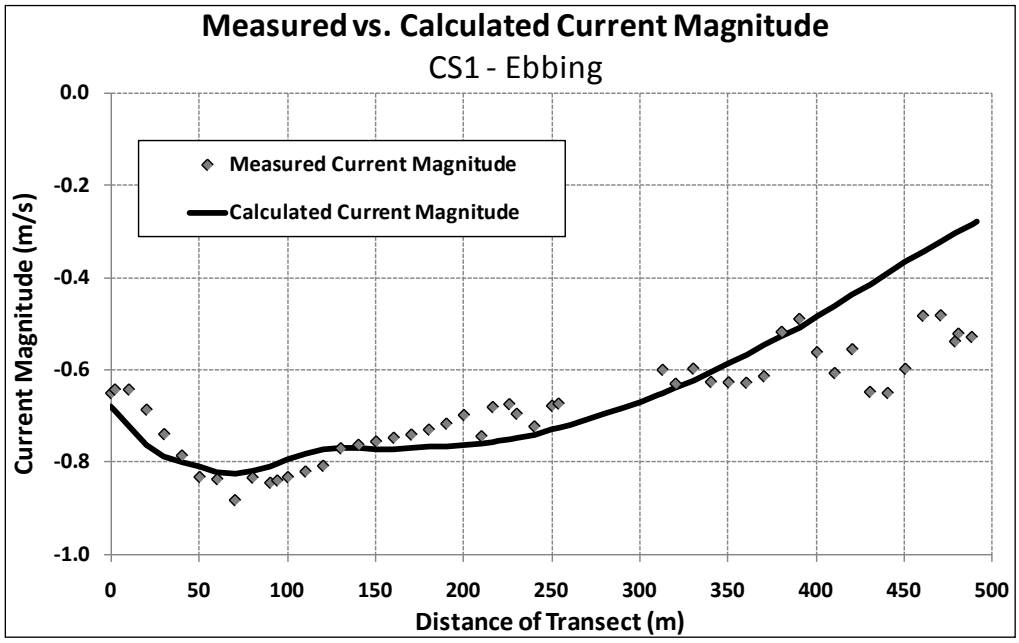

Figure 55. Measured and calculated current speeds for CS1 on April 9, 2010 during an ebbing tide; model time: 14:40; measurement time: 14:14, distance is measured from south to north.

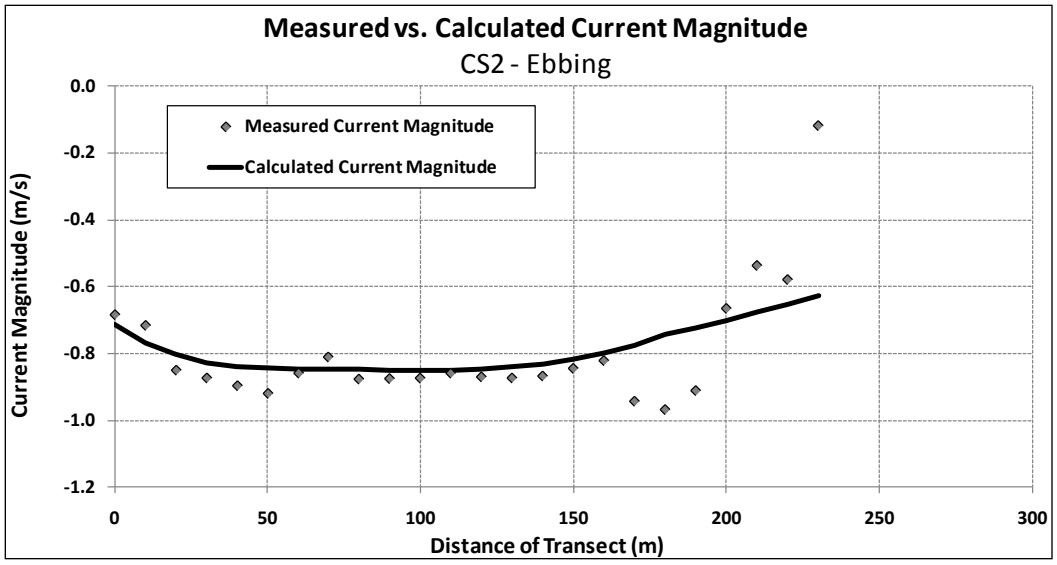

Figure 56. Measured and calculated current speeds for CS2 on 9 April 2010 during an ebbing tide; model time: 14:40; measurement time: 14:04, distance is measured from south to north.

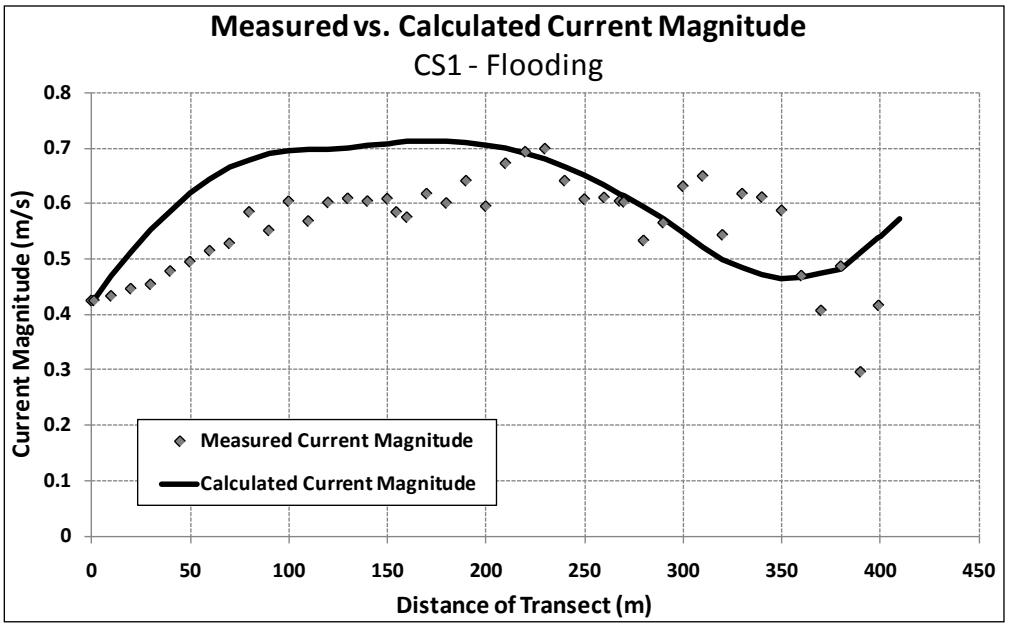

Figure 57. Measured and calculated current speed for CS1 on 9 April 2010 during a flooding tide; model time: 20:00; measurement time: 20:18, distance is measured from south to north.

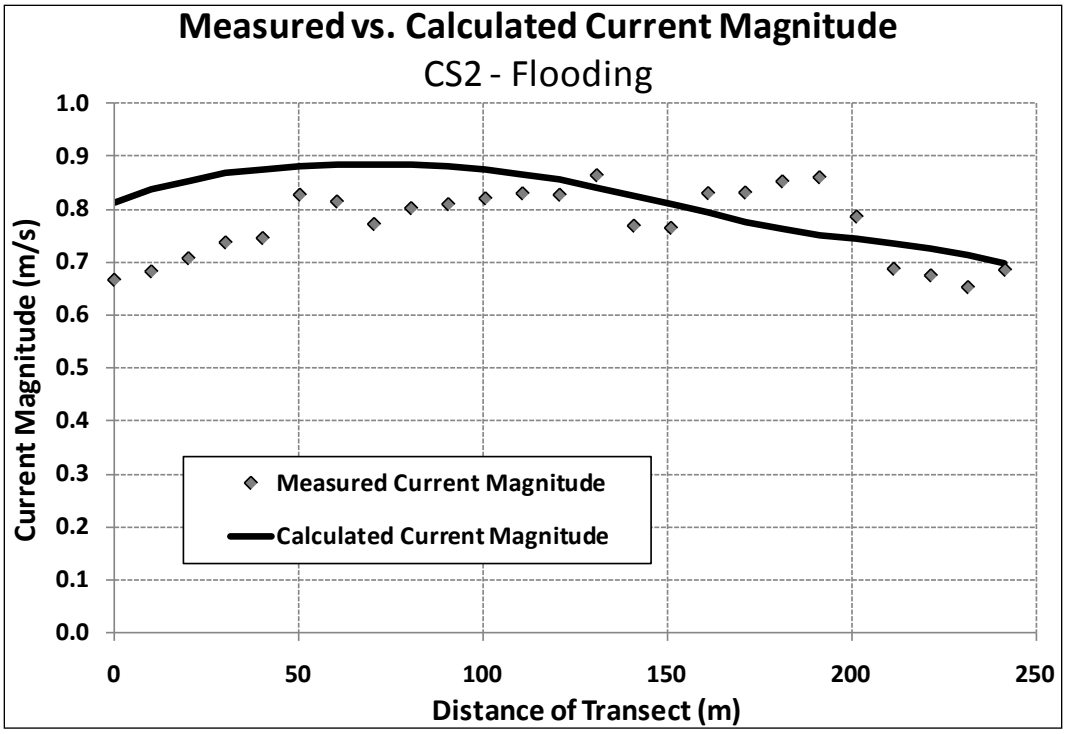

Figure 58. Measured and calculated current speed for CS2 on 9 April 2010 during flooding tide; model time: 20:00; measurement time: 20:26, distance is measured from south to north.

A set of two transects over the ebb shoal trace the main ebb jet through the channel and over the northern lobe of the shoal is shown in Figures 59 and 60. The measured and calculated currents speeds have a NMAE of 8 to 18 percent.

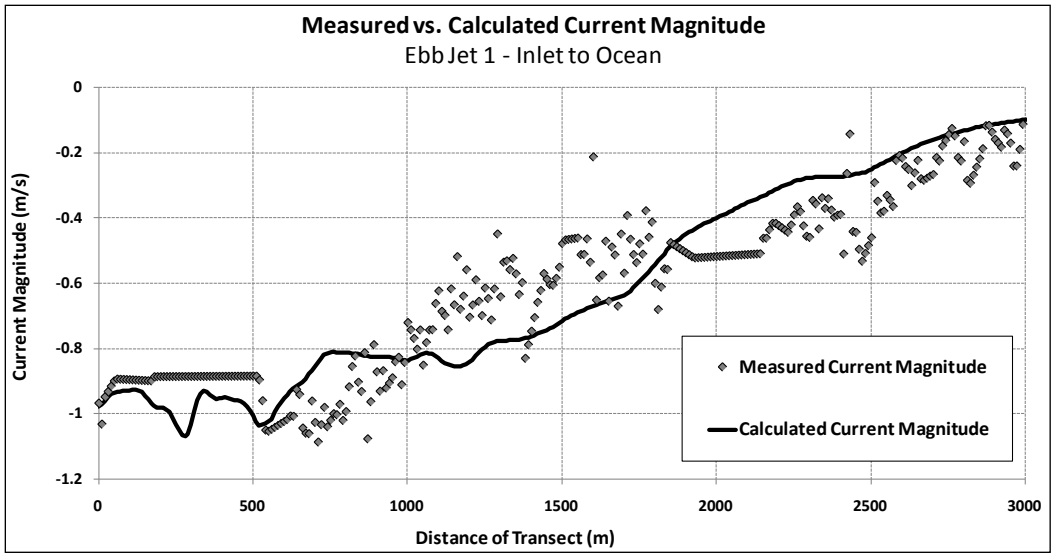

Figure 59. Measured and calculated current speeds for Ebb Jet 1 on 9 April 2010 during an ebbing tide; model time: 12:10; measurement time: 12:48, distance is measured from west to east.

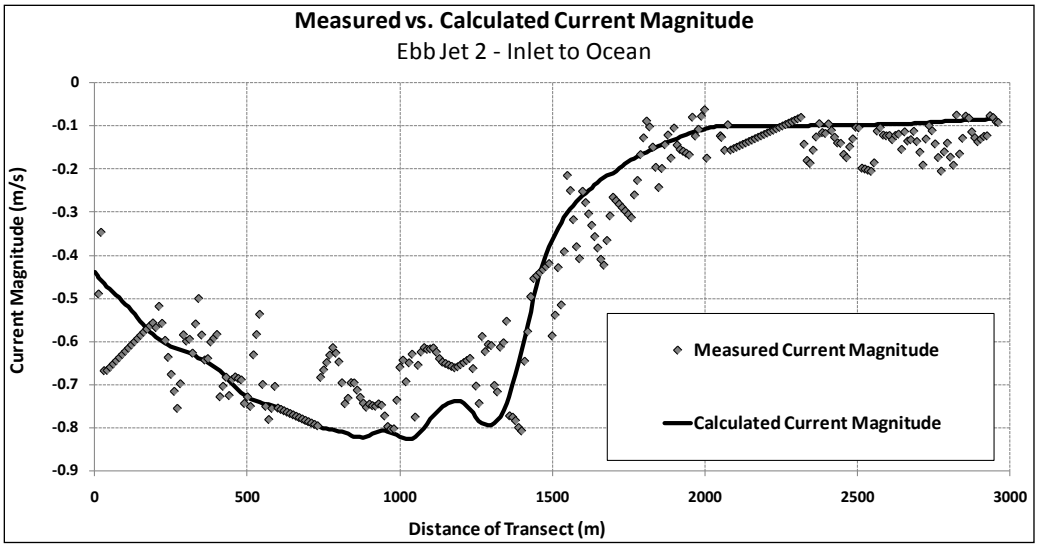

Figure 60. Measured and calculated current speed for Ebb Jet 2 on 9 April 2010 during an ebbing tide; model time: 12:30; measurement time: 13:12, distance is measured from west to east.

Additional model comparisons with D-ADCP transects within the bay can be seen on the CIRP wiki website at http://cirp.usace.army.mil/wiki/. The high correlation between the measurements and the calculations illustrates the degree of calibration of the model. Also, modeled currents do not include waves and yet still capture the ebb jet trends, illustrating the dominance of tidal driven flow over the ebb shoal. In summary, the model is able to reproduce the current speed within 20 percent of measured values.

4.5.4 Conclusions

The CMS was applied to a coastal inlet with tidal forcing. Calculated water levels agreed with two measurement locations with a correlation coefficient R^2 equal to 0.82-0.93 for the two measurement gauges. Measurements were made within the inlet throat, across the ebb shoal, and in the bay, totaling 12 transects, on 9 April 2010. These transects included three within the inlet throat and two across the ebb shoal during ebb flow, and three within the inlet throat and four within the bay on flood flow. Ebbing transects had normalized errors between calculated and measured values ranging from 1 to 11 percent for the inlet throat and 8 to 18 percent across the ebb shoal. For flooding transects, normalized errors ranged from 4 to 8 percent through inlet throat and up to 20 percent for bay transects during flood tide. This application demonstrates the ability of CMS to accurately calculate water level and current within a tidally-dominated inlet system.

4.6 Test C3-Ex5: Shark River Inlet, New Jersey

4.6.1 Purpose

The CMS performance was tested with water levels and currents at Shark River Inlet, NJ. Water level data from Belmar, NJ, a site within Shark River Estuary (Figure 61), were compared to CMS calculations for a 10-day period from 15-25 August2009. Peak currents across three channel transects within the throat of Shark River Inlet measured during a complete tidal cycle on 20 August 2009 were also compared to CMS simulation results. The implicit time marching scheme of CMS-Flow was used and the model was forced with water level measurements at the Sandy Hook ocean tide gauge. Water level measurements at the Belmar tide gauge were used for model calibration. The case is useful for testing the CMS hydrodynamic performance for a relatively small bay and dual-jettied entrance. This test case is borrowed from Beck and Kraus (2010), where study details are available for interested readers.

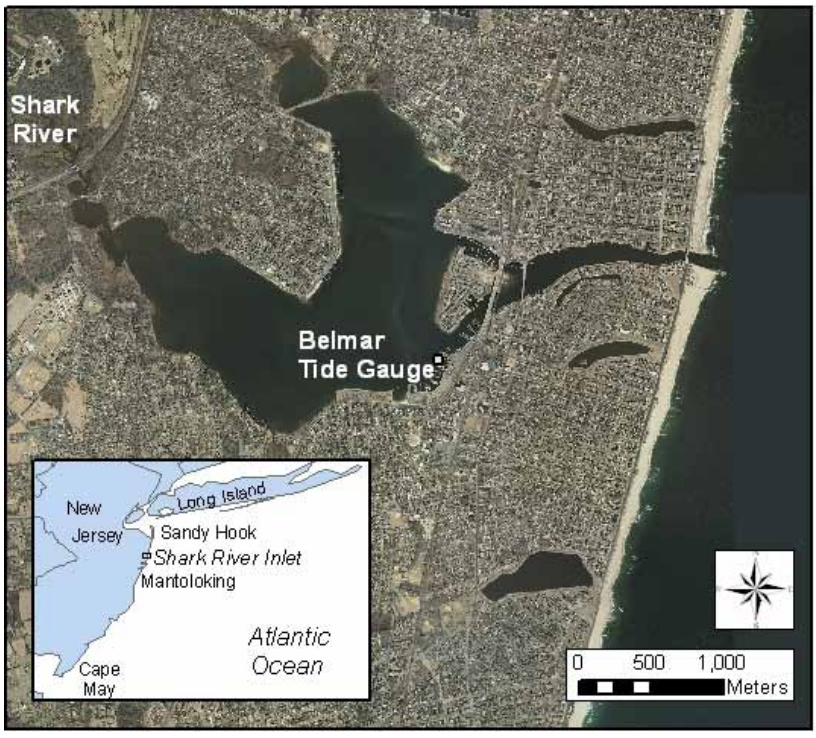

Figure 61. Location map for Shark River Inlet, NJ showing the Belmar tide gage.

4.6.2 Model setup

The CMS-Flow model grid domain covered a local scale of approximately 11 km centrally located around Shark River Inlet (Figure 62) with a cross-

shore distance covering the backbay and extending seaward 3.5 km. The grid was oriented to the shoreline at an 11 deg angle to North. The telescoping grid was developed with 8-m cell resolutions within the main throat of the inlet, extending out to 128-m cell size in the ocean. Resolution around the groins north and south of the study area and beach was kept to a 16-m cell size, bringing the ocean cell total to 20,000 cells.

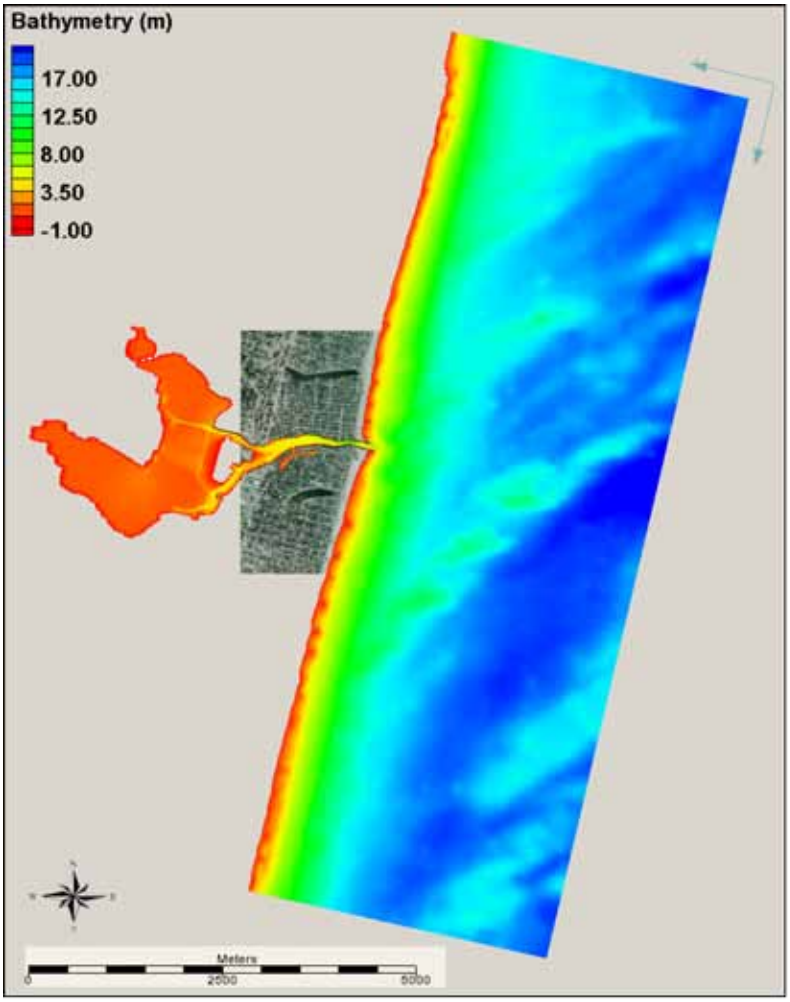

Figure 62. CMS model domain for the Shark River Inlet, NJ test.

Bathymetry needed to develop the model grid for the backbay, entrance channel, and ocean was assembled from several datasets and converted to mean sea level (MSL) as given by the local tidal datum for Long Branch, NJ (NOAA). Bay bathymetry consisted of data collected by the USACE and New Jersey State, as well as data collected during the August 2009 field measurements. The nearshore and ocean bathymetric datasets were a combination of 2005 LIDAR (NOAA) and the National Geodetic Data

Center's Coastal Relief Model (NOAA) at a spatial resolution of 3 sec geographic coordinates. CMS-Flow was driven with measured open ocean tide from a tidal gage at Sandy Hook, NJ, approximately 30 km north of Shark River Inlet. Table 40 show parameters used to set up CMS for this application.

Table 40 CMS-Flow setup parameters for the Shark River Inlet, NJ field test case.

Parameter	Value
Solution scheme	Implicit
Simulation duration	Tidal cycle ~10 days
Ramp period	12 hour
Time step	15 min
Manning's n coefficient	0.025 – 0.06 sec/m$^{1/3}$

Due to the constricted nature of the main channel for Shark River Inlet from multiple shoals and bridge crossings, Manning's *n* was modified at discrete locations of the grid. Three bridges cross the channels, two of which cross the north and south split bay channels, have more than five pilings each, and are situated over shallow shoals covered in oyster beds. To account for this increase in friction at these locations, the Manning's *n* was increased to 0.06 sec/m$^{1/3}$ for a series of 3 to 5 rows of cells (Figure 63). The inclusion of this extra frictional factor improved the current velocity calibration through each channel.

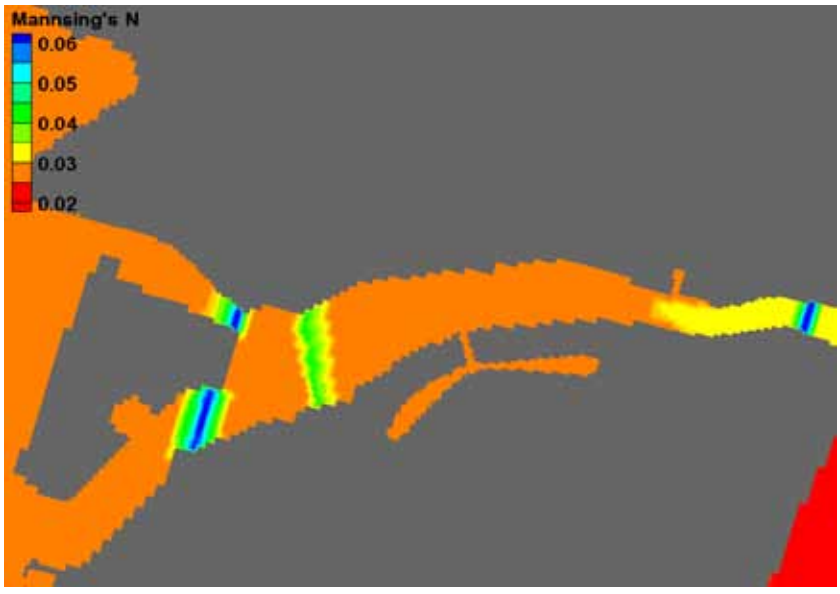

Figure 63. Manning's roughness coefficient in the main, north, and south channels of Shark River Inlet, NJ.

4.6.3 Results and discussion

The study was completed in two parts: first, through comparison of measured and calculated hydrodynamics discussed herein, and second, through comparison of channel infilling rates and morphologic patterns (see Sánchez et al. 2011, Report IV). Water level comparison of the results was done by sampling the location of the Belmar bay gage, plotted in SMS, and then exported to another program (Microsoft Excel) to compare to measured water levels. Figure 64 shows the water level forcing from Sandy Hook, and measured and calculated at Belmar. Table 41 compares the tidal constituents derived from each of these tidal signals, and shows good calculation of tidal amplitude and phase. The NMAE for the amplitude and phase are 2 and 20 percent, respectively.

Beck and Kraus (2010) compared measured and calculated current velocity at peak flood in the three main channels (Figures 65 and 66). The measurements were collected near the split from the main channel to form the north and south reaches to calibrate the actual volumes of water moving through each reach. Manning's *n* coefficient was modified around the bridges to account for the presence of piles. Measurements and calculations show close correspondence for the main channel (CS1) and south channel (CS3) with a NMAE of 3 to 5 percent, and a NMAE of 9 percent for the north channel (CS2) (Figure 66).

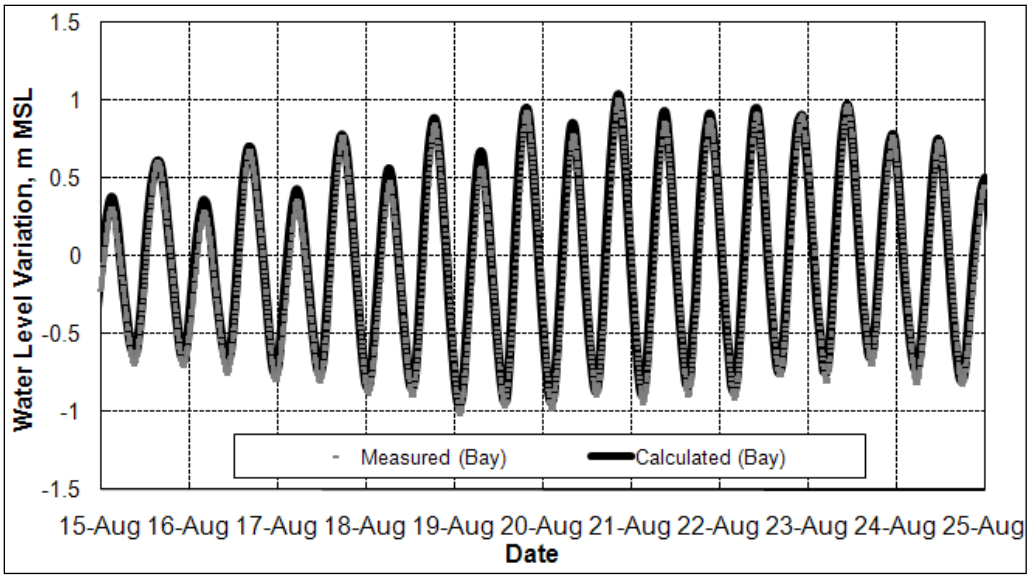

Figure 64. Measured water level at Sandy Hook and Belmar (Bay) and calculated water level at Belmar

Table 41. Measured and calculated tidal constituents at Sandy Hook and Belmar*.

	Measured				Calculated Belmar	
	Sandy Hook		Belmar			
Constituent	Amplitude, m	Phase, deg	Amplitude, m	Phase, deg	Amplitude, m	Phase, deg
Q1	0.014	303.3	0.014	307.5	0.011	310.3
O1	0.06	63.8	0.062	67.6	0.054	74.5
K1	0.105	120.2	0.109	126.3	0.09	133.6
N2	0.170	87.2	0.150	95.56	0.13	109.9
M2	0.687	139.5	0.599	201.2	0.561	213.3
S2	0.145	283.1	0.123	297.0	0.115	311.2
M4	0.022	295.2	0.021	322.4	0.026	3.0
M6	0.014	296.9	0.020	236.2	0.016	281.7

*Sandy Hook water levels were used as model forcing and therefore the calculated tidal constituents are at this station are equivalent to the measured values.

Figure 65. Location of measured currents on 20 August 2009.

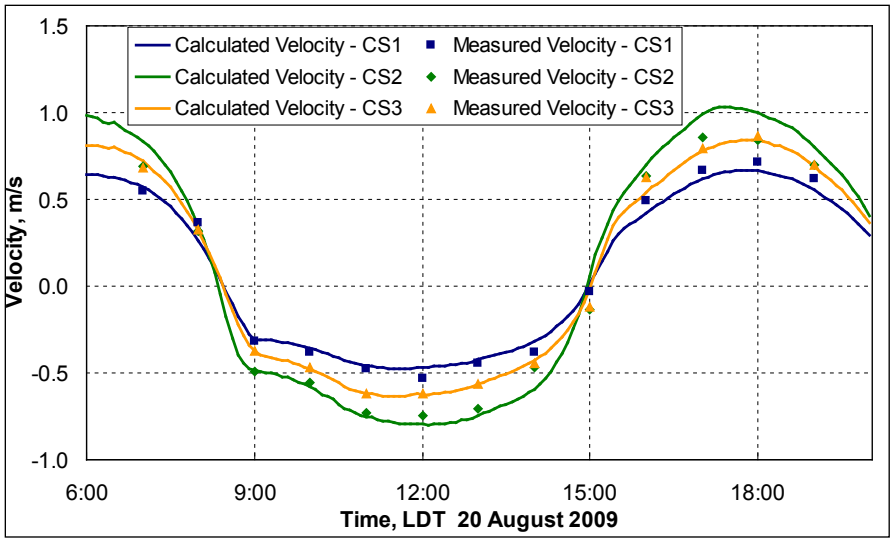

Figure 66. Measured and calculated currents for three channel transects over a tidal cycle on 20 August 2009.

4.6.4 Conclusions

The CMS was applied to a coastal dual-jettied inlet with tidal current forcing provided to CMS-Flow from a gage 30 km north of the project site. Calculated water levels agreed with those measured in the project bay with a NRMSE of 6 percent in magnitude and phase. Currents measured over a tidal cycle for three inlet cross-sections agreed with calculations with a NMAE ranging from 3 to 9 percent. This application demonstrates the ability of CMS to calculate water level and current accurately within a complex tidally-forced inlet system.

4.7 Test C3-Ex6: Galveston Bay, TX

4.7.1 Purpose

The purpose of this validation case is to test CMS performance for tide and wind induced hydrodynamics in Galveston Bay. Measured data, described below, was compared to model results to calibrate and validate the model. Circulation in Galveston Bay is heavily dependent on wind forcing, providing an opportunity to test the capability of CMS to simulate these conditions.

4.7.2 Physical setting and description

Galveston Bay is located on the upper Texas coast adjacent the Houston metroplex with three inlets to the Gulf of Mexico (see Figure 67) and a

federal deep-draft navigation channel from the Galveston Entrance Channel to the Port of Houston in the upper bay. There are numerous tide and meteorological stations across the bay, providing data for model forcing, calibration, and validation.

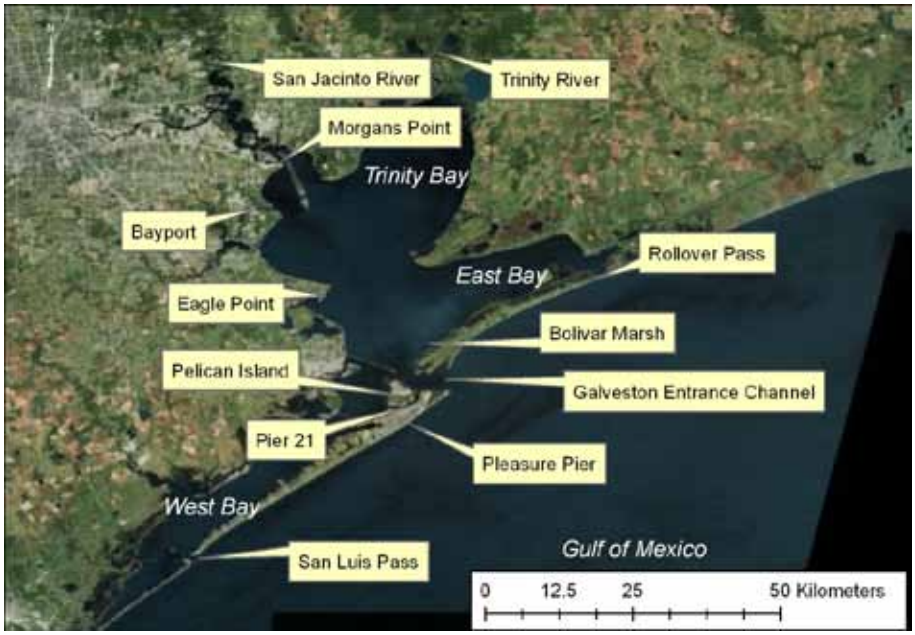

Figure 67. Galveston Bay overview map.

Hydrodynamic data were collected near the Galveston Entrance Channel in 2010 over two time periods; the first was February–March, and the second was in late June. Figure 68 shows data collection stations for the February–March time period (described in URS 2010). Measurements at platforms A–D included currents, waves, and turbidity (calibrated to measure total suspended solids). Additional data measured included passing vessel wake, sediment erodibility, cross-channel ADCP transects, side-scan and multi-beam surveys, and other point measurements of hydrodynamics and sediments.

Data collection stations for the June deployments are shown in Figure 69. ADCP's capable of measuring currents and waves were deployed on instrument pods (PODs 1–3). Complications during data collection caused the loss of both PODs 1 and 2, therefore only POD 3 data are available for model verification. Additional data collected included sediment erodibility, cross-channel ADCP transects, multibeam surveys, and point measurements of suspended sediment concentration and surficial bottom grain size distribution.

Figure 68. Location of data collection stations in the Galveston Entrance and Channel during February – March 2010.

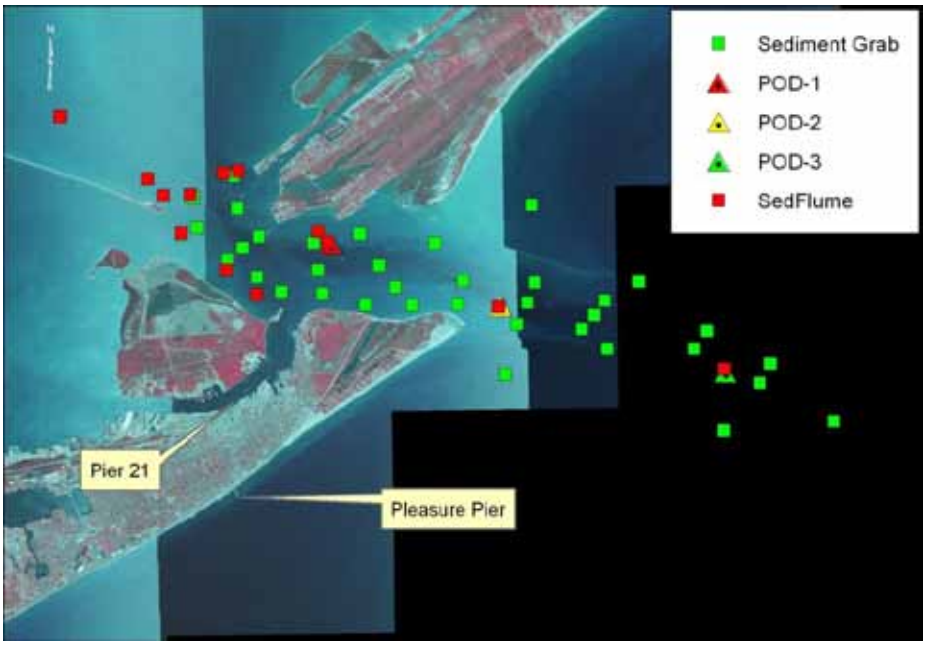

Figure 69. Location of data collection stations in the Galveston Entrance during the June 2010 field study.

4.7.3 Model setup

The computational grid and bathymetry for CMS-Flow is shown in Figure 70. The grid has 121,581 cells with variable resolution from 30 to 1,920 m. A list of basic model setup parameters are shown in Table 42. The implicit time marching scheme was used for this study.

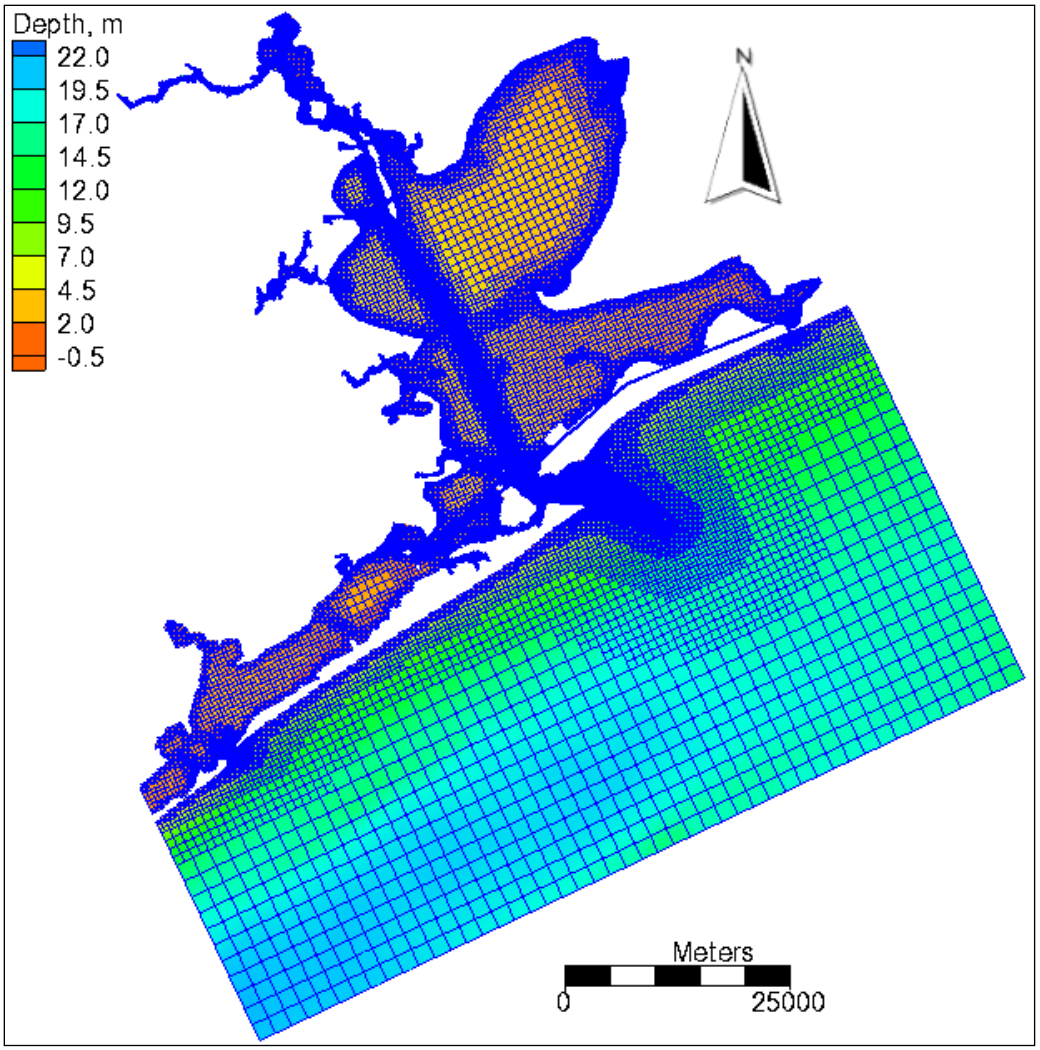

Figure 70. CMS-Flow telescoping grid for the Galveston Bay, TX test case. Colors indicate the local water depth.

Table 42. CMS-Flow general model parameter settings for the Galveston Bay test case.

Parameter	Value
Solution scheme	Implicit
Time step	5 min
Simulation durations	83 hr, 576 hr
Ramp period duration	0.25 hr
Manning's coefficient	0.015 s/m$^{1/3}$

Spatially constant water level measured at Pleasure Pier was applied on the ocean boundary. Temporally varying and spatially constant wind forcing, measured at Eagle Point, was applied. Comparison of winds at

Eagle Point, Pleasure Pier, and Morgan's Point was conducted for the modeled time periods to verify this assumption. A wall boundary condition was used at all boundaries inside the bay. The Manning's coefficient was the only parameter varied for calibration in this study. Freshwater inflow from the two rivers shown in Figure 67 was neglected, because both time periods investigated coincided with low river flows.

4.7.4 Results and discussion

Comparison between measured and calculated water level and currents are presented for model validation at Galveston Bay, TX. Four goodness-of-fit statistics are used to assess the model performance and are defined in Appendix A.

4.7.4.1 Calibration results (February – March 2010)

CMS was calibrated over a period of about 2 weeks between February – March 2010 using data described previously. Calibration was achieved by varying Manning's n until error between model results and measurements was minimized (n = 0.015 sec/m$^{1/3}$ was the best fit). Figure 71 compares NOAA measured and CMS water level at Eagle Point. Figures 72–73 plot measured and modeled currents along the principle axis at two selected data collection platforms (location shown in Figure 68). Statistics representing goodness-of-fit for currents at the data collection platforms and water level at Pier 21 and Eagle Point are listed in Table 43. Overall, the model represents circulation very well, as shown, except for currents between the Galveston and Pelican Islands.

Scatter diagrams of the measured and computed current velocities are available at http://cirp.usace.army.mil/wiki/Galveston. The flow direction was well captured in the entrance channel, but less so in the channel between the islands. Some of measurements in Galveston channel showed the presence of two principle components while the computed velocities showed only one principle component, indicating complex local flow patterns due to local topography. Errors in current direction are associated usually with errors in the bathymetry and lack of grid resolution. In the Galveston channel, the bathymetry is complicated by the shape of berthing facilities and the presence of large vessels.

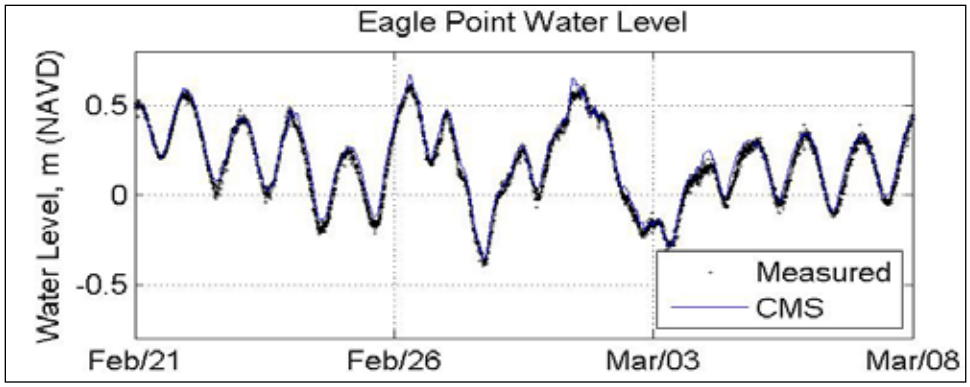

Figure 71. Comparison between CMS and measured water level at Eagle Point.

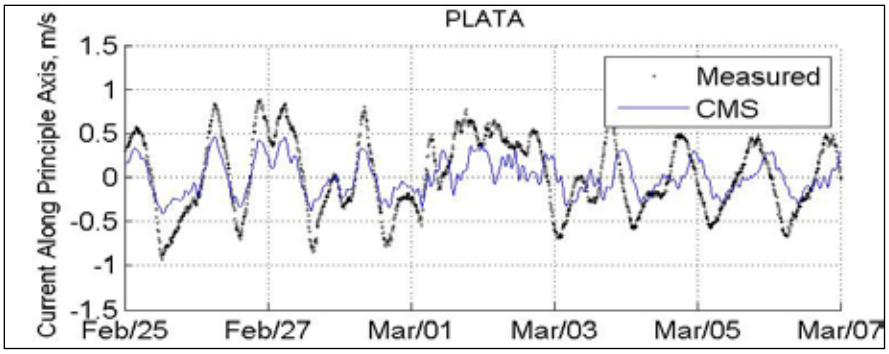

Figure 72. CMS and measured currents along the principle axis at platform A.

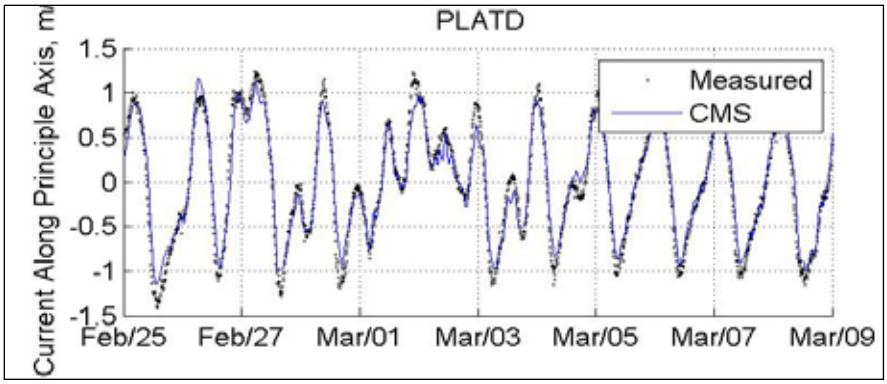

Figure 73. CMS and measured currents along the principle axis at platform D.

Table 43. Goodness-of-fit statistics for currents and water level for calibration.

Station	NRMSE, %	NMAE, %	R^2	Bias
PLAT A	36	30	0.63	-0.01 m/sec
PLAT B	39	28	0.45	0.01 m/sec
PLAT C	39	32	0.26	0.01 m/sec
PLAT D	7	5	0.98	0.00 m/sec
Eagle Point	4	3	0.99	0.03 m
Pier 21	3	3	0.99	0.00 m

4.7.4.2 Validation results (June 2010)

Field measurements from the June 2010 field study were used for validation. The simulation was carried using the same setup parameters as the calibration period (February-March 2010). Figure 74 shows measured and modeled water levels at Eagle Point. Current directions at POD 3 were not well measured due a problem with the instrument making it difficult to make velocity comparisons along the principle axis. Therefore, measured current magnitudes were used for the model result comparison at POD 3 (see Figure 75). Goodness-of-fit statistics for principle currents at POD 3 and water levels at Pier 21 and Eagle Point are presented in Table 44. Additional validation results and plots are available at http://cirp.usace.army.mil/wiki/Galveston.

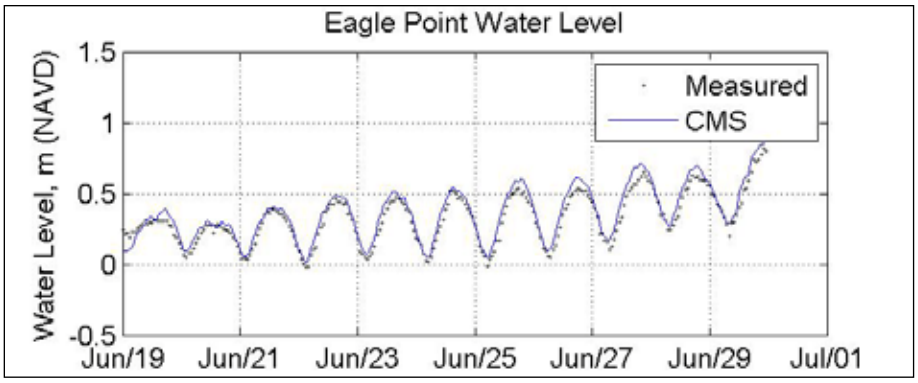

Figure 74. Measured and calculated water levels at Eagle Point for the June 2010 Galveston Bay, TX field study.

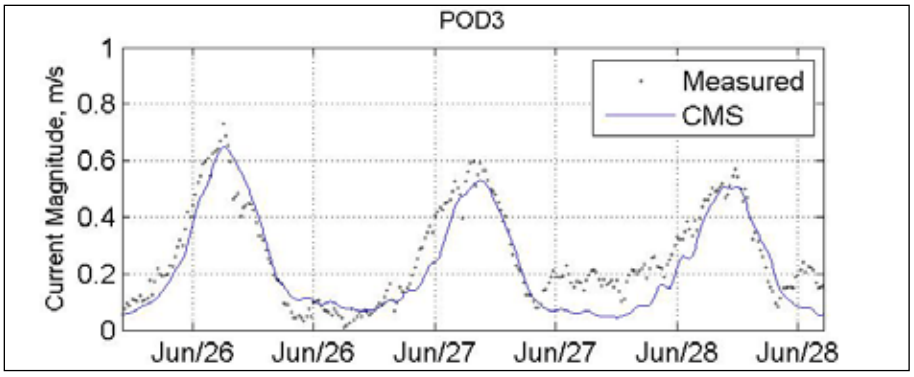

Figure 75. Measured and calculated current speed at POD 3 for the June 2010 Galveston Bay, TX field study.

Table 44. Goodness-of-fit statistics* for the June 2010 Galveston Bay field test case.

Station	NRMSE, %	NMAE, %	R^2	Bias
POD 3	12	10	0.92	-0.04 m/sec
Eagle Point	19	15	0.58	0.01 m
Pier 21	17	14	0.80	0.04 m

*defined in Appendix A

4.7.5 Conclusions

Data collected during two time periods in 2010 were applied to validate the CMS for circulation. Measurements of water level and currents were compared with CMS results at multiple locations including the Galveston Entrance Channel, the channel between Galveston and Pelican Islands, mid- bay, and the Gulf of Mexico offshore of the inlet. CMS was run using default settings. A spatially constant Manning's coefficient was calibrated to n = 0.015 sec/m$^{1/3}$ using measurements from one field study and applied to a separate field study as a validation case. Water levels were well represented at all measurement locations as quantified by the goodness-of-fit statistics in Tables 43 and 44. Measured currents compare well to modeled currents (quantified in Tables 43 and 44), except within the channel between Galveston and Pelican Islands. Between the islands, magnitude of current speed is well captured; however, flow direction and phase are not. Increased resolution in the channel, accounting for the presence of large vessels, may improve results in this area.

4.7.6 Recommendations for practical applications

The following recommendations are offered based on lessons learned during this model application:

Spatially constant wind forcing may be applied for Galveston Bay, TX, for non-storm conditions. Although only Galveston Bay is tested, the same is probably true for other bays of similar or smaller size in Texas. It is recommended that this assumption should be tested for each application and time period by comparing observed winds at multiple stations across the domain. Model results will be less accurate as the winds become less constant in space.

Poor resolution or bathymetry over complex topography could result in locally less accurate results; however, lower resolution is often necessary away from the area of interest to increase computational speed.

When calibrating a model, it is recommended to start by comparing water levels and then current velocities. This is because water levels are generally easier to calibrate and are less sensitive to errors in local bathymetry or poor grid resolution.

Manning's roughness coefficient was varied for calibration. In general, the value for this parameter should always be based on comparison of model results to measurements.

4.8 Test C3-Ex7: Ship Island, MS

4.8.1 Purpose

The purpose of this validation case is to test CMS performance for tide and wind induced hydrodynamics around Ship Island, MS, with and without regional model forcing.

4.8.2 Physical setting and description

CMS was applied to a section of the Mississippi coast in the vicinity of Ship Island, MS. Model results are compared to measured data collected by NOAA (NOAA 2010), roving Acoustic Doppler Current Profiler (ADCP) and two wave gages.

4.8.3 Model setup

Grid boundaries were selected to optimize computations in the vicinity of Ship Island. Larger grid sizes would require one to account for spatially variable winds and tide potentials for this location. Figure 76 shows the CMS telescoping grid used for initial calibration and validation. Grid cell sizes between 25 and 800 m are used, depending on the expected flow gradients and spatial resolution required. Updated bathymetry and topographic LIDAR data were provided by the Mobile District based on surveys conducted either by the District or the USGS (MCIP 2011) for this study. The grid was adjusted to the Mean Sea Level (MSL) datum. Water level forcing occurs at the water boundaries. Table 45 summarizes the CMS-Flow model settings for this case.

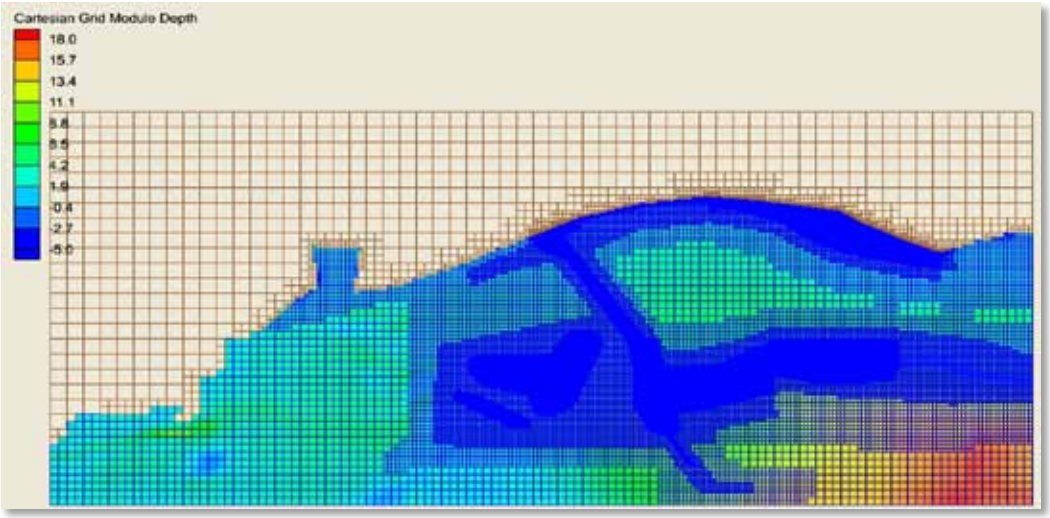

Figure 76. CMS-Flow telescoping grid for Ship Island, MS.

Table 45. CMS-Flow model parameter settings for the Ship Island, MS test case.

Parameter	Value
Time step	10 min
Simulation duration	120 hr
Ramp period duration	1 hr
Manning's *n* – Measured water levels Manning's *n* – ADCIRC	0.017 sec/$m^{1/3}$ 0.012 sec/$m^{1/3}$

4.8.4 Field data description

Figure 77 shows the location of available permanent water level or current measuring sensors. These sensors are maintained and operated either by the U.S. Army Corps of Engineers, NOAA, or the USGS. ADCP measurements were collected on March 31, 2010. The validation period selected was 30March- 3 April 2010.

4.8.4.1 Model forcing - winds

Winds from the National Ocean Service Gulfport Outer range station, (gpom6) were used. The winds from this exposed on-the-water station are typically higher than the winds at nearby Gulfport Harbor (Figure 77). Due to the relatively small tidal range and shallow depths, the wind is a major influence on water movement in the Mississippi sound. The model was run with uniform winds over the modeling grid. It is notable that during the validation period, a significant wind shift occurred, providing a good test for the model. Bunch et al. (2003) showed the importance of winds in the Mississippi Sound for water levels and currents.

Figure 77. Location of field measurement stations for the Ship Island, MS field test case.

4.8.4.1 Model forcing - water levels

Two types of water levels were used to force CMS: ADCIRC water levels and NOAA tide gauges. Water levels were extracted from regional ADCIRC model simulations carried out by MCIP (2011). The ADCIRC simulations were forced with astronomical tides and spatially variable winds. The coverage of the ADCIRC model grid is shown in Figure 78.

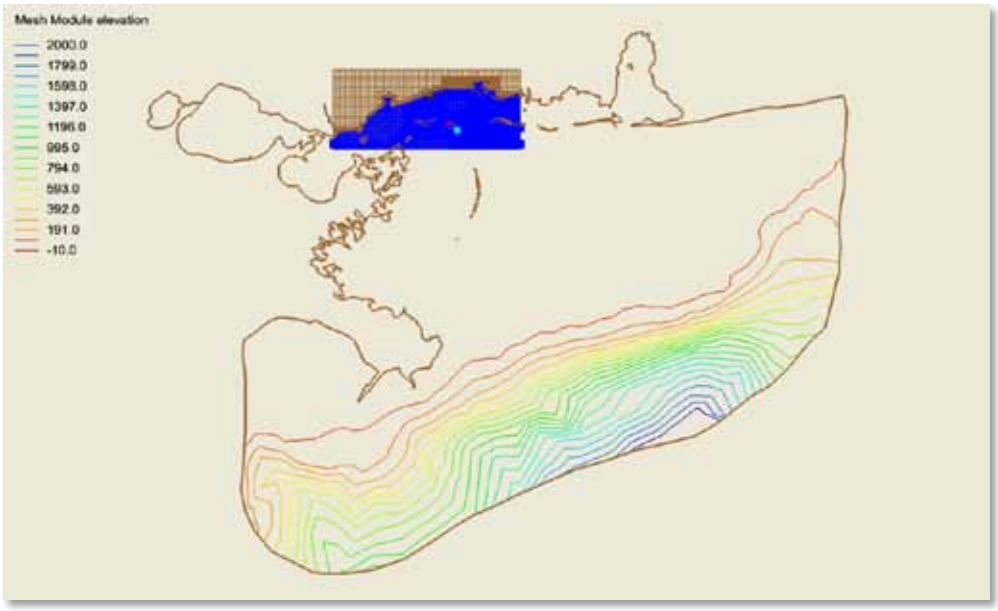

Figure 78. CMS (brown/blue) and ADCIRC extents of water level values were extracted from ADCIRC for CMS boundary forcing

Several NOAA tide gages are deployed on the Mississippi coast with the Dauphin Island gage being the closest to providing an open coast boundary condition. Water levels from the Gulfport tide gage were also used to force the model uniformly along the open boundary condition.

4.8.5 Results and discussion

The primary exchange with the Gulf of Mexico is in the North-South direction, but the meteorological response varies with direction. Southerly winds act over much longer distance than the other directions. Consequently, the effects of those winds need to be included in any offshore forcing. The winds from other directions are more local to the Mississippi sound area, particularly from the North, and the goal is to handle the observed response in the model domain.

4.8.5.1 Water levels

The ADCIRC computed water levels (sampled at 0.5-hr intervals from the offshore CMS boundary) incorporate the effects of the winds and tides. For predicting responses during possible extreme events, a regional model should be used since the water levels may vary in unforeseeable ways due to effects the complicated topography would have on water levels as it becomes inundated.

Figure 79 shows measured and computed water levels at the Gulfport station using extracted water levels from ADCIRC. Note that the measured data show a relative increase in water level for the Gulfport gage at hour 60 due to southerly wind acting on the water surface causing an increase in water surface elevation against the land. While at hour 10, a set down occurs due to a northerly wind.

The computed water levels do not agree fully with the measurements (primarily wind driven). Although uniform winds were used in the CMS model, the computed water levels are largely dependent on the input boundary forcing. The figure also shows computed water levels at the wave gages compared to measured data. Table 46 shows computed statistics where the best agreement was obtained at the Gulf gage, which is least influenced by the wind forcing. Similar results and trends are obtained when measured Gulfport tide levels are used to force the model (see Figure 80 and Table 47).

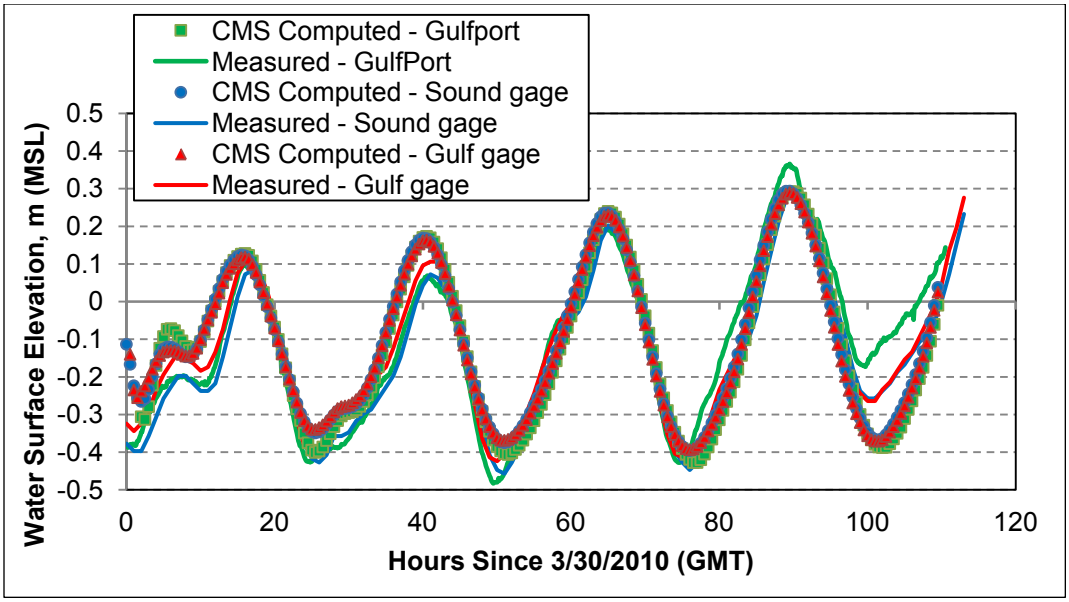

Figure 79. CMS computed GulfPort water levels with boundary conditions from ADCIRC.

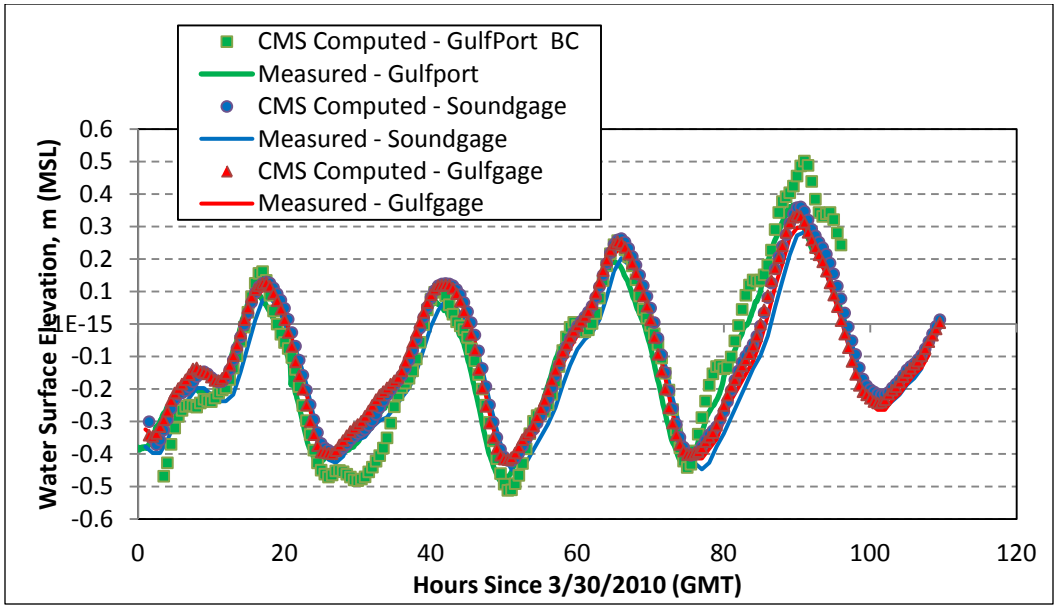

Figure 80. Measured and calculated water levels with boundary conditions from measured Gulfport Data compared to measurements.

Table 46. Water level goodness-of-fit statistics* for the CMS forced with ADCIRC water levels.

Statistic	Gulf gage	Sound gage	Gulfport
RMSE, m	0.079	0.114	0.108
R^2	0.9169	0.8506	0.8599
Bias, m	-0.0104	-0.0429	0.0054
MAE, m	0.255	0.311	0.298

*defined in Appendix A

Table 48. Water level goodness-of-fit statistics* for the CMS run with Gulfport water levels.

Statistic	Gulf gage	Sound gage	Gulfport
RMSE, m	0.283	0.0635	0.0813
R^2	0.9927	0.9847	0.9607
Bias, m	-0.016	-0.052	-0.017
MAE, m	0.155	0.235	0.253

*defined in Appendix A

4.8.5.2 Currents

Figure 77 showed the locations of the NOAA PORTS (NOAA 2010) current meters that were used primarily for model calibration and verification. The NOAA data were collected via ADCP current meters. The boat based roving Corps ADCP surveys showed that flow did not vary significantly with depth, confirming the 2-D depth-averaged flow assumption for CMS. Also, there are significant spatial current gradients in the vicinity of Ship Island, making the exact measurement time and location important. The current meter data are reported in 10 min intervals and they were smoothed with a 3-point moving average.

The CMS computed currents (the same forcing combinations described in the water level section were used) at NOAA gage CM26 are described in Figures 81 and 82. The data from NOAA gage CM32 were generally comparable, and the observed difference between the CM26 and CM32 were used to calibrate the Manning's *n* roughness coefficient. A Manning's coefficient of 0.012 sec/$m^{1/3}$ was used with ADCIRC forcing and a value of 0.017 sec/$m^{1/3}$ was used for all other runs.

Figure 81 shows the comparison between CMS results and measurements at CM 26 when ADCIRC results are used to force the model. The low current value at hour 6 is noticeable, as well as the obvious mistimed low and high currents at hours 18 and 24. These are likely due to imperfect winds over the ADCIRC domain. The large currents computed around hour 35 correspond to a high wind event coming from the westerly direction. Using exact spatially varying winds in CMS could possibly improve the computed levels and currents since the exposed location Gulfport Outer Range winds used are higher in magnitude than other locations within the model domain.

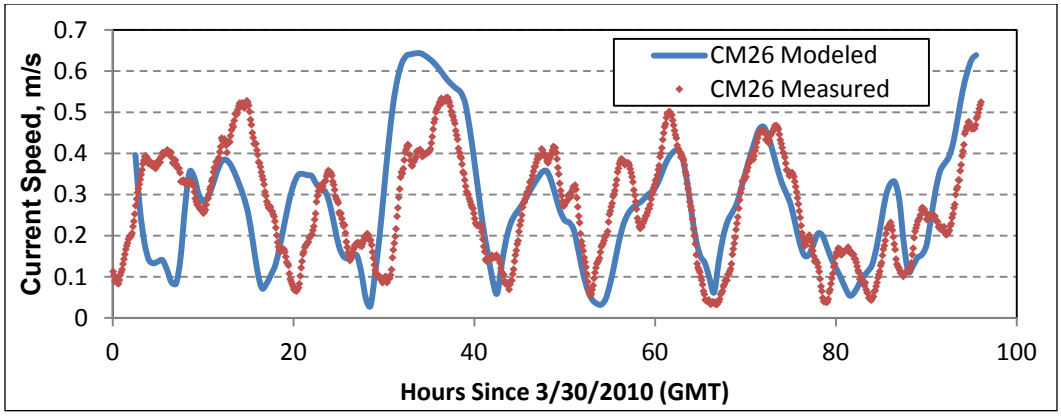

Figure 81. Measured and calculated current speeds at station CM26 for the run forced with ADCIRC water levels.

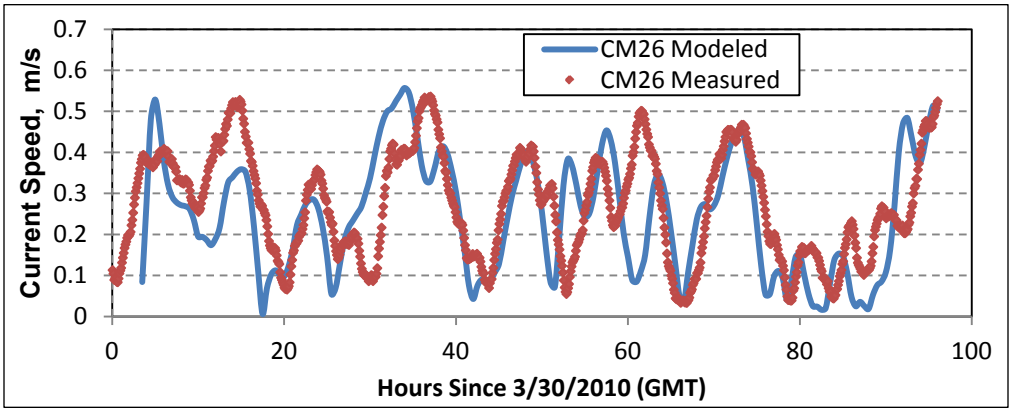

Figure 82. Measured and calculated current speeds at station CM26 for the run forced with Gulfport levels.

Figure 82 shows a comparison between CMS and the current observed at the NOAA CM 26 station when forced with the measured Gulfport water surface elevation data shown in Figure 79. The initial high current is due to ramp up time of the model and can be ignored. Generally, the computed current is within 0.1 to 0.15 m/sec of the observed current. The most notable exception is seen at hour 60 when the current decreases significantly when it should be increasing. This time corresponds with a significant wind shift. As stated earlier, the inshore Gulfport data used to force the model already incorporates the observed response to the incident tides and weather, so the effect of the wind in the model at this time leads to a significant difference between the computed slope of the water surface from offshore to inshore, affecting the computed current. The timing of the peak water level values (resulting in slack water) at hours 18 and 55 are also affected by this mechanism. The summary goodness-of-fit statistics shown in Table 48 has no clear winner between the model results from the two forcing scenarios described here.

Table 48. Water level goodness-of-fit statistics at Station CM26 using two different types of water level forcing.

Statistic	Water level forcing	
	Gulfport	ADCIRC
RMSE, m/sec	0.139	0.133
R2	0.522	0.584
Bias, m/sec	0.0177	-0.0036
MAE, m/sec	0.326	0.324

*defined in Appendix A

4.8.5.3 Comparison with roving ADCP measurements

The previous section showed the model-to-data comparison for currents at a single location in the area of interest. The ADCP measurements (MCIP 2011) show the observed currents over a larger area within the area of interest around Ship Island, MS. Recall that the CMS implicit model was run with a time step of 10 to 15 min, and the output was recorded every 30 min. Therefore, there are relatively few points to compare for each ADCP transect. However, in general, the observed data were found to follow the same trends as presented in the previous section, and have good agreement. Depth averaged ADCP transect data were loaded into the Surface Modeling System and overlaid with the model results.

Figure 83 shows an example ADCP transect collected near the time of 21:30 GMT on 31 March 2010. This time period is interesting since it is near the transition from flood to ebb, with changing flow patterns. The figure shows good agreement between computed and measured data on the right side of the transect (which most closely matches the 2,130 timestep in time). The flow increases during subsequent time steps, matching the remainder of the transect data. Figure 84 shows flow flooding between Ship and Cat Islands, while flow is ebbing through Camille Cut and between East Ship and Horn Islands, which matches the ADCP data. Note the gyre that formed near the tip of Ship Island.

4.8.6 Conclusions

CMS-Flow was evaluated by comparing measured and calculated water levels and currents near Ship Island, MS. The relatively small model domain allowed for the use of locally measured water levels and spatially uniform

wind data for (non-storm) conditions. Similar results were obtained when the model was forced with spatially variable water levels from ADCIRC model results. Uniform winds proved sufficient in this application.

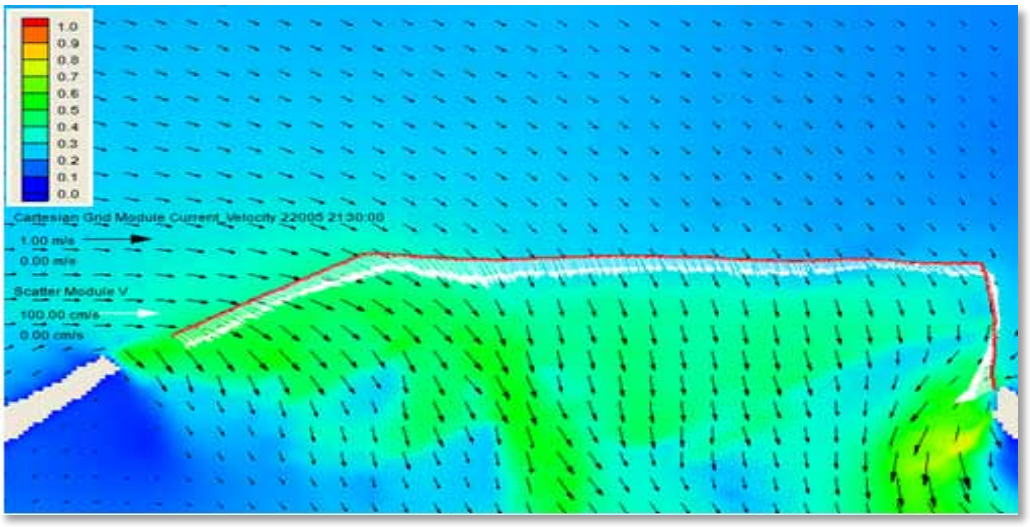

Figure 83. Ship to Horn Island transect on 30 March 2010 at 21:30 GMT. Right side transect values are closest in time to the timestep value.

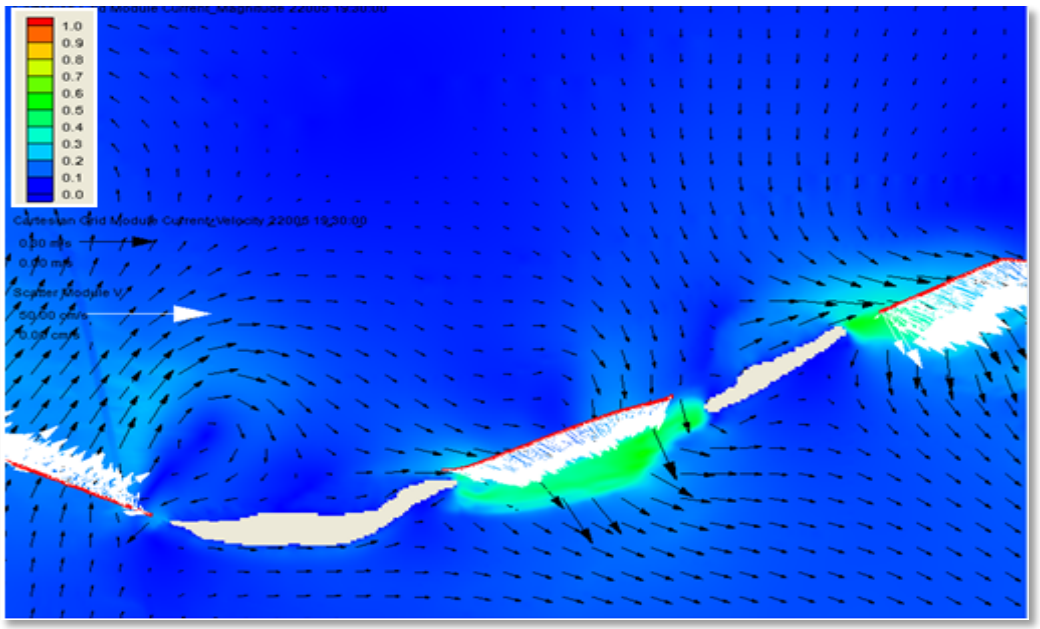

Figure 84. Flow at 30 March 2010 at 19:30 GMT overlaid with transects that also occur at that time.

4.8.7 Recommendations for practical applications

The use of a larger model domain to supply computed water levels and currents is needed to supply proper forcing for storm conditions in the

Mississippi Sound area. The presence of a NOAA PORTS system provides an abundance of data at certain locations for model calibration and validation. The presence of multiple simultaneous current measurements within a domain helps to calibrate model flow roughness. When uniform winds are used, the wind data should be validated against nearby anemometer locations. When dealing with wind dominated systems such as the Mississippi sound, the variation of winds measured between onshore locations and offshore locations should be understood.

4.9 Test C3-Ex8: Hazaki Oceanographic Research Facility, Japan

4.9.1 Purpose

The CMS is applied to a field case to test the model performance in predicting the cross-shore distribution of the wave height and long-shore current over a double barred beach.

4.9.2 Field study

Kuriyama and Ozaki (1993) measured the cross-shore distribution of longshore current and wave height at the Hazaki Oceanographic Research Facility (HORF) located on the Japan Pacific coast. Longshore current measurements were made from a 427-m-long pier using a float. The wave heights were calculated with ultrasonic wave gauges. The data presented here was taken on 28 March 1989. Table 49 shows a summary of offshore wave conditions.

Table 49 Offshore wave conditions for the HORF test case.

Variable	Value
Incident wave angle	27°
Offshore significant wave height	2.14 m
Wave period	8.86 sec

4.9.3 Model setup

A non-uniform Cartesian grid is used with a variable resolution of 3 to 10 m in the cross-shore direction and a constant resolution of 4 m in the long-shore direction (see Figure 85). A constant zero water level was specified at the east (offshore) boundary, and cross-shore boundary conditions were used at the north and south boundaries. At the cross-shore boundaries, a

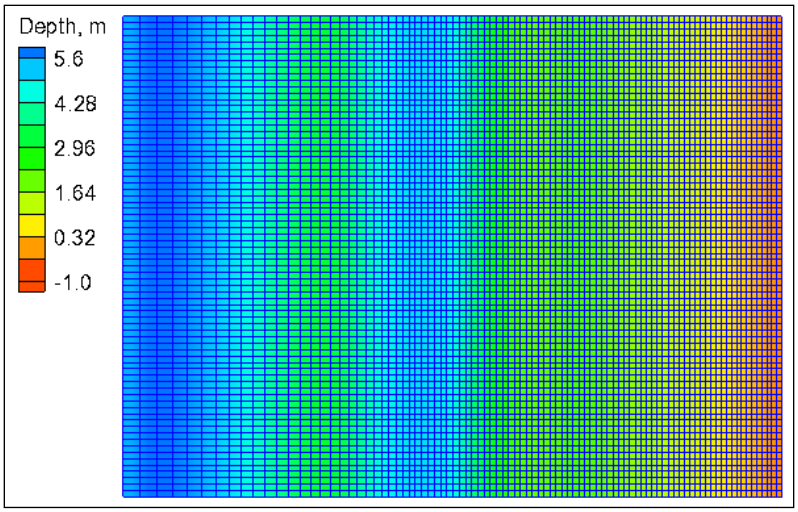

Figure 85. Computational grid for the HORF test case.

Table 50. CMS-Flow setup parameters for the HORF field test case.

Setting	Value
Solution scheme	Implicit
Time step	1 min
Simulation duration	3 hr
Ramp duration	2 hr
Manning's coefficient	0.032 sec/m$^{1/3}$
Clock time	2.8 min

Table 51. CMS-Wave setup parameters for the HORF field test case.

Setting	Value
Wave breaking	Battjes and Jansen (1978)
Spectrum	TMA
Directional spreading distribution	Cosine Power
Directional spreading parameter γ	3.3
Bottom friction	Off (default)
Steering interval	0.25 hr
Roller (Stive and De Vriend 1994)	Off, On
Roller efficiency factor	1.0
Roller dissipation coefficient	0.1

longshore flux was given for inflow conditions and a water level that includes wave setup is specified for outflow conditions. This field case was simulated as a steady state condition, for which the model was ramped from still water by using a pseudo-time stepping procedure. The nearshore bathymetry is assumed to be uniform in the longshore direction and the longshore currents and water levels to be well developed. Tide and wind are not included in the simulation. The important settings for CMS-Flow and CMS-Wave are provided in Tables 50 and 51.

4.9.4 Results and discussion

The computed significant wave heights are compared to field measurements in Figure 86. The wave height profile is characterized by strong wave breaking near the offshore bar and the inner bar and less intense wave breaking on the beach face. In general, good agreement is obtained between the measured and computed wave heights as illustrated by the goodness of fit statistics shown in Table 52. The computed longshore currents with and without the surface roller are compared to the measurements in Figure 87. The cross-shore distribution of the longshore current is characterized by two peaks due to the double barred beach profile. The magnitude of the longshore current is proportional to the reduction of the wave height squared which explains why the offshore longshore current peak is stronger than the nearshore peak. The location of the longshore current peaks is captured better when the roller is included. The default value for the roller dissipation coefficient of 0.1 is used. It is expected that further improvement of the longshore current could be obtained by calibrating the roller dissipation coefficient.

4.9.5 Conclusions and recommendations

The implicit CMS was validated with data from the Kuriyama and Ozaki (1993) field experiment for wave height and longshore current distribution across a double barred surf zone. The case was run without and with the wave roller effect. For both simulations, wave height distribution across the surf zone was not influenced significantly by inclusion of the wave roller, and calculations had errors within 3 to 5 percent of measurements.

However, the longshore current calculations with the surface roller gave a better agreement. Both the peak location and the magnitude of the longshore current were better calculated with the roller effect. Since the roller model computation only accounts for less than 1 percent of the total

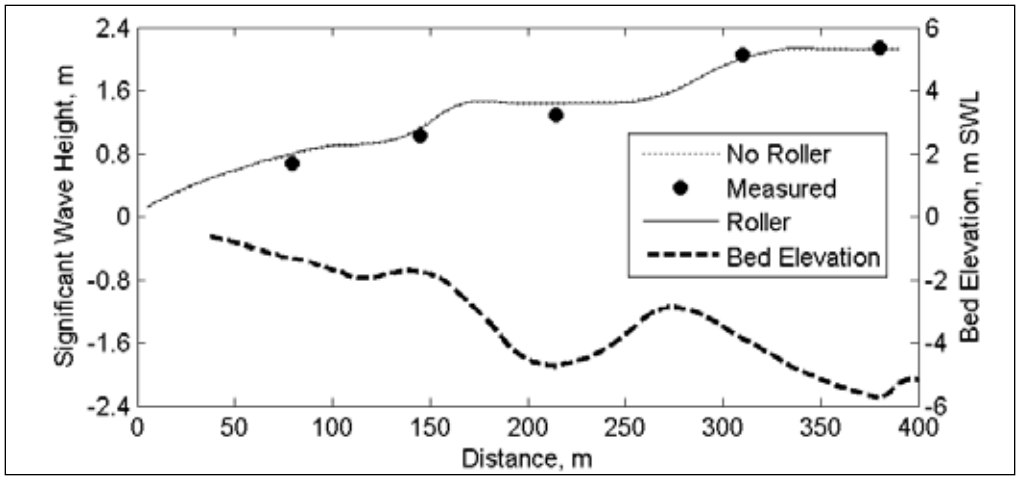

Figure 86. Comparison of measured and calculated significant wave heights for the HORF field experiment. The beach profile is also shown for reference.

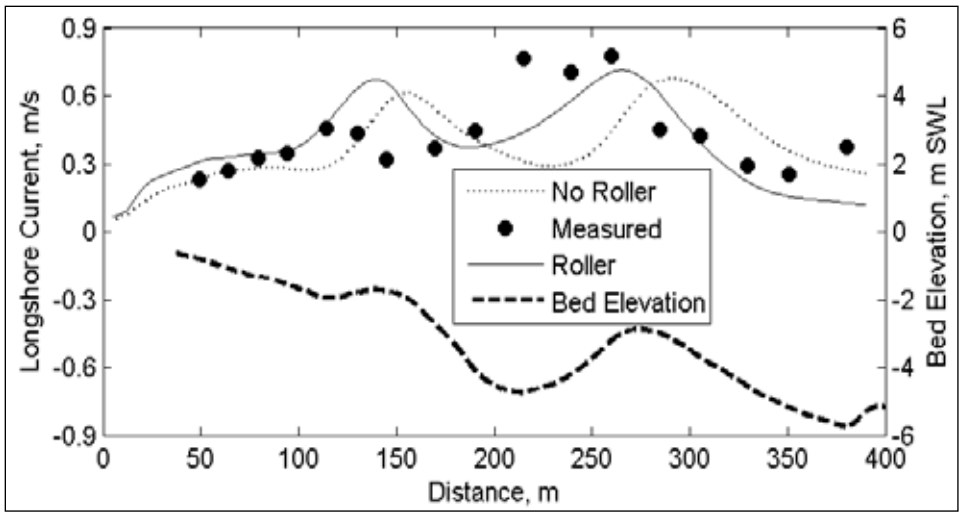

Figure 87. Comparison of measured and calculated longshore currents for the HORF field experiment. The beach profile is also shown for reference.

Table 52. Wave height and longshore current goodness-of-fit statistics* for the HORF field case.

	No Roller		Roller	
Statistic	Hs, m	V, m/sec	Hs, m	V, m/sec
NRMSE, %	6.95	38.51	6.65	28.26
NMAE, %	5.89	30.01	5.61	21.44
R^2	0.994	0.0015	0.995	0.3236
Bias	0.066	-0.028	0.062	-0.006

*see Appendix A.

computational time, adding the roller calculation does not have a significant impact on the total computational time. Besides improving the accuracy of the longshore current, the roller has also added the benefit of improving model stability because it tends to spread out the combined wave and roller forcing. In the absence of longshore current measurements, it is recommended that the surface roller should be turned on for practical applications in the surf zone.

4.10 Test C3-Ex9: Duck, NC, DELILAH field experiment

4.10.1 Purpose

The purpose of this effort was to test the CMS performance in predicting nearshore hydrodynamics, specifically the wave height and longshore current on a barred beach profile. The specific model features to be tested are the inline flow and wave coupling and surface roller.

4.10.2 Field experiment

Waves and currents were measured at Duck, NC, during the DELILAH field experiment held from 1-19 October 1990. Data presented here were measured along a cross-shore array of instruments with conditions recorded approximately every 3 hr. For additional details on the DELILAH field experiment, the reader is referred to Smith et al. (1993). The datasets presented here were collected on 14 October 1990 for which the beach profile consisted of a pronounced longshore bar.

4.10.3 Model setup

A non-uniform Cartesian grid was used with a variable resolution in the cross-shore direction between 2 to 6 m, and a constant resolution in the longshore direction of 6 m (Figure 88). Table 53 shows the offshore wave conditions at an 8-m water depth.

The implicit CMS with steering between the flow and wave calculation was run with a time step of 2 min with a 3-hr ramp period and simulation duration of 3.5 hr. The simulation required 1.2 min to execute on a single 2.67 GHz processor. A summary of the CMS-Flow setup parameters is provided in Table 54.

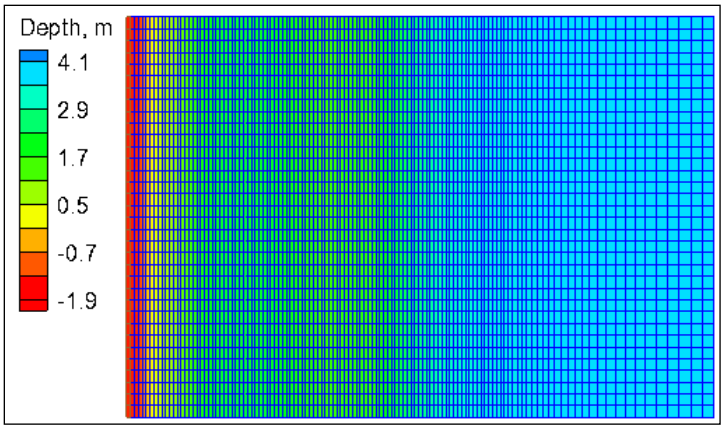

Figure 88. Computational grid for the DELILAH test case.

Table 53. Offshore wave conditions for the DELILAH test case at 8-m depth.

Variable	Value
Incident wave angle	32°
Offshore significant wave height	0.94 m
Wave period	9.7 sec

Table 54. CMS-Flow setup parameters for the DELILAH test case.

Setting	Value
Solution scheme	Implicit
Time step	2 min
Simulation duration	3.5 hr
Ramp duration	3 hr

The wave breaking formula applied was Battjes and Jansen (1978) because it is the recommended wave breaking formula when using the implicit CMS-Flow with inline CMS-Wave model. Two simulations are presented herein with the wave roller terms turned on and off to illustrate the significance of the wave roller process. Bottom friction was turned off in the wave model. Sensitivity tests showed that the wave bottom friction had a negligible influence on the wave height over such a small distance and that the wave breaking was the dominant form of dissipation. The TMA spectrum was applied with a cosine directional spreading with $\gamma = 3.3$ to represent the wave spectrum in shallow water. The steering interval between the wave and flow calculations was 0.25 hour (Table 55).

Table 55. CMS-Wave setup parameters for the DELILAH test case.

Setting	Value
Wave breaking	Battjes and Janssen (1978)
Spectrum	TMA
Directional spreading distribution	Cosine Power
Directional spreading parameter γ	3.3
Bottom friction	Off
Steering interval	0.25 hr
Roller	Off, On
Roller dissipation coefficient, β_D	0.02,0.05
Roller efficiency factor	1.0

4.10.4 Results and discussion

Figure 89 shows the cross-shore profile with the measured and calculated significant wave heights, H_s, in the cross-shore array for measurements at 1:00 AM on 14 October 1990. The inclusion of the wave roller effect is nearly insignificant in the calculation of the wave height across shore. However, in terms of the calculated longshore current, V, the wave roller effect is important. Figure 90 shows the same profile with the measured and calculated longshore current. Three calculations are shown: no roller, the roller with roller dissipation coefficient, β_D = 0.05 and β_D = 0.02. Inclusion of the roller effect more accurately captures the location of the peak in the longshore current further inshore, and also provides a better representation of the magnitude of the current.

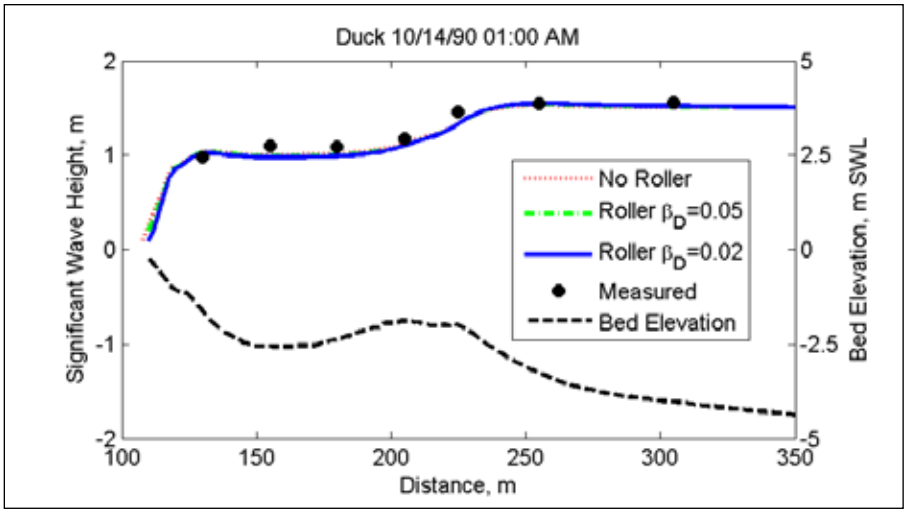

Figure 89. Comparison of measured and calculated significant wave heights for the DELILAH field experiment.

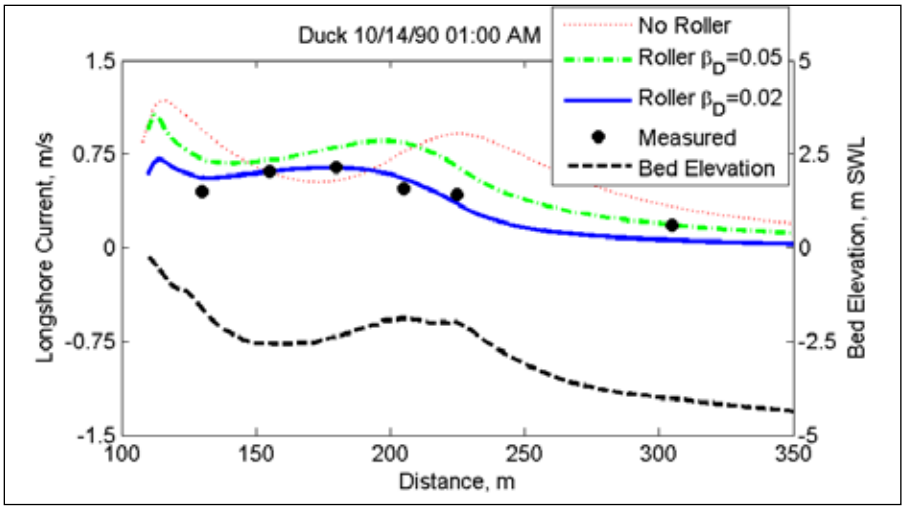

Figure 90. Comparison of measured and calculated longshore currents for the DELILAH field experiment.

Table 56 shows goodness-of-fit statistics for this case, and quantifies how the roller affects the calculations. Errors for calculation of wave height actually increase very slightly when the roller is included, although this error is insignificant because it is likely within the accuracy of the measurements and numerical calculations. However, error decreases quite significantly for the longshore current when the roller is included, from between 37 to 46 percent error to 9 to 12 percent with roller and β_D = 0.02. The most accurate calculation was obtained with the roller β_D = 0.02, resulting in the squared correlation coefficient R^2 =0.927 and 0.915 for the significant wave height and longshore current speed, respectively.

Table 56. Goodness-of-fit statistics* for the DELILAH field experiment at 1 am on October 14, 1990.

Roller	Variable	NRMSE, %	NMAE, %	R^2	Bias
Off	H_s	4.50	4.05	0.933	-0.040 m
	V	46.23	37.11	0.400	0.206 m/sec
On β_D = 0.05	H_s	4.97	4.37	0.926	-0.046 m
	V	31.81	26.29	0.864	0.169 m/sec
On β_D = 0.02	H_s	5.18	4.41	0.927	-0.049 m
	V	11.53	8.72	0.915	-0.000 m/sec

*defined in Appendix A

A second case for data collected during DELILAH at 10 am on 14 October 1990 was run for validation of these parameters. Figure 91 shows the cross-shore profile and distribution of significant wav e height across the profile. Similar to the previous case, inclusion of the roller does not have a

significant effect on the wave height calculation. However, as with the previous case, the wave roller more accurately calculates the location of the peak in the longshore current as well as the magnitude of the longshore current (Figure 92).

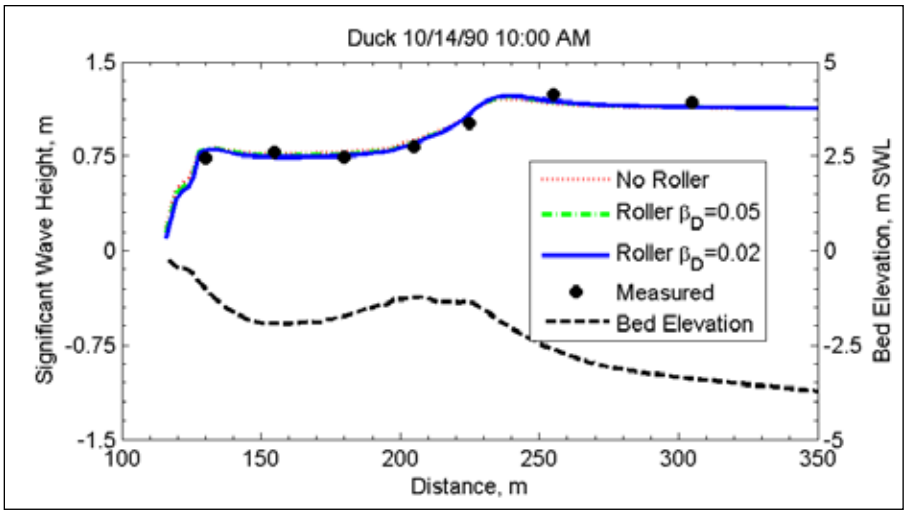

Figure 91. Comparison of measured and calculated significant wave heights for the DELILAH field experiment.

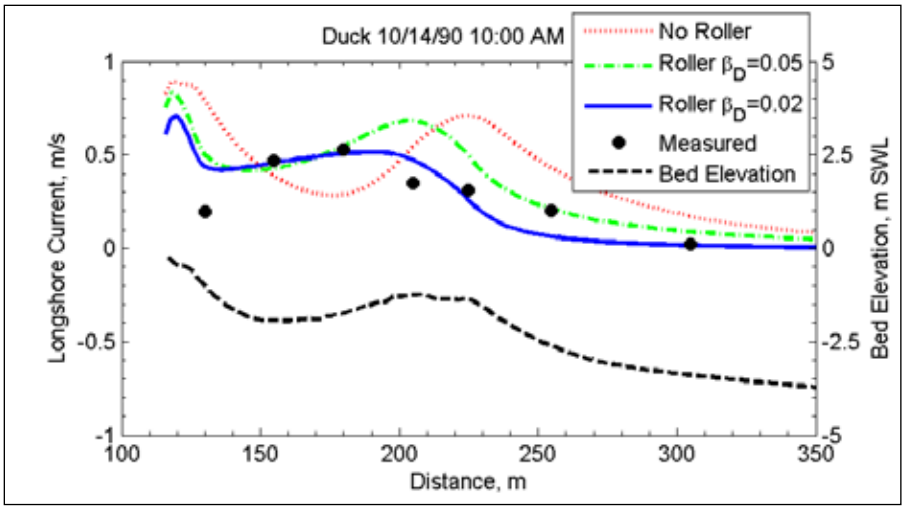

Figure 92. Comparison of measured and calculated longshore currents for the DELILAH field experiment.

Table 57 compares the goodness-of-fit statistics for this case. As opposed to the previous case, the error appears to decrease slightly for the calculated wave height when the roller is included (from 4 to 4.2 percent to 3.4 to 3.7 percent error), although once again this improvement is likely within the accuracy of the measurements and calculations. Error in longshore current speeds decreases significantly when the roller is included, from 58 percent

for the NRMSE without the roller to 25 percent. Once again, the best squared correlation coefficient, R^2 occurs with β_D = 0.02, resulting in R^2 = 0.945 and 0.699 for the significant wave height and longshore current speed, respectively. Typical roller dissipation coefficient values are within 0.05 to 0.1 and the default value in CMS is 0.05. These results indicate that the roller dissipation coefficient may have values smaller than 0.05. More research is needed in better defining the roller dissipation coefficient based on field conditions.

Table 57. Goodness-of-fit statistics for the DELILAH field experiment at 10 am on October 14, 1990.

		NRMSE, %	NMAE, %	R^2	Bias
No Roller	H_s	4.23	3.98	0.943	0.019 m
	V	58.53	51.10	0.202	0.189 m/sec
Roller β_D = 0.05	H_s	3.84	3.58	0.947	0.014 m
	V	37.16	28.65	0.663	0.141 m/sec
Roller β_D = 0.02	H_s	3.70	3.43	0.945	0.010 m
	V	25.21	19.02	0.699	0.044 m/sec

*defined in Appendix A

4.10.5 Conclusions and recommendations

The implicit CMS was validated with data from the DELILAH field experiment, for wave height and longshore current distribution across the surf zone. Two cases were run without and with the wave roller effect. For both cases, wave height distribution across the surf zone was not influenced significantly by inclusion of the wave roller, and calculations were accurate within 3 to 5 percent of measurements for all cases with and without the roller. The roller with a dissipation coefficient β_D = 0.02 gave the best correlation for longshore current speed which is lower than the typical range of 0.05 to 0.1. More research is needed in determining the roller dissipation coefficient as a function of the field wave conditions. Both the location of the peak in the distribution of the longshore current and the magnitude of the longshore current were best calculated with the roller effect. This case demonstrates the accuracy of CMS to calculate wave height transformation and longshore current speed in the surf zone.

4.11 Test C3-Ex10: Matagorda Ship Channel, TX

4.11.1 Description

The purpose of this validation case was to test CMS performance for tide and wind induced hydrodynamics in Matagorda Bay and Matagorda Ship Channel Entrance.

4.11.2 Physical setting and description

The Matagorda Ship Channel (MSC) is a deep-draft channel located on the central Texas coast (Figure 93) and connects the Gulf of Mexico and the Port of Port Lavaca-Point Comfort. The MSC is about 25-miles long and passes through Matagorda Bay, where it intersects the Gulf Intracoastal Waterway (GIWW). The MSC Entrance (MSCE) cuts through the Matagorda Peninsula for approximately 1 mile. The distance between the jetties on the Gulf of Mexico side is 2,000 ft. In the landcut, however, the channel narrows to 950 ft (referred to as the bottleneck), greatly focusing the flow and increasing the current velocity in this area and on the Matagorda Bay side.

Figure 93. Map of Matagorda Ship Channel Entrance and surroundings (from Google Earth).

CMS was applied in this study to evaluate changes to waves and currents at the entrance to the inlet and morphology change at Sundown Island, a dredged material placement site in Matagorda Bay (see Figure 93). One objective of the CMS modeling was to reveal any subtle unintended

consequences of bottleneck removal and dredged material placement alternatives under the complex conditions of rapid tidal flow, wind-induced flow, and waves.

A successful solution would be removal of the bottleneck to decrease current magnitudes while not compromising operation and maintenance of the GIWW (Kraus et al. 2000), nor stability of the adjacent natural inlet, Pass Cavallo, while enhancing the beneficial use of dredged material. Building upon previous studies and in consultation with the sponsor, a jetty configuration alternative that included removing the bottleneck was evaluated with a combined wave, sediment, and hydrodynamic numerical model that was first validated to the existing condition (Rosati et al. 2011).

4.11.3 Model setup

The computational grid and bathymetry for CMS-Flow is shown in Figure 94. The grid has approximately 70,000 active cells with resolution varying between 7.5 and 1,600 m (prototype scale). The grid was oriented to be parallel to the entrance jetties.

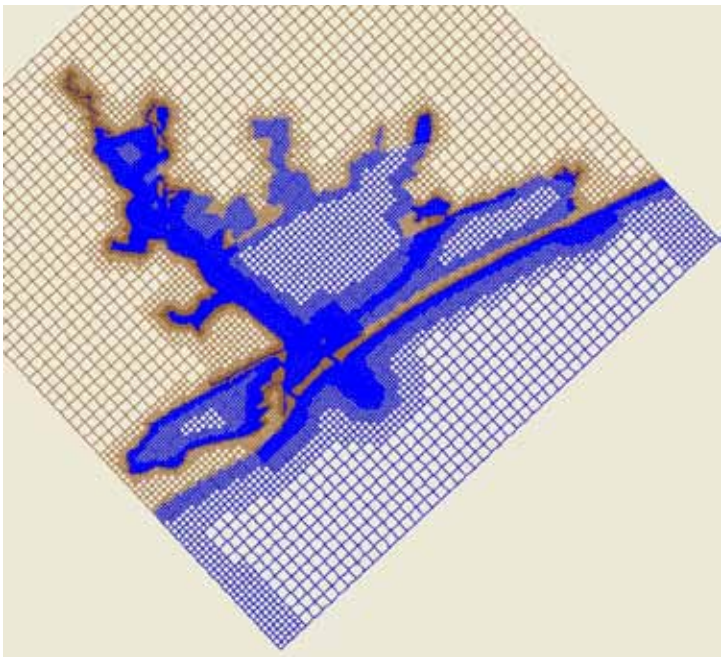

Figure 94. CMS computational grid configuration showing the various sized grid cells for Matagorda Ship Channel, TX.

A list of the basic model setup parameters is shown in Table 58. The implicit code was used for this study. Spatially constant water level measured at Pleasure Pier, approximately 108 miles from the project, was applied on the

ocean boundary. Temporally varying and spatially constant wind forcing, measured at Port O'Connor (shown in Figure 93), was applied. A wall boundary condition was used at all boundaries inside the bay.

Table 58. CMS-Flow parameter settings for Matagorda Bay test case.

Parameter	Value
Flow time step	900 sec
Simulation durations	744 hr
Ramp time	6 hr
Manning's n	0.025 sec/m$^{1/3}$

4.11.4 Results and discussion

The CMS was calibrated against data published in previous reports and is documented in Rosati et al. (2011) and not reproduced here. Validation for calculated and measured water levels is shown in Figures 95-98. In Texas bays, wind in winter and seasonal highs and lows in Gulf of Mexico water levels can exceed changes in water level generated by astronomical tides. Therefore, previous studies examined representative summer and winter conditions (for which the most complete data were available). Seasonal highs occur around May and October, and seasonal lows occur around August and December-January. There is approximately about a 0.3 m (~1 ft) difference between summer highs and winter lows. Tidal range is greater typically in summer than in winter.

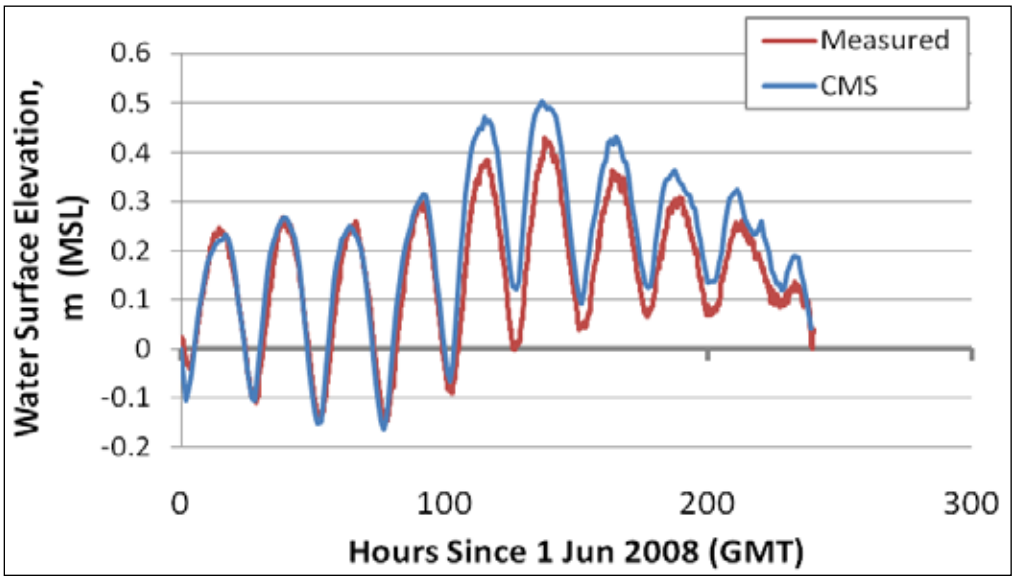

Figure 95. Measured and calculated summer water levels at Port O'Connor.

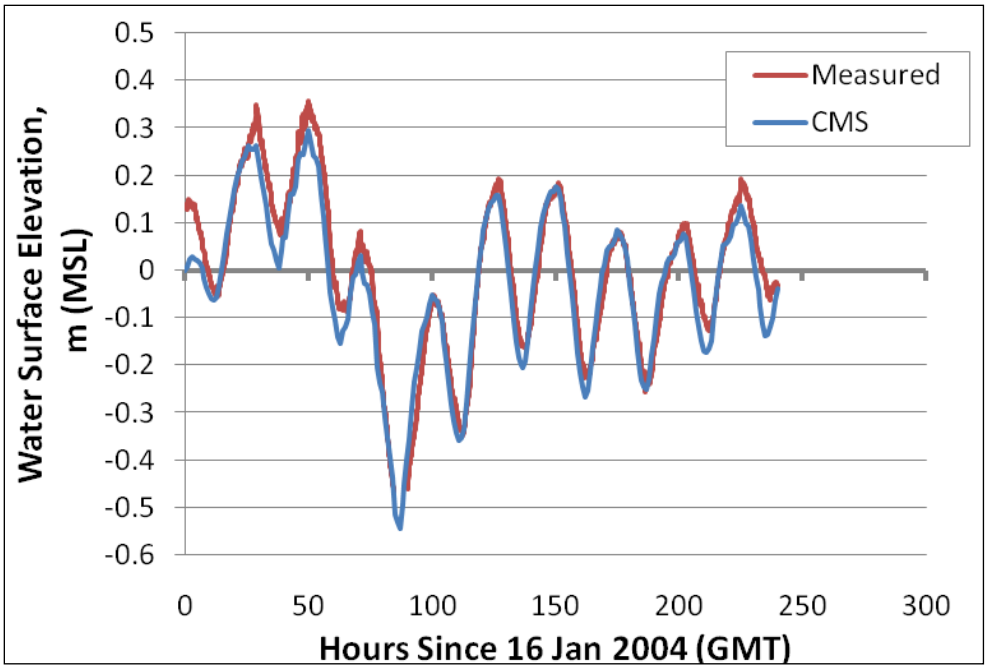

Figure 96. Measured and calculated winter water levels at Port O'Connor.

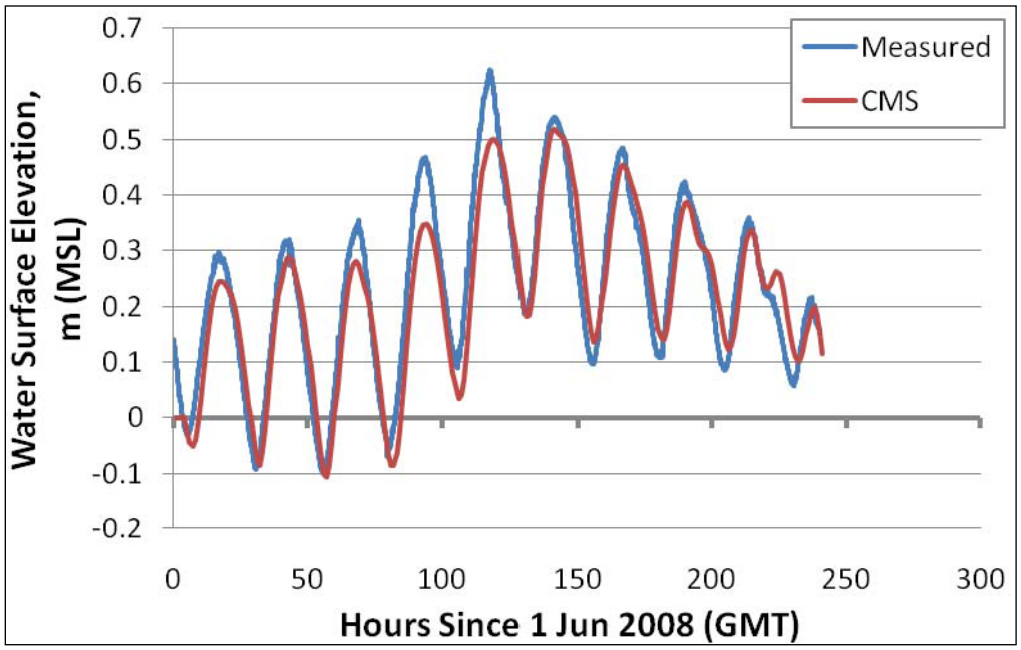

Figure 97. Measured and calculated summer water levels at Port Lavaca.

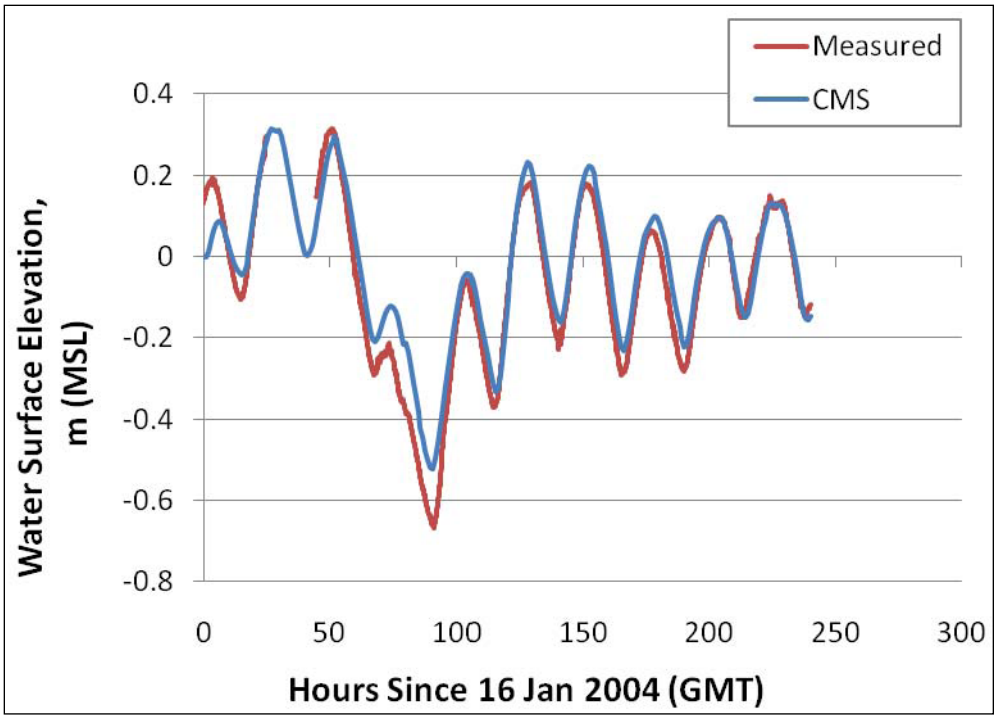

Figure 98. Measured and calculated winter water levels at Port Lavaca.

Gulf of Mexico forcing was specified by data available from the National Oceanic and Atmospheric Administration (NOAA) water level gauge at the Galveston Pleasure (Flagship) Pier. This gauge includes water level as influenced by wind blowing over the gulf in its vicinity. Wind on the present project grid was specified by measurements at the Port O'Connor gauge. Figures 95-98 indicate a close agreement between the water level measurements at Port Lavaca (close to the State Highway bridge) and at Port O'Connor. Main discrepancies occur during wind events, but even so, trends in the increase or decrease in bay water levels are maintained. For the summer period at Port O'Connor, both the measured and calculated water levels are elevated after 100 hr (4 June 2008) because of a summer storm wind that elevated the bay water level. For the winter period at Port O'Connor, there is a sharp decrease in water level around hour 80, caused by wind, which was well reproduced by the CMS. The summer water levels at Port Lavaca show a relatively high mean water level which is typical for the summer season. Table 59 summarizes the goodness-of-fit statistics.

Roving Acoustic Doppler Current Profile (ADCP) measurements were made through the MSC and near Sundown Island on 17 November 2004. Figure 99 displays sample transects of ADCP data along one of the data-collection boat paths. The white arrows display the velocity and magnitude of the measurements, and the black arrows show the CMS calculations.

Table 59. Water level goodness-of-fit statistics* for the Matagorda Ship Channel, TX field test. case.

Statistic	Port Lavaca 2008	Port Lavaca 2004	Port O'Connor 2008	Port O'Connor 2004
RMSE, m	0.0477	0.0595	0.0674	0.0433
R	0.9595	0.9537	0.9613	0.8908
Bias, m	0.0147	-0.0318	-0.0496	0.0230
MAE, m	0.1944	0.2110	0.2349	0.1850

*defined in Appendix A

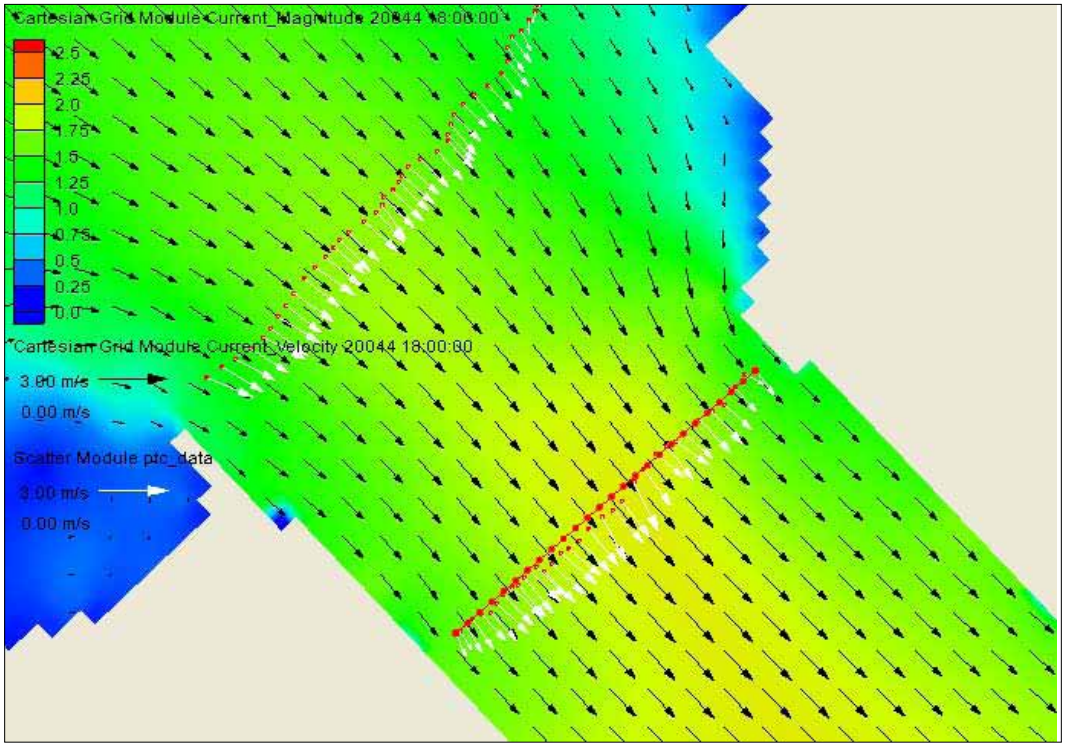

Figure 99. Measured and calculated current velocities along two ADCP transects near the bay side of the Matagorda Inlet. The location of transect 30 is provided for reference.

The CMS computed with a time step of 15 min and a minimum grid size of 12.5 m. The ADCP measurement points are measured typically about 5 sec apart along the moving boat path. Both the CMS calculations and ADCP data are depth averaged.

CMS was validated with currents measured at ADCP transect 30, which was located inside the inlet and was sampled at near peak ebb tide (Figure 100). The ADCP data were averaged to be compatible with the spatial scale of the CMS computational cells. CMS slightly under-predicts

the peak currents for this transect, while capturing the overall shape of the cross-channel current. The main driving force controlling the current for a given bathymetry condition is the amount of the difference in water level inside and outside the inlet. As stated in a previous report (Kraus et al. 2006), uncertainties in bathymetry and offshore forcing conditions are considered to be the main factors contributing to differences between observed and computed current speeds. Goodness-of-fit statistics are shown in Table 60.

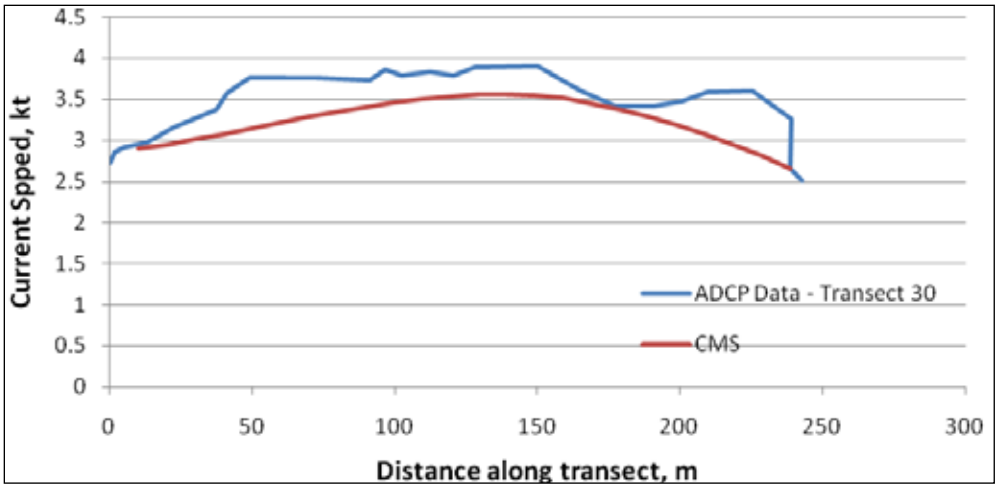

Figure 100. Measured and calculated current speeds along ADCP transect 30 (located in channel as shown in Figure 99). Distance measured from south-west to north-east.

Table 60. Current velocity goodness-of-fit statistics*.

Statistic	Transect 30
RMSE, m/sec	0.336
R^2	0.869
Bias, m/sec	0.245
MAE, m/sec	0.524

*defined in Appendix A

4.11.5 Conclusions

CMS-Flow was calibrated to water level data in the literature and then validated for water level data at two stations for typical summer and winter water levels, with correlation coefficients ranging from 89 to 96 percent. ADCP current measurements across the inlet throat were compared to CMS calculations at the same location. Results validated CMS for current speed with a correlation coefficient of 87 percent.

4.11.6 Recommendations for practical applications

The following recommendations are offered based on lessons learned during this model application:

- Spatially constant wind forcing may be applied over bay-scale domains, even when it is a significant process. Although not specifically demonstrated for this case, it is important to test this assumption for each time period by comparing observed winds at multiple stations across the domain. Model results will be less accurate as the winds become less constant in space.
- Incorporating higher resolution to resolve spatial features such as coastal structures could result in longer run times. Depending on the area of interest and study objectives, lower resolution is often acceptable away from the area of interest to increase computational speed.

4.12 Test C3-Ex11: Matagorda Ship Channel, TX (salinity transport)

4.12.1 Description

The Coastal Modeling System (CMS) is applied to Matagorda Bay, TX, to calculate depth-averaged salinity transport. Matagorda Ship Channel (MSC) is a federally-maintained inlet that, together with Pass Cavallo, connects the Matagorda Bay to the Gulf of Mexico and the Gulf Intracoastal Waterway (GIWW) (Kraus et al. 2006). The bay has an average water depth of 2 m and the hydrodynamics in this shallow bay are frequently dominated by wind. The mean tidal range is only 0.26 m, which very often results in a weak tidal forcing in the bay. Strong wind provides sufficient energy to mix water vertically, indicating that depth-averaged circulation and salinity simulations are applicable to the bay as the salinity is well mixed over the water column.

An extensive field measurement program was conducted by Evans-Hamilton, Inc. (EHI 2006). The data collected include currents, water levels, salinity, total suspended solids, and waves throughout the bay. Freshwater inflows at the Colorado River and Lavaca River gages were available for this study from the U. S. Geological Survey (USGS) website. The salinity measurements inside the bay were used to validate the CMS salinity calculations from 29 November - 10 December 2005.

4.12.2 Model setup and parameters

Figure 101 shows the quadtree grid with 78,000 cells and bathymetric features of Matagorda Bay and MSC. The CMS grid permits fine resolution of 25 to 100 m in areas of high interest such as channels, the bay, and the river and coarse resolution of more than 1 km in the offshore area. The implicit scheme of the CMS with a large time step of 15 minutes was applied for the simulation. Comparing to the explicit scheme, the computation time for the implicit solver was reduced by more than 50 percent. The basic model parameters are listed in Table 61.

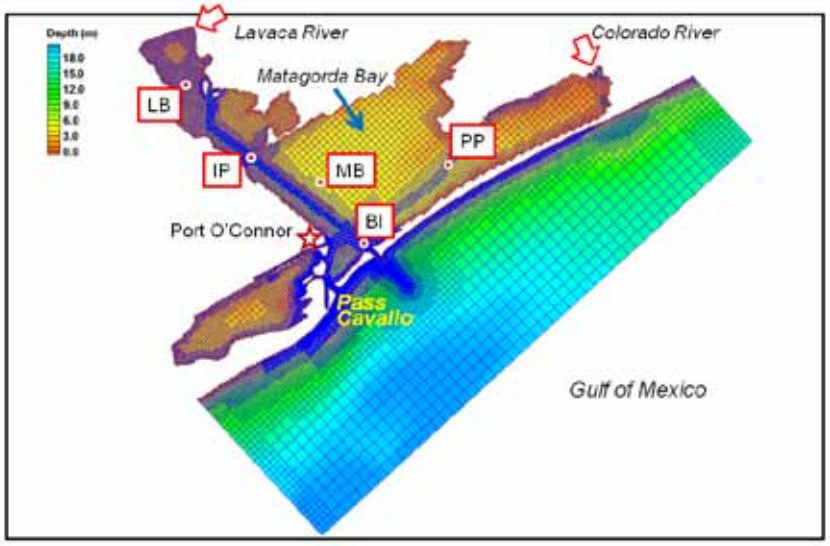

Figure 101. CMS domain and survey stations, Bird Island (BI), Matagorda Bay (MB), Port of Palacios (PP), Indian Point (IP), and Lavaca Bay (LB), in Matagorda Bay.

Table 61. Model parameters.

Parameter	Value	Default
Hydrodynamic time step	900 s	None
Simulation duration	31 d	None
Ramp time	6 hr	None
Manning's n	0.025	0.025
Advection scheme	Exponential	Exponential
Turbulence model	Sub-grid	Sub-grid
Wetting/drying	0.05 m	0.05 m
Steering interval	3 hr	None

Arrows and red dots in Figure 101 indicate the station locations where freshwater inflows and salinity data were collected. Table 62 lists the instrument latitude/longitude locations and the sensor depths. Daily freshwater flows are available at two USGS gages, Lavaca River near Edna and Colorado River near Bay City. Salinity data were collected at Stations Matagorda Bay (MB), Port of Palacios (PP), Bird Island (BI), Lavaca Bay (LB), and Indian Point (IP); wind data were measured at Port O'Connor.

Table 62. Salinity instrument locations and sensor depths.

Station	Layer	Depth (m)	Latitude (N, degree)	Longitude (W, degree)
BI	Surface	1.22	28.44182	96.34500
	Mid	3.05	28.44182	96.34500
MB	Bottom	4.11	28.52142	96.40705
PP	Mid	2.13	28.53990	96.22090
IP	Surface	0.91	28.55227	96.50432
	Mid	3.05	28.55227	96.50432
	Bottom	5.79	28.55227	96.50432
LB	Mid	1.52	28.65192	96.59573

4.12.3 Discussion of results

Depth-averaged current and salinity fields in the bay and MSC were retrieved from two snapshots of the CMS results, corresponding to the ebb and flood currents, respectively (Figure 102).

The calculated current speed was more than 1.5 m/sec at the entrance of the bay during the ebb and flood tides. Relatively stronger currents push salty water into the bay and bring freshwater into Gulf of Mexico along MSC during the flood and ebb tides, respectively. The calculated salinity at the MSC entrance varied from 29.0 to 32.0 ppt during the tidal cycle (Figure 102). A salt front in the bay separates the high salinity water along MSC and the low salinity water in the shallow area of the bay clearly, indicating the interaction between freshwater inflows and ocean water intrusion. Because meteorological tides dominate the astronomical tide in Matagorda Bay (Kraus et al. 2006), the salinity variations mostly respond to weather events or seasonal wind conditions.

Figure 103 shows the salinity comparisons at Stations MB, PP, BI, LB, and IP. Salinity variability is generally less than 1.0 ppt under normal tidal

conditions at stations MB, PP, and BI, and the variability is relatively larger at coastal stations near freshwater sources. There were a few occasions when salinity decreased by 4.0 to 5.0 ppt at Station BI. By examining wind data at Port O'Connor, it was found that those significant salinity changes are most likely associated with weather events (Figure 104). These significant changes in salinity occurred when cold air passed the bay area and a strong northerly wind with a maximum speed greater than 15 m/s pushed fresher, coastal water southward into the bay and resulted in the large salinity drop at Station BI.

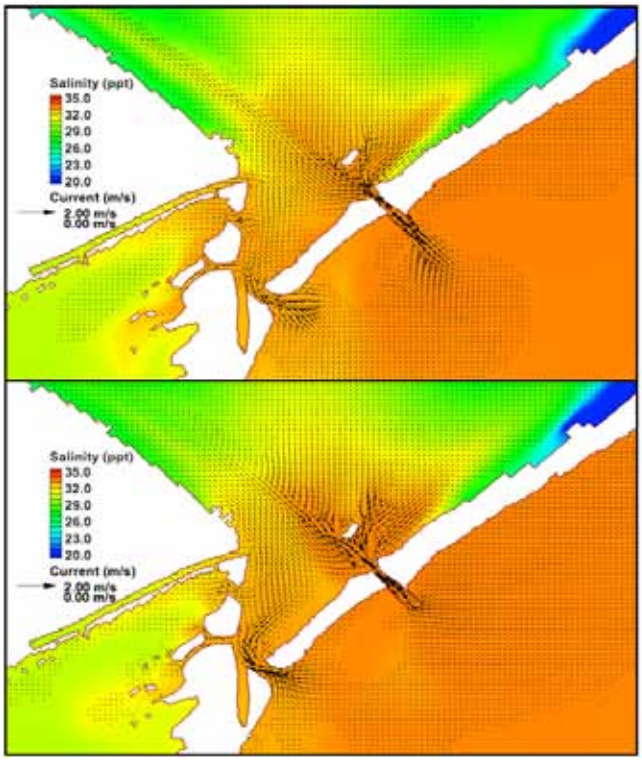

Figure 102. Current and salinity distribution during the ebb (top) and flood (bottom) tide; arrows indicate current and color indicates salinity.

The CMS simulations represented the salinity variations in the bay with NRMSE ranging from 13.3 to 26.9 percent. Lack of freshwater inflow and salinity distribution data in the bay created difficulties in determining initial conditions for freshwater input and salinity for the CMS calculations, which could explain the model and data discrepancies at stations LB and IP and the underestimate of salinity decreases during cold air passage through the region. Table 63 shows correlation coefficient, RMSE, and NRMSE, between the model output and the measurements at the five survey stations.

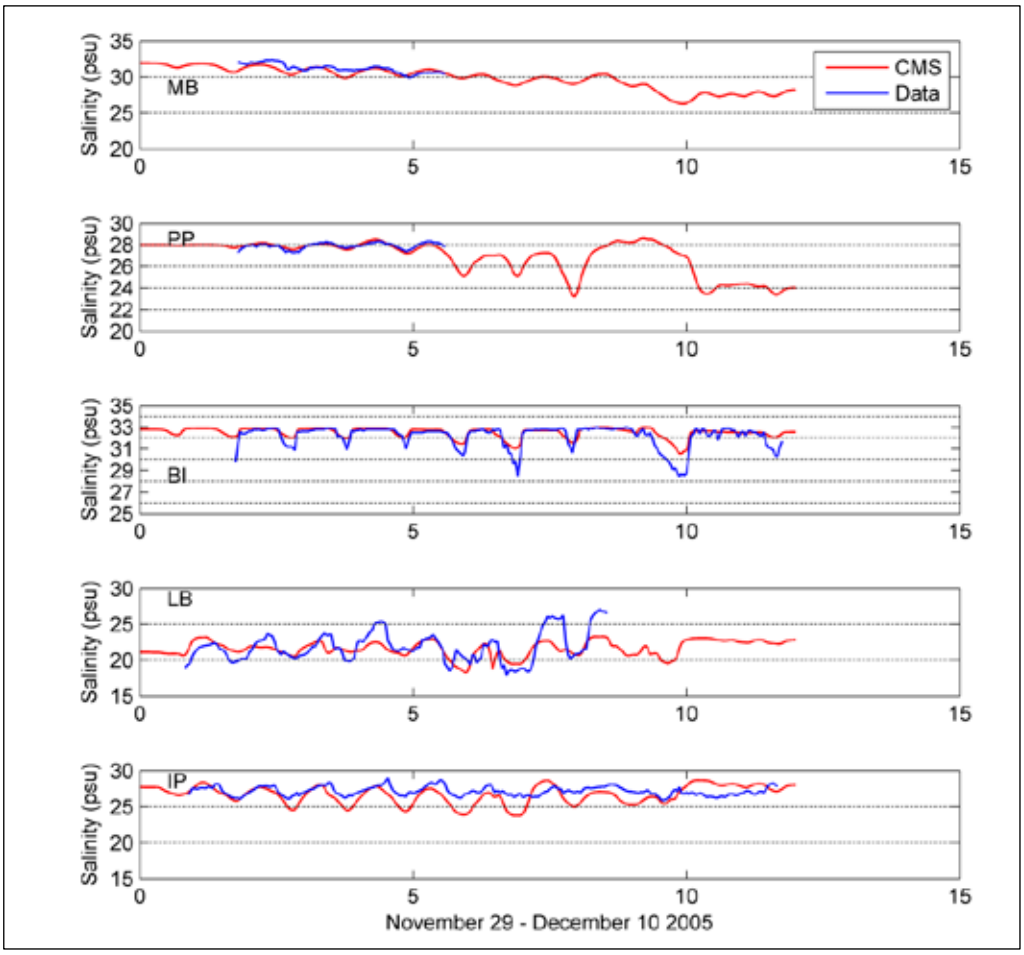

Figure 103. Measured and calculated salinity at the five survey stations.

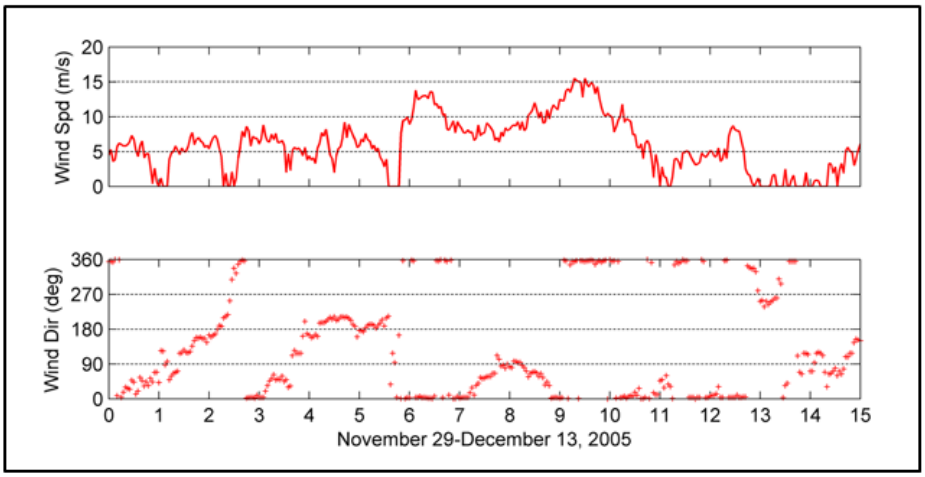

Figure 104. Wind during the simulation period.

Table 63. Correlation coefficients, root mean square errors (RMSE), and relative RMSEs (RRMSE) for computed and measured salinity.

Station	Correlation Coefficient	RMSE	NRMSE (%)
BI	0.888	0.666	13.3
MB	0.629	0.578	19.3
PP	0.698	0.221	14.7
IP	0.344	1.344	26.9
LB	0.598	1.626	18.1

4.12.4 Conclusions

Depth-averaged salinity calculations by the CMS were validated in Matagorda Bay with NRMSE ranging from 13 to 27 percent. The model output showed close correlation with the observations and proper responses to wind and tide forcing. Small computational errors are presented by RMSEs and NRMSEs. The coupled waves and current model demonstrates a successful application of salinity calculations in this shallow, well-mixed bay.

4.12.5 Recommendations for practical applications

The simulation of salinity can often require a 3-D solution due to the presence of vertical salinity gradients that can influence the flow significantly. It is therefore important to understand the limitations of 2-D salinity simulations, and to apply them only when the assumptions inherent in 2-D simulations are valid. However, when the application is well-mixed, a 2-D solution with CMS can represent salinity variation with forcing processes.

5 Summary and Recommendations

This report summarizes the comprehensive V&V study of hydrodynamics for CMS-Flow. The model was evaluated with a large number of analytical, laboratory, and field applications with a wide variety of conditions. The V&V provided an in-depth assessment of various features and capabilities of the CMS-Flow model. Additional analyses will be conducted in subsequent technical documents to extend the Verification and Validation of this model. Applications considered in this V&V study covered coastal inlets, navigation channels, estuaries and bays, adjacent beach surf zone processes, and coastal structures. For each test case, the CMS-Flow model setup was described, and recommendations for default values of the computational parameters were provided for similar practical applications. Limitations of the flow model were described in the discussion of results for each test case. These are briefly discussed next, with a summary of the completed V&V studies, including major conclusions and recommendations for future application of the CMS.

- CMS-Flow was verified with five analytical cases for wind-induced flow, tidal propagation, transcritical flow, and long-wave runup.
- Verification tests demonstrated the model accuracy in representing wind-induced currents, geostrophic balance, nonlinear long-wave transformation, wetting and drying, flux, water level, and land-water boundary conditions.
- Both the non-uniform Cartesian grid and telescoping mesh were verified with analytical test cases. The stretched telescoping grid with a grid cell aspect ratio different than one is recommended since it can reduce the number of cells significantly.
- For boundaries which are not aligned with the Cartesian grid, errors associated with the staircase representation of the boundary may be reduced by increasing the local resolution either by subdivided the local cells, as in the case of the telescoping mesh, or by refining the resolution locally in the case of non-uniform Cartesian grids.
- For practical applications, it is recommended that open boundaries should be specified along straight boundaries since the stair-case representation of curved open boundaries may lead to errors. For most practical applications, straight open boundaries are simpler to implement and curved open boundaries are not necessary.

- When applying the implicit flow solver to applications with sharp discontinuities in flow or extensive wetting and drying, smaller time steps are recommended to resolve the physics associated with the rapidly changing conditions. The model will reduce the time step automatically to insure stability but will reduce the model efficiency. For problems which require small time steps due to large wetting and drying or rapidly varying conditions, use of the explicit flow solver is recommended.
- CMS-Flow hydrodynamics were validated with four laboratory experiments: a rectangular flume with spur dike extending into a steady flow, a steady flow with sudden expansion in the flume width, and two cases of wave-induced currents and water levels.
- Both the non-uniform Cartesian grid and telescoping grid have been tested using laboratory experiment cases.
- The inline flow and wave coupling (steering) was tested using laboratory cases in which both the flow and wave models shared the same grid. Using the same grid for flow and waves avoids interpolation and extrapolation errors and is recommended whenever possible.
- The flux, water level, cross-shore, and land-water boundary conditions were tested for laboratory conditions and performed well without spurious flows or instabilities.
- Both the mixing-length and subgrid turbulence model performed well for laboratory test cases.
- For these laboratory cases with regular monochromatic waves, the best results were obtained with the wave surface roller turned on. However, the optimal roller dissipation coefficient and efficiency factor varied for different tests.
- CMS was applied to ten field data sets, including inlet systems connected to large estuaries, one with primarily river and tidal forcing, and the rest with wind, wave, and tidal forcing; beaches adjacent to a large coastal inlet with strong tidal and wave forcing; and two nearshore experiments with high-quality surf zone measurements.
- For comparisons with two different field data sites, inclusion of the roller did not change the wave height distribution across the surf zone significantly, but the wave roller did improve significantly the magnitude and location of the peak in the longshore current. In the absence of longshore current measurements, it is recommended that the roller should be included in nearshore simulations for best representation of the longshore current.

- Depending on the geometry of the application, either the non-uniform or telescoping Cartesian grid can be used. For most practical applications, the telescoping grid provides more flexibility and efficiency. Use of a stretched telescoping grid is recommended whenever possible to reduce the number of cells.
- Default horizontal eddy viscosity and bottom friction parameters appeared to be appropriate for most cases. However, results can be sensitive to the bottom roughness. Therefore, it is recommended that the bottom roughness (e.g., Manning's coefficient) should be calibrated using field measurements, estimated from coverage maps, or at least varied to obtain the model result sensitivity.
- When calibrating a model using both water levels and current velocities, starting with the water levels is recommended because they are generally easier to calibrate and are less sensitive to errors in local bathymetry or poor grid resolution. The main calibration parameter is usually the bottom roughness (e.g., Manning's roughness coefficient). The bottom roughness should be estimated based on the bottom type (e.g., sand, mud, coral reef, rock, etc.), and then adjusted based on field measurements of water levels and current velocities. Test cases of wave-induced nearshore currents and water levels showed that the results can be sensitive to the surface roller breaking and efficiency coefficients. Lastly, the turbulent eddy viscosity is important for representing the nearshore hydrodynamics (e.g., longshore current profile, ebb/flood jet, rip currents, etc.) accurately. The default turbulence settings were found to work well for most practical applications. However, the optimal turbulence model and empirical parameters varied for different cases. Further research on the turbulence parameters is needed.
- It seems reasonable to apply spatially constant wind forcing over bay-scale domains for non-storm conditions, even when wind is a significant process. It is important to test this assumption for each time period by comparing observed winds at multiple stations across the domain. When simulating storms, the use of both spatially variable winds and atmospheric pressure is recommended.
- For inlets connected to large tidal bays and estuaries such as Grays Harbor, WA, the application of a spin-up period of 10 to 11 days or more for the system reaches dynamic equilibrium is recommended. The user can determine whether the system has reached dynamic equilibrium by comparing measured and computed water levels and

current velocities and ensuring that the agreement between measurements and calculations does not continue to improve.

- All laboratory cases studied were for steady conditions. In the future, laboratory hydrodynamic tests for unsteady conditions should be conducted.
- Turbulence calculations performed well in the test cases discussed herein. However, optimal empirical coefficients for each turbulence model varied depending on the case. Although these tests provide a reference for similar applications, they are not sufficient to provide guidance for different applications. More tests are necessary for developing comprehensive guidance for turbulence coefficients. Presently, all of the turbulence models in CMS assume local equilibrium between turbulence production and dissipation. This has the advantage of not having to solve additional transport equations for turbulence and possibly other turbulence variables (e.g., energy dissipation, frequency of dissipation, etc). However, more sophisticated turbulence models may prove to be beneficial for some coastal applications and require less calibration than simpler models. This topic will be researched further in the near future.
- Inclusion of the surface roller improved significantly the magnitude and location of the peak longshore current. The surface roller has also the added benefit of increasing model stability. However, in one case, the best value of the dissipation coefficient was 0.02 which varied from the recommended range of 0.05 to 0.1. More case studies should be evaluated to determine the best magnitude of this parameter as a function of field forcing, and guidance provided for estimating this parameter in the absence of longshore current data.
- In the SMS 11.0 interface, only telescoping grids with a spatially constant cell aspect ratio can be generated. The present numerical discretization of the telescoping grid allows for anisotropic grid refinement and spatially variable aspect ratios. However, these options have not yet been implemented in the interface.
- It was noted earlier that errors at curved boundaries can be minimized by applying a local refinement to better resolve the curvature along a boundary. However, this increases the number of cells and still produces a staircase representation of curved boundaries. In the future, this problem could be eliminated by implementing a boundary fitting method, such as a cut-cell, shaved-cell techniques (e.g., Popinet and Rickard 2007) or immersed boundaries (e.g., Ye et al. 1999), or an unstructured grid or hybrid mesh scheme.

- For the CMS implicit solver, the governing equations are discretized into a linear system of equations. The resulting matrix is solved using one of four general solvers for sparse unsymmetrical matrices for all of the governing equations. Improved efficiencies can be obtained by implementing solvers specific to the structure of the matrices such as the Alternate Direct Implicit (ADI) and Strongly Implicit Procedure (SIP). These take advantage of the mesh structure and are more efficient for regular Cartesian grids.
- The turbulence models in CMS assume local equilibrium, meaning that the local production and dissipation of turbulence are equal. In the future, an improved turbulence model should also be implemented to simulate the production, transport and dissipation of turbulence (e.g., Rastogi and Rodi 1978).
- All the data sets discussed in this report can be used for verification and validation of other numerical models, and are available from the CIRP website[1].

Pre and post-processing Matlab codes are available on the CIRP wiki at http://cirp.usace.army.mil.

[1] http://cirp.usace.army.mil/

References

Batten, B.K., and N.C. Kraus. 2006. Evaluation of Downdrift Shore Erosion, Mattituck Inlet, New York: Section 111 Study. *Technical Report ERDC/CHL-TR-06-1*, US Army Engineer Research and Development Center, Coastal and Hydraulics Laboratory, Vicksburg, Mississippi.

Battjes, J.A., J.P.F.M. Janssen. 1978. Energy loss and set-up due to breaking of random waves. *Proc. 16th International Conference on Coastal Engineering*, ASCE, 569–588.

Beck, T.B., and N.C. Kraus. 2010. Shark River Inlet, New Jersey, Entrance Shoaling: Report 2, Analysis with Coastal Modeling System. *Technical Report ERDC/CHL-TR-10-4*, U.S. Army Engineer Research and Development Center, Coastal and Hydraulics Laboratory, Vicksburg, MS.

Bunch, B.W., R.S. Chapman, M.B. Gravens, A.S. Grzegorzewski, B.D. Johnson, R.L. Permenter and M.W. Tubman. 2003. "Evaluation of Island and Nearshore Confined Disposal Facility Alternatives, Pascagoula River Harbor Dredged Material Management Plan," Technical Report ERDC TR-03-3, U.S. Army Engineer Research and Development Center, Coastal and Hydraulics Laboratory, Vicksburg, MS.

Buttolph, A. M., C.W. Reed, N.C. Kraus, N. Ono, M. Larson, B. Camenen, H. Hanson, T. Wamsley and A.K. Zundel. 2006a. Two-dimensional depth-averaged circulation model CMS-M2D: Version 3.0, Report 2: Sediment transport and morphology change. *Technical Report ERDC/CHL TR-06-09*, U.S. Army Engineer Research and Development Center, Coastal and Hydraulics Laboratory, Vicksburg, MS. http://cirp.usace.army.mil/pubs/html/buttolph-etal-06.html, accessed June 2011.

Buttolph, A.M., W.G. Grosskopf, G.P. Bass and N.C. Kraus. 2006b. Natural Sand Bypassing and Response of Ebb Shoal to Jetty Rehabilitation, Ocean City Inlet, Maryland, USA. *Proceedings 30th Coastal Engineering Conference*, World Scientific Press, pp. 3344-3356.

Byrnes, M.R., S.F. Griffee and M.S. Osler. 2010. Channel Dredging and Geomorphic Response at and Adjacent to Mobile Pass, Alabama. *Technical Report ERDC/CHL-TR-10-8*, U.S. Army Engineer Research and Development Center, Coastal and Hydraulics Laboratory, Vicksburg, MS. http://cirp.usace.army.mil/pubs/html/10-Byrnes_TR-10-8.html, accessed June 2011.

Caleffi, V., A. Valiani and A. Zanni. 2003. Finite volume method for simulating extreme flood events in natural channels. *Journal of Hydraulic Research*, 41(2), 167-177.

Carrier, G., T.T. Wu and H. Yeh. 2003. Tsunami runup and draw-down on a plane beach. *Journal of Fluid Mechanics*, 475, 79-99.

Dean, R.G., and R.A. Dalrymple. 1984. Water wave mechanics for scientist and engineers. Prentice-Hall, Inc., Englewood Cliffs, New Jersey, 353 p.

Demirbilek, Z., L. Lin and W.C. Seabergh. 2009. Laboratory and numerical modeling studies of hydrodynamics near jetties, *Coastal Engineering Journal*, 51(2), 143-175.

Demirbilek, Z., and J.D. Rosati. 2011. Verification and validation of the Coastal Modeling System: Executive Synopsis. *Technical Report ERDC/CHL-TR-11-XX*, U.S. Army Engineer Research and Development Center, Coastal and Hydraulics Laboratory, Vicksburg, MS.

Dupont, F. 2001. Comparison of numerical methods for modelling ocean circulation in basins with irregular coasts. Ph.D. Thesis, McGill University, Montreal.

EHI. 2006. Data Report: Matagorda Bay Field Data Collection. Report to URS, Houston, Texas. 3/27/2006.

Fredsoe, J. 1984. Turbulent boundary layer in wave-current motion. *Journal of Hydraulic Engineering*, ASCE, 110, 1103-1120.

Kraus, N.C., D.J. Mark and S. Sarruff. 2000. DMS: Diagnostic Modeling System Report 1, Reduction of Sediment Shoaling by Relocation of the Gulf Intracoastal Waterway, Matagorda Bay, Texas. *Technical Report ERDC/CHL TR-99-19*, U.S. Army Engineer Research and Development Center, Coastal and Hydraulics Laboratory, Vicksburg, MS

Kraus, N.C., L. Lin, B.K. Batten and G.L. Brown. 2006. Matagorda Ship Channel, Texas. Jetty Stability Study. *Technical Report ERDC/CHL TR-06-7*, U.S. Army Engineer Research and Development Center, Coastal and Hydraulics Laboratory, Vicksburg, MS.

Li, H., M.E. Brown, T.D. Smith and J.H. Podoski. 2009. Evaluation of Proposed Channel on Circulation and Morphology Change at Kawaihae Harbor and Pelekane Bay, Island of Hawaii, HI. *Technical Report ERDC/CHL-TR-09-19*, U.S. Army Engineer Research and Development Center, Coastal and Hydraulics Laboratory, Vicksburg, MS.

Li, H., L. Lin, C. Lu and A.T. Shak. 2011. Evaluation of Breakwaters and Sedimentation at Dana Point Harbor, CA**.** *Proceedings Coastal Sediments*. http://cirp.usace.army.mil/pubs/html/CS11_Li-Lin.html, accessed July 2011.

Li, Z.H., K.D. Nguyen, J.C. Brun-Cottan and J.M. Martin. 1994. Numerical simulation of the turbidity maximum transport in the Gironde Estuary (France). *Oceanologica Acta*, 17(5), 479–500.

Lin, L., and Z. Demirbilek. 2005. Evaluation of two numerical wave models with inlet physical model. *Journal of Waterway, Port, Coastal, and Ocean Engineering* 131(4):149-161, ASCE.

Lin, L., Z. Demirbilek, H. Mase, and J. Zheng. 2008. CMS-Wave: A nearshore spectral wave processes model for coastal inlets and navigation projects. *Technical Report ERDC/CHL TR-08-13*, U.S. Army Engineer Research and Development Center, Coastal and Hydraulics Laboratory, Vicksburg, MS.

Lin, L., Z. Demirbilek, R. Thomas and J. Rosati. 2011. Verification and Validation of the Coastal Modeling System: Report II, CMS-Wave. *Tech. Report ERDC/CHL-TR-11-xx*, U.S. Army Engineer Research and Development Center, Coastal and Hydraulics Laboratory, Vicksburg, MS.

Luettich, R.A., J.J. Westerink and N.W. Scheffner. 1992. ADCIRC: An advanced three-dimensional circulation model for shelves, coasts, and estuaries; Report 1, Theory and methodology of ADCIRC-2DDI and ADCIRC-3DL. *Technical Report DRP-92-6*, Vicksburg, MS: U.S. Army Engineer Waterways Experiment Station.

Lynch, D.R., and W.G. Gray. 1978. Analytical solutions for computer flow model testing. *J. Hydraulics Division*, 104, 1409-28.

Kuriyama, Y., and Y. Ozaki. 1993. Longshore current distribution on a bar-trough beach, Field measurements at HORF and numerical model. *Report of Port and Harbour Research Institute 32(3)*, Ministry of Transport, Japan, 3-37.

Mase, H., K. Oki, T.S. Hedges and H.J. Li. 2005. Extended energy-balance-equation wave model for multidirectional random wave transformation. *Ocean Engineering*, 32(8-9), 961-985.

MacDonald, N. J., M.H. Davies, A.K. Zundel, J.D. Howlett, Z. Demirbilek, J.Z. Gailani, T.C. Lackey and J. Smith. 2006. PTM: Particle Tracking Model; Report 1: Model Theory, Implementation, and Example Applications, *ERDC/CHL-TR-06-20*, U.S. Army Engineer Research and Development Center, Coastal and Hydraulics Laboratory, Vicksburg, MS.

Militello, A., C.W. Reed, A.K. Zundel and N.C. Kraus. 2004. Two-dimensional depth-averaged circulation model CMS-M2D: Version 2.0, Report 1, Technical documentation and user's guide. *Technical Report ERDC/CHL TR-04-02*, U.S. Army Engineer Research and Development Center, Coastal and Hydraulics Laboratory, Vicksburg, MS.

Osborne, P.D., D.B. Herricks, N.C. Kraus and R.M. Parry. 2002. Wide-Area Measurements of Sediment Transport at a Large Inlet, Grays Harbor, WA. *Proceedings 28th Coastal Engineering Conference*, World Scientific, 3053-3064.

Phillips, O.M. 1977. Dynamics of the upper ocean. *Cambridge University Press*. 261 p,

Popinet, S., and G. Rickard. 2007. A tree-based solver for adaptive ocean modeling. *Ocean Modeling*, 16, 224-249.

Rajaratnam, N. and B.A. Nwachukwu. 1983. Flow near groin-like structures. *Journal of Hydraulic Engineering*, 109(3), 463-480.

Rastogi, A.K., and W. Rodi. 1978. Predictions of heat and mass transfer in open channels. *Journal of the Hydraulic Division*, ASCE, 104(HY3), 397-420.

Reed, C.W., M.E. Brown, A. Sánchez, W. Wu and A.M. Buttolph. 2011. The Coastal Modeling System Flow Model (CMS-Flow): Past and Present. *Journal of Coastal Research*, Special Edition, 59, 1-6.

Reed, C.W., and L. Lin. 2011. Analysis of Packery Channel Public Access Boat Ramp Shoreline Failure. *Journal of Coastal Research Special Edition*, Coastal Education and Research Foundation, Inc., Special Issue, 59, 150-155.

Reed, C. W., and A. Militello. 2005. Wave-Adjusted Boundary Condition for Longshore Current in Finite-Volume Circulation Models. *Ocean Engineering*, 32, 2121-2134.

Rhie, T.M. and A. Chow. 1983. Numerical study of the turbulent flow past an isolated airfoil with trailing-edge separation. *AIAA J.*, 21, 1525–1532.

Rosati, J.R., A.E. Frey, M.E. Brown and L. Lin. 2011. Analysis of Dredged Material Placement Alternatives for Bottleneck Removal, Matagorda Ship Channel, Texas. *ERDC/CHL-TR-11-2*, U.S. Army Engineer Research and Development Center, Coastal and Hydraulics Laboratory, Vicksburg, MS. http://cirp.usace.army.mil/pubs/html/11-Rosati-Frey-TR-11-2.html, accessed 7 June 2011.

Sánchez, A., and W. Wu. 2011. A Non-equilibrium Sediment Transport Model for Coastal Inlets and Navigation Channels. *Journal of Coastal Research Special Issue*, 59, 39-48.

Sánchez, A., W. Wu, T.M. Beck, J.D. Rosati, Z. Demirbilek, H. Li, and M.E. Brown. 2011. Verification, Calibration and Validation of the Coastal Modeling System: Report IV, Sediment Transport and Morphology Change. Tech. *Report ERDC/CHL-TR-11-xx*, U.S. Army Engineer Research and Development Center, Coastal and Hydraulics Laboratory, Vicksburg, MS.

Seabergh, W. C., L. Lin, and Z. Demirbilek. 2005. Laboratory study of hydrodynamics near absorbing and fully reflecting jetties. *Technical Report ERDC/CHL (in press)*, Coastal and Hydraulics Laboratory, U.S. Army Engineer Research and Development Center, Vicksburg, MS.

Smagorinsky, J. 1963. General circulation experiments with the primitive equations, i. the basic experiment. *Monthly Weather Review*, 91, 99-164.

Smith, J.M., M. Larson and N.C. Kraus. 1993. Longshore current on a barred beach: Field measurements and calculation. *Journal of Geophysical Research*, 98(C12), 22,717-22,731.

Stive, M.J.F., and H.J. De Vriend. 1994. Shear stress and mean flow in shoaling and breaking waves. in *Proceedings 24th International Coastal Engineering Conference*, ASCE, New York, 594-608 pp.

Svendsen, I.A. 2006. Introduction to nearshore hydrodynamics. *Advanced Series on Ocean Engineering*, 124, World Scientific Publishing, 722 p.

URS. 2010. Implementation of Bathymetric Survey Plan and Sampling and Monitoring Plan. Report to U. S. Army Corps of Engineers, Galveston District. 4/20/2010.

Visser, R. J. 1991. Laboratory measurements of uniform longshore currents. *Coastal Engineering*, 15, 563-593.

MCIP. 2011. Mississippi Coastal Improvement Program, Barrier Island Restoration Numerical Modeling. Wamsley, T.V. editor with contributions by Bunch, B.W., Chapman, R.S., Gravens, M.B., Grzegorzewski, A.S., Johnson, B.J., Permenter, R.L., Tubman, M.W., [Draft]

NOAA. 2010. Tides and currents. National Oceanographic and Atmospheric Administration, http://tidesandcurrents.noaa.gov/, accessed 17 April 2011.

U.S. Army Engineer District, Jacksonville. 2010. St. Augustine Inlet, Florida, Response to Florida Department of Environmental Protection Request for Additional Information. Draft report.

Wang, P. and T.M. Beck. 2011. Modeling Regional-Scale Sediment Transport and Medium-term Morphology Change at a Dual-Inlet System Examined with the Coastal Modeling System (CMS): A Case Study at Johns Pass and Blind Pass, West-central Florida. *Journal of Coastal Research Special Issue*, 59, 49-60.

Watts, I. M., J. D. Rosati, M. Borelli. 2011. Re-Establishing a Historical Inlet at East Harbor, Cape Cod. *Coastal Sediments '11 Conference Proceedings*, Miami, FL, 419-429.

Wu, W., A. Sánchez, and M. Zhang. 2011a. An Implicit 2-D Depth-Averaged Finite-Volume Model of Flow and Sediment Transport in Coastal Waters. *Proceedings, International Conference on Coastal Engineering*.

Wu, W., A. Sánchez, and M. Zhang. 2011b. An Implicit 2-D Shallow Water Flow Model on Unstructured Quadtree Rectangular Mesh. *Journal of Coastal Research Special Issue*, 59, 15-26.

Wu, W., A. Sánchez, M. Zhang. 2010. An implicit 2-D depth-averaged finite volume model of flow and sediment transport in coastal waters. *Proceeding of the International Conference on Coastal Engineering*. Available at: http://journals.tdl.org/ICCE/article/view/1431. Date accessed: June 12.

Wu, W., and S.S.Y. Wang. 2004. Depth-averaged 2-D calculation of tidal flow, salinity and cohesive sediment transport in estuaries. *International Journal of Sediment Research*, 19(3), 172-190.

Xie, B.L. 1996. Experiment on flow in a sudden-expanded channel. *Technical Report*, Wuhan University of Hydraulic and Electric Engineering, China.

Ye, T., R. Mittal, H.S. Udaykumar, and W. Shyy. 1999. An accurate Cartesian grid method for viscous incompressible flows with complex immersed boundaries. *Journal of Computational Physics*, 156, 209-240.

Zarillo, G. A., and F.G.A. Brehin. 2007. Hydrodynamic and Morphologic Modeling at Sebastian Inlet, FL. *Proceedings Coastal Sediments '07 Conference*, ASCE Press, Reston, VA, 1297-1310.

Zundel, A. 2006. Surface-water modeling system reference manual – Version 9.2, Brigham Young University Environmental Modeling Research Laboratory, Provo, UT.

Appendix A: Goodness-of-Fit Statistics

In this report, the Root Mean Squared Error (RMSE) is defined as

$$\mathrm{RMSE} = \sqrt{\left\langle (x_c - x_m)^2 \right\rangle} \tag{A1}$$

The RMSE has the same units as the measured data. Lower values of RMSE indicate a better match between measured and computed values.

The Normalized Root Mean Squared Error (NRMSE) is defined as

$$\mathrm{NRMSE} = \frac{\mathrm{RMSE}}{\mathrm{range}(x_m)} \tag{A2}$$

The NRMSE is often expressed as percent and in units of data. The measured data range $\mathrm{range}(x_m)$ can be estimated as $\max(x_m) - \min(x_m)$. Lower values of NRMSE indicate a better agreement between measured and computed values.

The Mean Absolute Error (MAE) is defined as

$$\mathrm{MAE} = \left\langle \left| x_c - x_m \right| \right\rangle \tag{A3}$$

Similarly, the Normalized Mean Absolute Error (NMAE) is given by

$$\mathrm{NMAE} = \frac{\mathrm{MAE}}{\mathrm{range}(x_m)} \tag{A4}$$

The NMAE is also expressed as percent quantity and in units of data. Smaller values of NMAE indicate a better agreement between measured and calculated values.

Correlation is a measure of the strength and direction of a linear relationship between two variables. The correlation coefficient R is defined as

$$R = \frac{\left\langle x_m x_c \right\rangle - \left\langle x_m \right\rangle \left\langle x_c \right\rangle}{\sqrt{\left\langle x_m^2 \right\rangle - \left\langle x_m \right\rangle^2} \sqrt{\left\langle x_c^2 \right\rangle - \left\langle x_c \right\rangle^2}} \tag{A5}$$

A correlation of 1 indicates a perfect one-to-one linear relationship and -1 indicates a negative relationship. The square of the correlation coefficient is the variance between two variables as described by a linear fit. The interpretation of the correlation coefficient depends on the context and purposes for which this statistical measure is used. In the present work, the following interpretations apply to model-to-data comparisons: $0.7<R^2<1$ for a strong correlation, $0.4<R^2<0.7$ for a medium correlation, $0.2<R^2<0.4$ for a weak or small correlation, and $R^2<0.2$ for no correlation.

The Bias is defined as

$$\text{Bias} = \left\langle x_c - x_m \right\rangle \tag{A5}$$

Positive values indicate over-prediction and negative values indicate under-prediction.

REPORT DOCUMENTATION PAGE

Form Approved
OMB No. 0704-0188

1. REPORT DATE *(DD-MM-YYYY)*	2. REPORT TYPE	3. DATES COVERED *(From - To)*
December 2011	Report 3 of a series	

4. TITLE AND SUBTITLE

Verification and Validation of the Coastal Modeling System, Report 3: Hydrodynamics

5a. CONTRACT NUMBER

5b. GRANT NUMBER

5c. PROGRAM ELEMENT NUMBER

6. AUTHOR(S)

Alejandro Sánchez, Weiming Wu, Tanya M. Beck, Honghai Li, James Rosati III,
Robert Thomas, Julie Dean Rosati, Zeki Demirbilek, Mitchell Brown, and Christopher Reed

5d. PROJECT NUMBER

5e. TASK NUMBER

5f. WORK UNIT NUMBER

7. PERFORMING ORGANIZATION NAME(S) AND ADDRESS(ES)

U.S. Army Engineer Research and Development Center
Coastal and Hydraulics Laboratory
3909 Halls Ferry Road
Vicksburg, MS 39180-6199

8. PERFORMING ORGANIZATION REPORT NUMBER

ERDC/CHL TR-11-10

9. SPONSORING / MONITORING AGENCY NAME(S) AND ADDRESS(ES)

10. SPONSOR/MONITOR'S ACRONYM(S)

11. SPONSOR/MONITOR'S REPORT NUMBER(S)

12. DISTRIBUTION / AVAILABILITY STATEMENT

Approved for public release. Distribution is unlimited.

13. SUPPLEMENTARY NOTES

14. ABSTRACT

This is the third report, Report 3, in a series of four reports toward the Verification, and Validation (V&V) of the Coastal Modeling System (CMS). All details of the V&V study specific to the hydrodynamic modeling are provided in this report. The primary goal of this study task was to perform a comprehensive assessment of the predictive skills of the CMS-Flow model for a wide range of problems encountered in coastal applications, with an emphasis on applications for coastal inlets and navigation projects. The evaluation study began by considering some simple and idealized test cases for checking the basic physics and computational algorithms implemented in the CMS-Flow model. After these fundamental comparisons, the model was evaluated with a large number of test cases representing real world problems. These application-oriented tests were selected carefully and only those which had data available from laboratory and field studies were considered. Included in this report are the descriptions of each test case, model setup, the boundary conditions used for each numerical simulation, and an assessment of the modeling results. Major findings and default parameters are provided as guidance to users for practical applications of CMS-Flow.

15. SUBJECT TERMS

Circulation	Data	Numerical models	Simulations	Waves
Coastal Modeling System	Errors	Performance of models	Statistics	
	Field and laboratory tests	Sediment transport modeling	Verification and validation	

16. SECURITY CLASSIFICATION OF:			17. LIMITATION OF ABSTRACT	18. NUMBER OF PAGES	19a. NAME OF RESPONSIBLE PERSON
a. REPORT	b. ABSTRACT	c. THIS PAGE			19b. TELEPHONE NUMBER *(include area code)*
UNCLASSIFIED	UNCLASSIFIED	UNCLASSIFIED		147	